SHEAR STRENGTH OF PARTIALLY GROUTED SQUAT MASONRY SHEAR WALLS

By

JAMAL H. ELMAPRUK

A thesis submitted in partial fulfillment of
the requirements for the degree of

MASTER OF SCIENCE IN CIVIL ENGINEERING

WASHINGTON STATE UNIVERSITY
Department of Civil and Environmental Engineering

AUGUST 2010

To the Faculty of Washington State University:

The members of the Committee appointed to examine the thesis of JAMAL H. ELMAPRUK find it satisfactory and recommend that it be accepted.

Mohamed ElGawady, Ph.D., Chair

David I. McLean, Ph.D.

William F. Cofer, Ph.D.

Acknowledgement

I wish to express my special thanks to Dr. Mohamed ElGawady, my M.Sc. advisor, for his guidance, interest, and support during my work in this research. I would also like to extend my thanks to Dr. David McLean and Dr. William Cofer, my thesis committee members, for their dedication, help and guidance.

Other deep thanks are due to Dr. David McLean for his patience and help to test the masonry and reinforcement samples. Thanks are also due to National Concrete Masonry Association, the Northwest Concrete Masonry Association, and the Eastern Washington Masonry Promotion Group for partial funding. Deep thanks to Bob Duncan and Scott Lewis at the Composite Materials and Engineering Center and Miles Pepper at the Engineering shop center for their help during the experimental part of the project.

Sincere thanks to my mother Selma and my wife Samira for their unlimited support, prayers, and encouragement. Without their support I would not have been able to be the one I am now. Moreover, I wish to deeply thank all my friends, Hitham, Shawn, Amin, Abbe, Abdulmanam, Hussain, Zakaria, and others who helped me through this project.

At the last but not the least, I would like to thank the higher minister of education in Libya for giving me this opportunity to pursue my M.Sc. degree in the USA.

SHEAR STRENGTH OF PARTIALLY GROUTED
SQUAT MASONRY SHEAR WALLS

Abstract
by JAMAL H. ELMAPRUK, M.S.
Washington State University
AUGUST 2010

Committee Chair: Mohamed ElGawady.

Partially grouted masonry shear walls are common structural systems in North America. This research examines the shear behavior of six partially grouted masonry shear walls. The walls ha an aspect ratio of 0.58, vertical reinforcement ratio of 0.33% and axial force of 11 kips (49 kN). They were subjected to in-plane lateral cyclic loading in a displacement control. The walls had grout horizontal spacing of 24, 32, and 48 in. (610, 813, and 1219 mm, respectively). Horizontal reinforcement ratios ranging from 0.127% to 0.254% were investigated as well.

The test results showed that the shear strength of the walls significantly depends on the grout horizontal spacing. In addition, there seems to be a threshold horizontal reinforcement ratio beyond which any increase in the reinforcement ratio does not result in increase in the shear strength of partially grouted shear walls.

The measured shear strengths of the test specimens were compared to the predicted shear strength using MSJC (2008) shear design equations. The comparisons showed that the MSJC overestimated the shear strength of partially grouted walls having grout horizontal spacing greater than 24 in. (610 mm). Finally, strut and tie models analysis were developed and were able to predict the shear strengths of the walls within ±20%.

Table of Contents

List of Figures

List of Tables

CHAPTER 1

INTRODUCTION

1.1 Background

Unreinforced masonry systems consist of a composite of bricks, often made from clay or concrete blocks, and mortar joints. Across the past centuries, masonry has been described as one of the most reliable and durable building systems that humans have built in many historic civilizations throughout the world, although they lack sufficient strength to resist strong ground motions. Nevertheless, the wide demand for such building systems also comes from their ease of construction and formation. Obviously, masonry systems are designed to carry out and resist vertical and the horizontal loads. However, during past and the recent earthquakes, the vulnerability of traditional masonry systems has been addressed. It has been noticed that the resistance of masonry buildings to tension or lateral dynamic loads, as well as vertical or compressive loads, is significantly different than in the case of isotropic or homogeneous materials.

Despite the wide use of some modern building materials such as steel and reinforced concrete, masonry building systems are still used. However, the development of a modern masonry construction system using fully reinforced or partially grouted masonry has improved the performance of masonry systems in terms of resisting the tension and the shear forces generated in high seismic activity regions.

Generally, the main structural elements in masonry building systems are shear walls. To illustrate, the structure relies on shear walls for lateral stability. Masonry shear

walls must be provided parallel to the direction of the lateral forces resisted. These shear walls are the mechanism by which lateral forces are ultimately transferred to the ground. The resistant behavior of masonry shear walls is influenced by several factors, including load conditions, properties of the material, block geometries, bond type, joint thickness, and the distribution and amount of the vertical and horizontal reinforcement. Depending on those factors, two distinct inelastic load deformation mechanisms can be identified in masonry shear walls subjected to forces acting in an in-plane direction. The first type of deformation mechanism is flexural failure, which is characterized by the tensile yield of vertical reinforcement followed by the crushing of masonry which occurs within the high compression zone at the diagonal loading corner. Since this type of failure is effective in terms of energy dissipation and ductility, it can be described as a perfect mode of failure.

The second type of deformation mechanism is shear failure, which can be characterized by diagonal tensile cracking along the loaded diagonal corner. This is an atypical mode of failure of masonry walls subjected to seismic loads. In addition, this mode takes place where the principal tensile stresses developed in the wall under a combination of vertical and horizontal loads exceed the tensile strength of the masonry. However, sliding shear failure can occur in the case of low vertical compressive stresses and poor mortar in conjunction with a high lateral load, thus causing sliding the upper part of the masonry walls at one or more of the horizontal mortar joints. Figure 1.1 illustrates the two modes of shear failure, as described above.

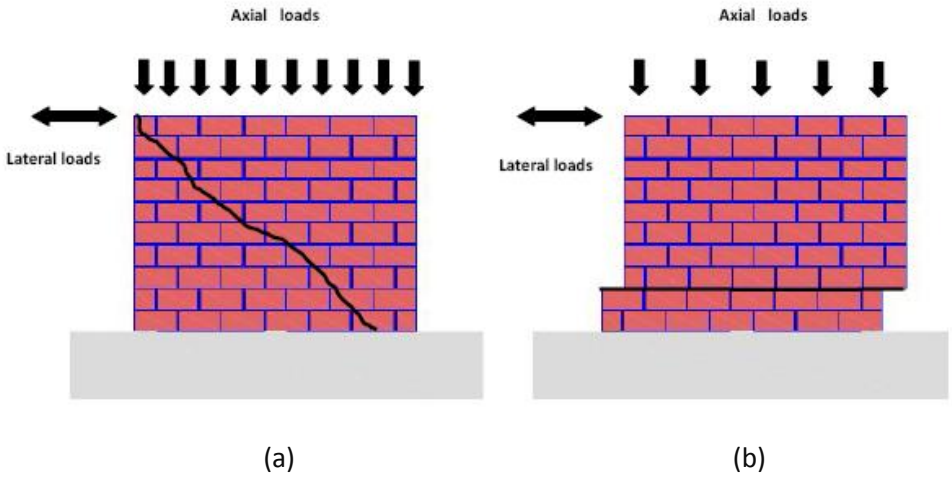

Figure 1.1 Shear failure mechanisms: a) diagonal cracks, b) bed joint cracks

Previous experimental studies (Priestley 1977; Matsumura 1988; Tomazevic 1988; Shing et al. 1990; Voon et al 2006) observed that masonry wall panels that fail predominantly in a shear mechanism tend to exhibit a more brittle behavior during the lateral load cycles than panels that fail in a flexural mechanism, which is more effective in terms of energy dissipation by yielding reinforcement. This brittle behavior is usually characterized by rapid strength degradation that occurs soon after the development of the maximum strength. However, some parameters such as tension of shear reinforcement, dowel action of vertical reinforcement, and aspect ratio as well as the level of applied axial stresses can influence and lead to shear dominated failure modes.

1.2 Research Significance and Objectives

The main objectives of this research are to study the performance of partially grouted reinforced masonry shear walls (PG-RM) subjected to lateral cyclic loads, and to

investigate the MSJC's (2008) shear design equations by comparing the calculated shear strength of 6 partially grouted masonry shear walls , tested in this research, to the measured experimental strength.

1.3 Scope

To achieve the study purposes and the research objectives, the test program consisting of six full scale reinforced masonry shear walls were constructed. In this program, it was decided that this number of walls would be sufficient to conduct the study. The work focused on studying the effect of different amounts of shear reinforcement and horizontal spacing of the vertical grouted cells including flexural reinforcement. All of the intended shear walls were tested under lateral cyclic loading combined with constant compressive stresses.

1.4 Literature Review

1.4.1 Introduction

Even though masonry shear walls have been used in the construction field for a very long time, they have only recently been utilized and designed based on engineering rules. Since the late 1950s, many research programs have been conducted to investigate the behavior of in-plane masonry shear walls. The earliest experimental program was created in 1956 and 1959 by Schneider to study the effect of vertical and horizontal reinforcement on shear strength of masonry shear walls using clay bricks and concrete blocks. The next section demonstrates a brief summary of some experimental studies related to this research; these efforts were focused on the in-plane behavior of reinforced masonry shear walls.

1.4.2 Studies on Behavior of Partially Grouted Masonry Shear Walls

Experimental studies were conducted in Japan by Matsumura (1985, 1987, 1990) on full-scale reinforced masonry shear walls. These experimental works were mainly conducted to study the effect of shear reinforcement ratio, shear span ratio, axial compressive stress, and strength of material.

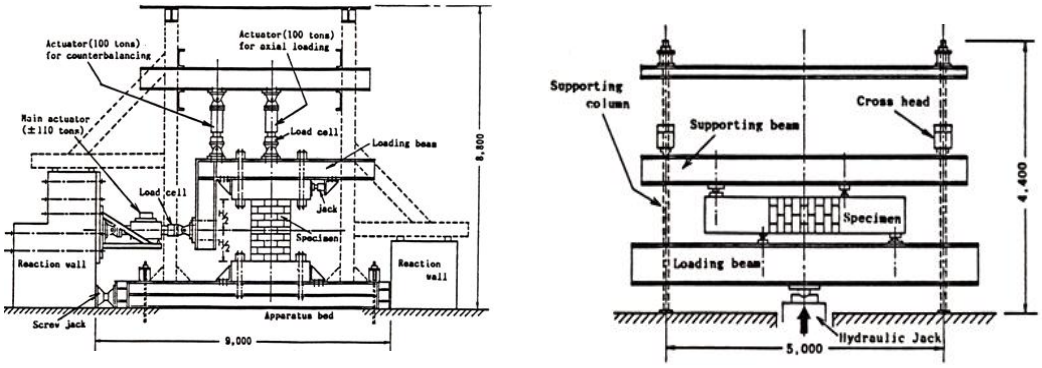

a) Wall type b) Beam type

Figure 1.2 Test setup used by Matsumura (Matsumura, 1985, 1986, and 1988)

In this research, most of the intended walls were partially grouted, and the remainders were fully grouted. For this purpose, 57 concrete masonry shear walls and 23 clay bricks walls were tested under two types of loading conditions, either the beam type or the wall type. To illustrate, in the wall type, the base of the walls were fixed with a free top. On the other hand, walls were laid horizontally and subjected to vertical loads in the beam type. Figure 1.2 shows both loading conditions examined in this study. These efforts concluded that shear strength increases by applying axial stresses on the wall. Matsumura also created a formula to predict the shear strength of fully grouted masonry shear walls.

Shing et al (1989, 1990) conducted a comprehensive study on resistance of in-plane reinforced masonry shear walls by testing a total of 22 walls. The purpose of their study was to examine and investigate the flexure and shear behavior of reinforced masonry shear walls under both cyclic and monotonic loads. Shing et al mentioned that before the diagonal cracks in a shear mode failure occurred, the masonry mainly relies on tensile strength and applied axial loads to resist lateral loads. They indicated that when diagonal cracks occur, the shear resistance will be distributed between the aggregate interlock, the horizontal reinforcement, and the dowel action of the vertical reinforcement. In addition, they also concluded that overall shear stiffness prior to major diagonal cracking tends to be proportional to the axial compressive stress and that the ductility of shear dominated walls is relatively low until a large amount of shear reinforcement is introduced. Shing et al reported that the flexural strength of shear walls might be predicted perfectly by using the flexure theory based on a simple plane section concept. Shing et al indicated that the Uniform Building Code (UBC 1988) specifications were over simplistic and too conservative to address the shear strength that is provided by the horizontal reinforcement in masonry shear walls.

In 1993, Fattal conducted a great deal of research in order to evaluate some of the equations provided by Matsumura**,** Okamoto, Shing et al**,** and UBC to predict and estimate the strength of partially grouted masonry shear walls for failure in the shear mode. Fattal compared the predicted strength calculated using these equations with test results taken from different previous experimental studies involving 72 wall specimens. The equation formulated by Matsumura was the closest predictor of ultimate shear

strength, although it appears to be inconsistent; the correlation provided by this equation was close for high strength walls, but it misestimates the shear strength in low strength walls, partially grouted walls and unreinforced masonry walls.

Some research on partially grouted masonry shear walls was carried out at Drexel University by Hamed and Ghanem (1990, 1992, 1993) using small scale models to investigate the effect of various design parameters and loading conditions such as axial loads, block strength, and the amount and spacing of horizontal and vertical reinforcement. Their results showed that by increasing the axial stresses, the ultimate load carrying capacity will be increased. Also, increasing the axial stresses leads to reduce the ductility, increased cracking strength, and change in the failure mode from flexure to shear. In this study, it was observed that, to avoid brittle behavior, the axial stress should not exceed five percent of the masonry compressive strength.

Schultz (1996) created an equation to determine the minimum horizontal reinforcement limits for seismic design in partially grouted masonry shear walls. Schultz also examined the behavior of partially grouted masonry shear walls under seismic loads using different parameters in order to find the correlation between predicted and measured shear strength. In the same year, Brunner and Shing (1996) tested three squat reinforced masonry shear walls with aspect ratio between 0.96 to 0.60. In order to promote the shear failure mode, the walls were heavily reinforced in the vertical direction. This research demonstrated that walls with low aspect ratio have a high stiffness and reach their maximum strength at small displacement. Two types of shear failure were specified in this research. The first type occurs with aspect ratio less than one in the compassion region

where the diagonal cracks intersect the base. They suggested that part of the vertical force can be transferred from the wall to the base at the compression toe, while the other part is transmitted across the diagonal cracks; this can lead to the generation of high aggregate interlock forces which add to the shear resistance of the wall. The other type is for walls that are squat, where the diagonal cracks intersect with the base away from the compression zone. In this situation, the aggregate interlock forces are relatively small, and the shear resistance can be provided by the entire area bounded by the compression block.

A single story concrete masonry shear wall was tested by Voon and Ingham (2004) in New Zealand. The main purpose of this study was to investigate the effect of the amount and the distribution of shear reinforcement, axial compressive stresses, wall aspect ratio, and type of grout on masonry shear wall strength. Different aspect ratios were used in this test. Eight walls were about 1.8 meters long with an aspect ratio equal to one; another wall was the same length with aspect ratio of 2; and the last wall was 3 meters long with an aspect ratio of 0.6. The research indicated that the distribution of the shear reinforcement along the wall height, as well as the axial compressive stress, can lead directly to improve the behavior of masonry shear walls by increasing the shear strength. Voon (2004) also included the benefit of decreasing the aspect ratio on increasing the shear strength. In term of grouting, Voon (2004) concluded that partially grouted masonry shear walls had about the same maximum shear strength that fully grouted walls had when net area shear stress is considered.

Minaie (2009) conducted a research in order to study the seismic performance of reinforced masonry shear walls. Both experimental and analytical approaches were used.

Four full-scale partially grouted and four fully grouted masonry shear walls, having different parameters, were investigated. The test parameters included wall aspect ratio, the level of vertical stress, and mortar type. It was found that the MSJC (2008) shear design equations significantly over-estimated the shear strength of masonry shear walls. For partially grouted walls, the over predictions increased with decreasing the specimens aspect ratios. The mortar type had no significant effect on the strength of fully grouted walls while it was not possible to determine such effect for partially grouted due to contradiction in the test results.

Nolph (2010) conduct an experimental study involved testing five partially grouted and one fully grouted masonry shear walls subjected to in-plane lateral cyclic loading. Both the grout horizontal spacing and horizontal reinforcement ratio were investigated. It was found that the current MSJC (2008) shear design equations over-estimated the strengths of partially grouted masonry shear walls with 48 in. (1219 mm) grout horizontal spacing. He also proposed couple of equations to improve the shear strength predictions of the MSJC (2008).

1.5 Conclusion

Previous studies have provided limited information to understand the behavior of partially grouted masonry shear walls subjected to in-plane lateral loads associated with low axial loads. There is also a lack of experimental data on the effects of spacing between vertical grouted cells on the strength and failure mechanism of partially grouted shear walls. In addition, no research has been conducted to either confirm or weaken that partially-grouted masonry shear walls perform similarly to masonry infilled reinforced

concrete frames or not. This behavior differs from the behavior that the provisions in the 2008 MSJC Code are based on.

In general, this study of previous research on partially grouted masonry shear walls under lateral loads has shown that a better evaluation for such issues requires carrying out more research and discovering more experimental evidence in order to evaluate and identify the current situation.

CHAPTER 2

DESCRIPTION OF EXPERIMENTAL PROGRAM

The experimental program in this research was designed to investigate the in-plane shear strength of squat partially grouted reinforced masonry shear walls. Six full-scale reinforced masonry shear walls having different amounts of shear reinforcement and grout horizontal spacing were constructed and tested under in-plane cyclic loading. This chapter discusses the construction details, material properties, and test setup used in this research.

2.1 Description of Test Specimens

The test specimens had identical nominal dimensions of 64 in. (1626 mm) high, 104 in. (2642 mm) wide, and 8 in. (194 mm) thick. Every specimen was assigned a name in the form of PG (partially grouted) followed by XXX-SP where XXX is the horizontal reinforcement ratio (ρ_h) multiplied by 10^5, followed by the horizontal grout spacing in inches. For example, specimen PG127-48 was a partially grouted specimen reinforced using a horizontal reinforcement ratio of 0.00127 and a horizontal grout spacing of 48 in.

The test specimens were built in a running bond with 8 in. (203 mm) hollow concrete masonry units using face shell mortar bedding. Standard 16 in. x 8 in. x 8 in. for full units and 8 in. x 8 in. x 8 in. for half-unit concrete masonry units (CMUs) were used for the construction of the test specimens. Knockout units were used in the 4^{th} and 8^{th} to 10^{th} masonry courses. Each wall consisted of 10 masonry courses high and 6½ masonry units long.

The specimens were reinforced horizontally and grouted at courses No. 4, 8, 9, and 10. Each one of these courses included 1#5 (D 16), except for specimens PG180-48 and PG254-48, where 1#6 (D 19) and 2#5 (D 16) were used, respectively. The horizontal reinforcements were hooked according to MSJC (2008) using a 180^{o} hook around the vertical bars in both outermost cells, as shown in Figure 2.1.

The walls were reinforced vertically using identical reinforcement ratio of 0.33% at horizontal spacing of 24 in. (610 mm), 32 in. (813 mm), and 48 in. (1219 mm). As shown in Tables 2.1 and 2.2 and Figure 2.2, all specimens except specimens PG127-32 and PG127-24 were reinforced using 2#6 at 48 in. (1219mm). Specimens PG127-32 and PG127-24 were reinforced using 2#6 in each outermost cell. Two inner cells was reinforced using 1# 6 in the case of specimen PG127-32. Three inner cells were reinforced using 1#5 in the case of specimen PG127-24. Each cell containing vertical reinforcement was grouted. The vertical flexural reinforcement rebar was extended from the foundation completely through the total height of the wall; i.e. there was no lap splice in any specimen.

Figure 2.1 The 180^{o} hook as used in the specimens

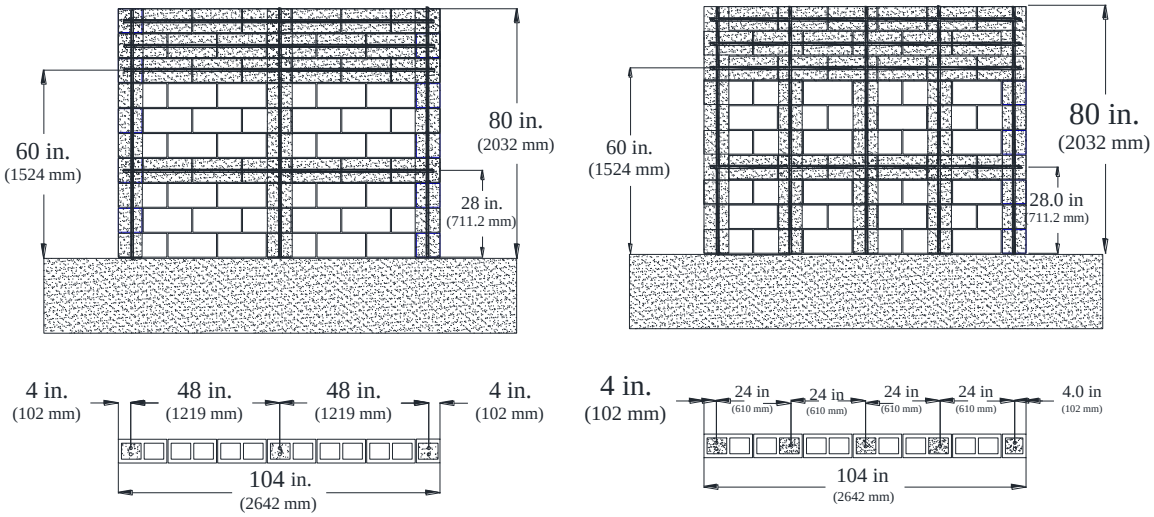

PG127-48, PG127-48I, PG180-48, and PG254-48

PG 127-32

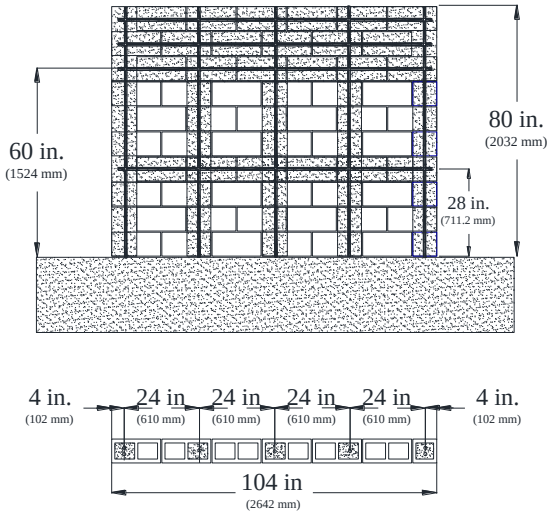

PG 127-24

Figure 2.2 Dimensions and reinforcement distribution for the tested walls

Table 2.1 Distribution of the vertical and horizontal reinforcement

Cell No.	PG 127-48	PG 127-48	PG 180-48	PG 127-32	PG 127-24	PG 127-48I
1	2 No. 6	2 No. 6	2 No. 6	2 No. 6	2 No. 6	2 No. 6
4					1 No. 5	
5				1 No. 6		
7	2 No. 6	2 No. 6	2 No. 6		1 No. 5	2 No. 6
9				1 No. 6		
10					1 No. 5	
13	2 No. 6	2 No. 6	2 No. 6	2 No. 6	2 No. 6	2 No. 6
ρ_v %	0.332	0.332	0.332	0.332	0.332	0.332
Spacing In. (mm)	48 (1219)	48 (1219)	48 (1219)	48 (1219)	24 (610)	48 (1219)
ρ_h %	0.127	0.127	0.180	0.254	0.127	0.127
HR	1 No. 5	1 No. 6	2 No. 5	1 No. 5	1 No. 5	1 No. 5

No. 5 = D 16 in metric size (A_b=0.31 in^2, 200 mm^2)
No. 6 = D19 in metric size (A_b=0.44 in^2, 284 mm^2)
HR= Horizontal reinforcement in every bond beam (at courses No.4, and 8)

2.2 Construction of Shear Wall Specimens

2.2.1 Reinforced concrete foundation

Each wall was constructed on a reinforced concrete foundation (Figure 2.3) having dimensions of 142 in. (3607 mm) long, 25 in. (635 mm) wide, and 19 in. (483 mm) high. Each footing had flexural reinforcement of 4 # 9 (D 29) as top reinforcement and 4 # 9 as well as in the bottom reinforcement. Stirrups consisting of #4 (D 13) @ 15 in (381 mm) were used as shear reinforcement. Each footing was fixed to the laboratory strong floor using eight 1.25 in. (31.75 mm) diameter high strength steel bolts. The bolts passed through PVC tubes which were placed vertically and fixed inside the foundation wood formwork prior to concrete pouring.

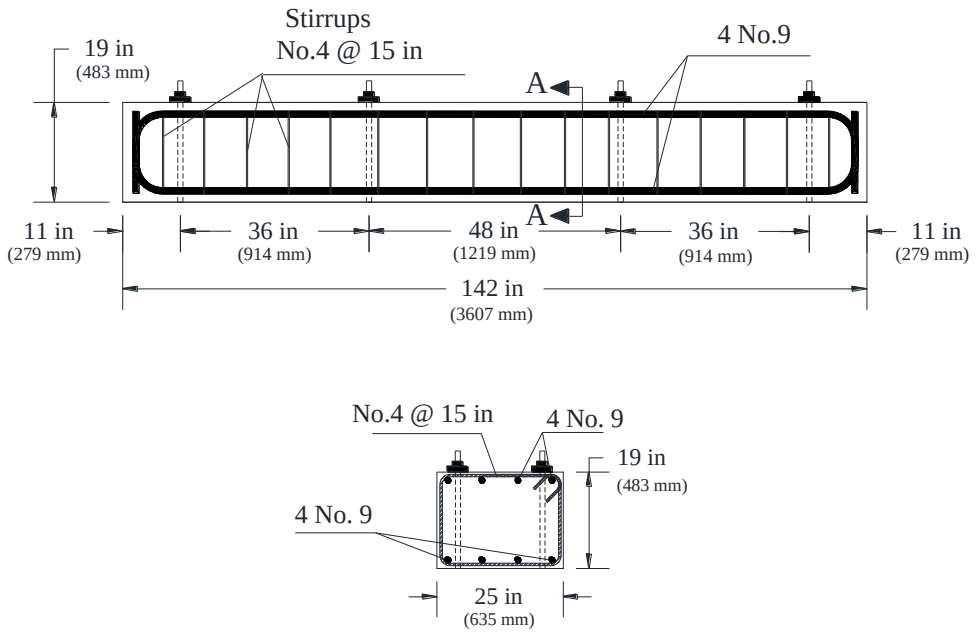

Figure 2.3 Details of reinforced concrete foundation

2.2.2 Wall specimens

The second stage involved construction of the masonry shear walls. Specimens were built in three days in the Composite Materials and Engineering Center at Washington State University by qualified masons in running bond with hollow concrete masonry units using a face shell mortar bedding only. Walls were placed over the reinforced concrete foundations as described in the previous section. Before wall construction, the vertical reinforcement was anchored in the concrete foundation and connected to the lower base reinforcement prior to concrete pouring to prevent any slip, and to provide a fixed connection between the wall and the concrete base. All walls were 8 courses high, and six and half wide. In addition, two more courses were added above course No. 8 in all walls to act as a cap beam where the lateral and vertical loads were applied. Plastic mesh was

placed below the course to be grouted along every horizontal bond beam to prevent the grout from flowing to the lower courses during pouring, as shown in Figure 2.4.

Figure 2.4 Specimens during construction

2.3 Construction Material Properties

2.3.1 Masonry prisms

Five grouted and five un-grouted two-block high single-block long prisms had an average height of 15.17 in. (385mm) and thickness of 7.625 in. (197 mm) were constructed and tested according to ASTM C1314-07 (2225) by the same masons crew using the same materials as was used for the construction of the walls. These prisms were tested to determine the masonry compressive stress $f`_m$. In these prisms, the face shells, the external and the internal webs were mortared. According to ASTM C1314-07, specimens have an average height to thickness of 1.99 have a correction factor of 0.997. The measured $f`_m$ for each tested specimens was multiplied by 0.997 and presented in table 2.2.

Table 2.2 Prism test results

Type	Sample No.	Load (Ib)	Area (in^2)	($f`_m$) (psi)	Corrected ($f`_m$) (psi)	Avg. of corrected $f`_m$ psi (MPa)
UNGROUTED	1	193,300	67.04	2883.3	2874.6	2530 (17.44)
	2	151,940	67.04	2266.4	2259.6	
	3	147,911	67.04	2206.3	2199.7	
	4	179872	67.04	2683.1	2675	
	5	178392	67.04	2661	2653	
GROUTED	1*	425752	119.15	3573.2	3562.5	3540 (24.40)
	2*	424255	119.15	3560.7	3550	
	3*	424342	119.15	3561.4	3551	
	4*	424198	119.15	3560.2	3549	
	5	414872	119.15	3482	3471.5	

Correction factor =0.997

* sample reached the machine's maximum load without rupture.

2.3.2 Mortar

Standard type S mortar containing ordinary Portland cement, lime, and dry sand was mixed at the construction site in the laboratory and used to construct the walls. Basically, the water was added to the previous combinations to satisfy the workability requirements. To ensure the mortar quality, five 2 in (51 mm) diameter by 4 in. (102 mm) high mortar cylinders were cast according to ASTM C780 (2090) during the construction. All the samples were air cured for 28 days, similar to the tested walls, and were subjected to uniaxial compressive load according to ASTM C780-09 (2220). The average compressive strength of the hardened mortar was 2160 psi (14.89 MPa). Table 2.3 shows the results of the test data for the mortar cylindrical samples.

Table 2.3 Compressive strength for the mortar cylinders

Sample No.	1	2	3	4	5	Average	COV%
Load (Ib)	6872.3	6119.8	7627.6	6375	6912.3		
Area (in^2)	3.14	3.14	3.14	3.14	3.14		
Strength psi (MPa)	2188.6	1948	2428	2029.2	2200.3	2160 (14.89)	8.6%

2.3.3 Grout

A high slump fine grout was mixed and poured to fill the cells and courses including either vertical or horizontal reinforcement. All six walls were constructed up to the first bond beam at the 4^{th} masonry course; then, the bond beam and the cells including the vertical reinforcement were grouted. The wall construction was completed on the second day. Then, on the third day, the remaining cells and courses, including reinforcement were grouted. Four grout prisms 4 x 4 x 8 in. (102 x 102 x 203 mm) were prepared and tested according to ASTM C1019-07 to determine the grout compressive

stress (Table 2.4). The test results indicated that the grout had an average compressive stress of 5200psi (35.85MPa). Table 2.4 shows the results of the compressive test on the grout prisms.

Table 2.4 Grout samples compressive strength results

Sample	1	2	3	4	Average	COV%
Load (Ib)	91357	72401	91080	88503		
Area (in^2)	16.71	16.32	16.53	16.44		
Strength Psi (MPa)	5467.2	4436.3	5510	5383.4	5200 (35.85)	9.8%

2.3.4 Reinforcement

The steel bars used in the walls construction were Grade 60 for both vertical and horizontal reinforcement. Uniaxial tensile tests on #5 and #6 (Table 2.5) indicated that the rebars had a yield stress of 65.6 ksi (452 Mpa) and 61.9 ksi (427 Mpa) respectively.

Table 2.5 Steel Reinforcement tensile strength results

Bar No.	Sample No.	Applied load Ib	Bar area in^2	(f_y) (psi)	Ave. of (f_y) Psi (MPa)	COV%
No. 5	1	20340	0.31	65613	65645 (452)	0.1%
	2	20360	0.31	65677		
No. 6	1	27300	0.44	62045	61932 (427)	0.3%
	2	27200	0.44	61810		

2.4 Test Procedures

2.4.1 Test Setup

The walls were fixed to the laboratory strong floor and the lateral load was applied at the 8^{th} masonry course as shown in Figure 2.5 and 2.6. The in-plane cyclic load was applied using a 225 kip (1000 kN) capacity hydraulic actuator. The actuator was fixed

from the southern end to the steel strong frame. The actuator was connected from the north end to two stiff C sections which were bolted at the 8th masonry course to both sides of each wall. The C sections were bolted using ¾ in. (19.1 mm) diameter shear studs passing through the thickness of each masonry wall. The holes for these studs were drilled after the walls had cured for approximately one week. A high strength anchorage epoxy meeting ASTM C881-02 (Type IV; Grade 3; Class A, B, C) was used to fill any tolerance between the bolts and holes.

The axial load was applied using two jacks operated by a manual hydraulic pump. The actuators were connected at their bottoms to the stiff hollow square steel section that was mounted on top of the wall, i.e. at the 10 masonry course, to uniformly distribute the applied axial load. The tops of the hydraulic jacks were connected to the main cross beam of the strong steel frame using a slippery plate to allow lateral movement of the actuator while applying the axial load.

In order to eliminate any sliding in the concrete base during the cyclic loading, the concrete base was braced using two stiff built-up steel angles bolted to the laboratory strong floor, as shown in Figure 2.5.

Figure 2.5 Shear wall test set up

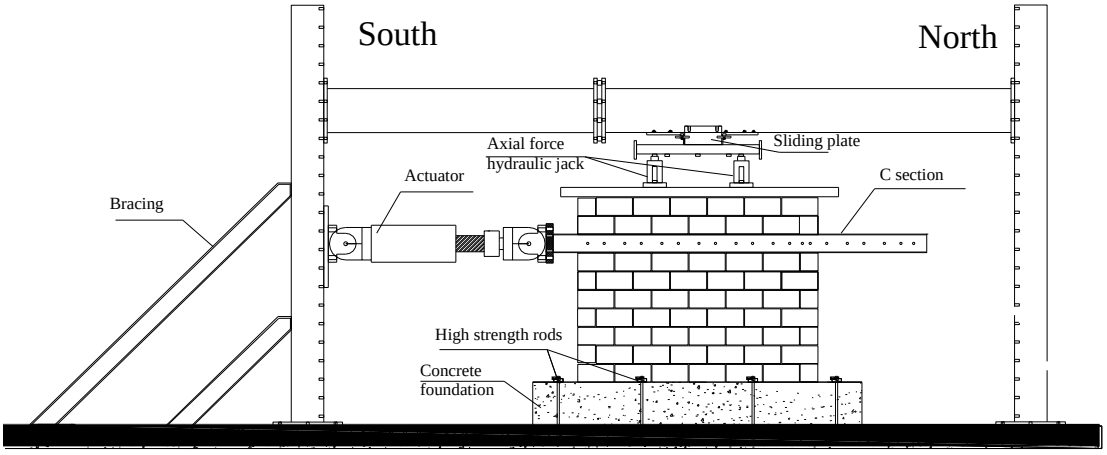

Figure 2.6 The test set up

2.4.2 Test protocol

The specimens were subjected to full reverse cyclic loading under displacement control. Three cycles at displacement levels of ±0.5, ±1, ±1.5, ±2, ±2.5, ±4, ±5, and ±6 multiplied by the theoretical yield displacement were used for testing the specimens (Fig 2.7). Theoretical yield displacement of 0.05 in. (1.27 mm) was calculated using Equation 2.1 and 2.2 (Priestley et al. 2007):

$$\theta_{y\_mw} = 0.6\varepsilon_y \cdot \frac{H_n}{l_w} \qquad \text{Eq. (2.1)}$$

$$\Delta_y = \theta_{y\_mw} \cdot H_e \qquad \text{Eq. (2.2)}$$

Where:

H_n = height of wall; H_n = 60 in. (1524 mm)

l_w = wall length; l_w = 103.6 in. (2631 mm)

H_e = effective height at yield; H_e = 60 in. (1524 mm)

ε_y = yield strain of the flexural steel; ε_y = 0.00207

θ_{y_mw} = yield drift of masonry wall

Δ_y = yield displacement

The loading rate was 0.1875 in/min (4.76 mm/min). The average duration of testing each of the shear walls to reach failure was approximately three hours.

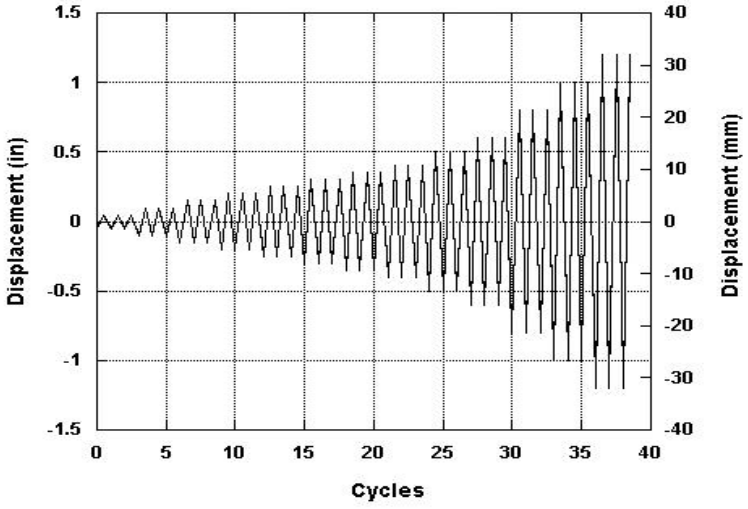

Figure 2.7 Loading protocol

2.4.3 Instrumentation

The lateral loads, displacement, and steel strains were measured at several positions of the wall during testing. A number of electrical strain gauges, each one having a length of 0.250 in. (6.3 mm) and a resistance of 250Ω, were installed on the steel rebar prior to the construction of the walls. A strain gauge was attached to the bottom of each flexural reinforcement rebar just above the foundation level. Another strain gauge was attached to each end of the shear reinforcement at the top and middle bond-beams, i.e. a total of 4

strain gauges were used. In addition, two strain gauges were attached to the rebar in the middle bond beam at the sides of the middle grouted vertical cells as shown in Figure 2.8.

For each wall, horizontal and vertical displacements were measured using a ten string potentiometers type (Micro-Epsilon WPS-500-MK30-P(01) and UniMeasure LX-PA-10) as shown in Figure 2.9. For each wall, the lateral in-plane displacements at the top bond beam, at the first masonry course, and at the top of the foundation were measured using three string potentiometers connected to independent frame in the north side of the wall. The displacement of the piston of the actuator and the deflection of the steel frame where the actuator was connected were measured using two string potentiometers connected to another independent frame installed at the southern side of the wall. Eight string potentiometers were used to measure the diagonal displacements across the masonry panels in each wall. Seven string potentiometers were used to measure the vertical displacement across the first masonry course at a height of 4 in (102 mm) from the bottom of the wall.

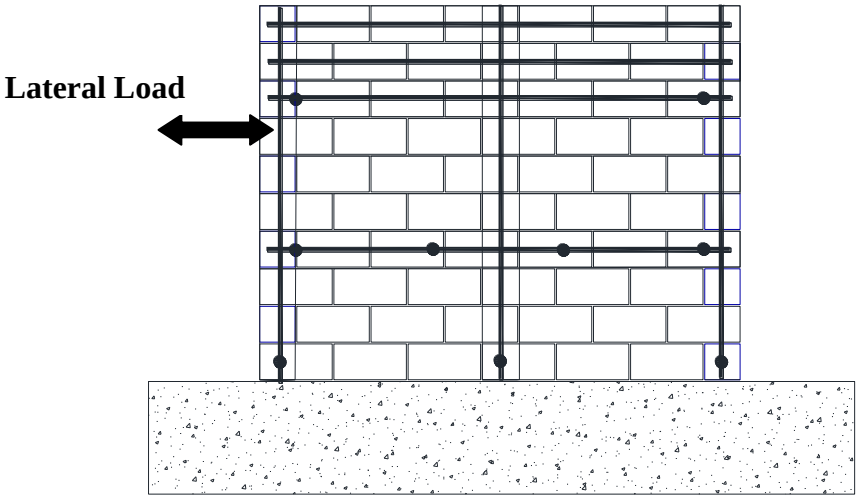

Figure 2.8 Strain gauge locations on vertical and horizontal bars

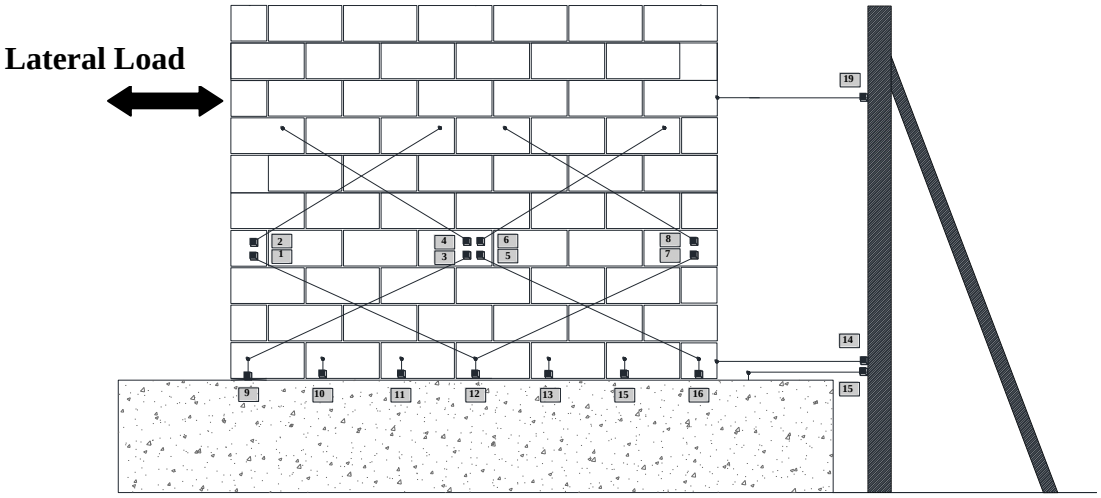

Figure 2.9 Displacement string potentiometers as distributed in the test

CHAPTER 3

EXPERIMENTAL RESULTS

3.1 Introduction

The response of partially grouted masonry shear walls under in-plane lateral loading was investigated in this research by testing six masonry shear walls designed to fail in shear mode. In these walls, the aspect ratio and the vertical reinforcement remained approximately constant. On the other hand, the horizontal reinforcement ratio and the grout horizontal spacing were variables. The walls were tested in displacement controlled cyclic loading. This chapter presents the experimental results of the tested specimens, including the failure mode, cracking pattern, and hysteretic behavior.

3.2 Specimen PG127-48

This specimen had grouted vertical cells and flexural reinforcement at horizontal spacing of 48 in (1219.2 mm). The flexural reinforcement consisted of 2 No. 6 (D 19) in every grouted cell i.e. ρ_v= 0.33%. The wall was reinforced horizontally using 1 No. 5 (D 16) in courses No. 4, and 8 (ρ_h= 0.127%). Courses No. 9 and 10 were also reinforced using 1 No. 5, each, to act as a rigid beam where the axial and the lateral loads were applied. The first crack was a hairline crack which occurred through the bed and head joints on the 3rd brick course at the southern side during pushing toward a drift angle of 0.06% and a lateral load of 36.8 kips (164 kN). More stair-step cracks occurred while the applied lateral load was increased. At a drift angle of 0.22% and a lateral load of 56.84 kips (253 kN), the specimen reached its maximum strength. At this drift angle 45^o cracks

occurred through the masonry units at the 2nd and 3rd masonry courses of the vertical grouted cells at the wall mid-length. More 45° cracks passing through the masonry units at the specimen's toes appeared with increasing the applied lateral displacement. At a lateral drift angle of 0.51% and lateral load of 45.72 kips (203kN), vertical splitting cracks occurred at the middle bond beam on the outer grouted cells in both load directions (Figure 3.1). The widths of the crack passing through the CMU units significantly increased by an applied lateral drift angle of 0.7% (Figure 3.1). During that drift angle, some mortar, and CMU parts at the compression zone started to fall down. On the south end of the wall and at a lateral drift angle of 1.1% and lateral load of 35.5 kips (158kN), the vertical splitting crack width increased and led to spalling of the masonry end shells of the end blocks at the third and fourth masonry courses as shown in Figure 3.3. The test was stopped when the lateral strength of the specimen dropped by 45% of the measured specimen's peak strength. No damage was observed on the top courses above the loading level (course No 9, and 10).

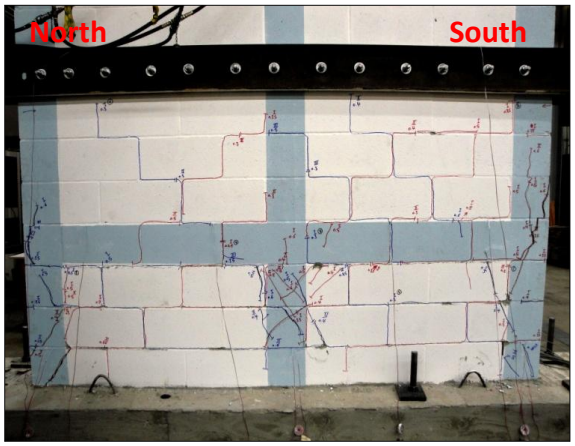

Figure 3.1 Wall at drift angle of 0.51% during the test

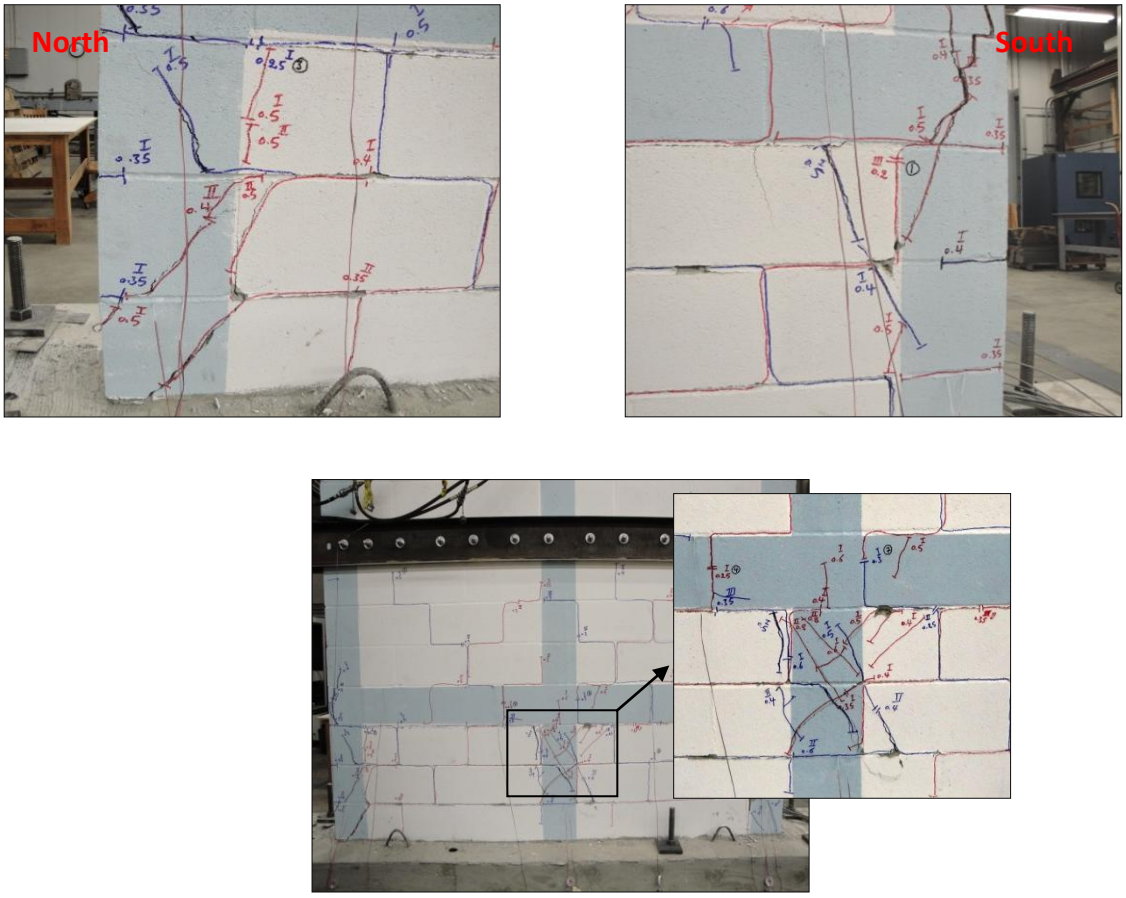

Figure 3.2 Opening of the cracks at drift angle of 0.7%

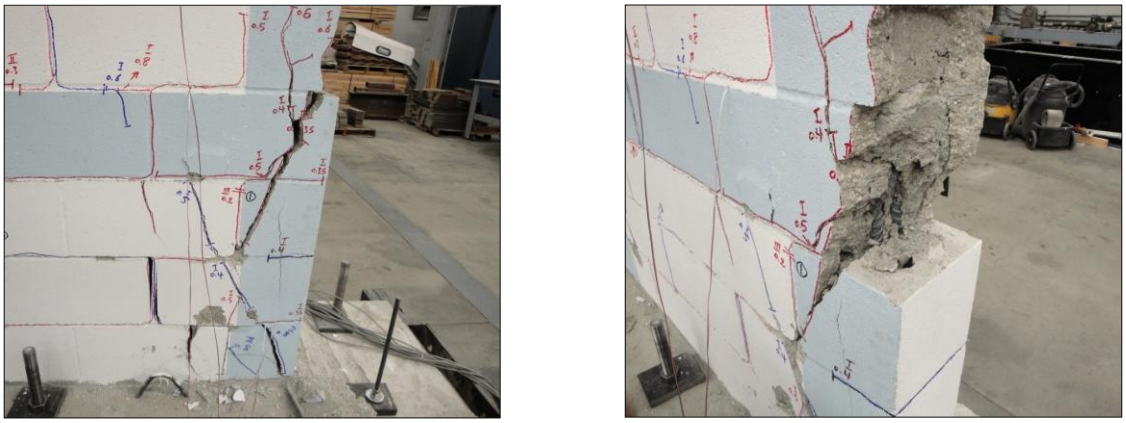

Figure 3.3 Failure in the grouted cells at drift of 1.1%

3.3 Specimen PG127-48I

This wall is identical to wall PG127-48 and was tested to investigate the repeatability of the test results. The observed crack patterns of PG127-48I were similar to those in wall PG127-48. The first crack was a stair-step crack and it was observed while pulling the specimen to a drift angle of 0.12% and lateral load of 39.9 kips (178 kN). The crack started from the middle of the middle bond beam until it reached the specimen concrete base through the bed and head joints in the northern bottom of the masonry panel. A similar crack appeared in the opposite direction when the load was reversed while the same loading cycle. The second stair-step crack appeared during testing the specimen to a lateral drift angle of 0.18% and a lateral load of 44.6 kips (198 kN). The crack extended from the top bond beam (i.e. the 8^{th} masonry course) to the middle bond beam through the top northern masonry panels. At a lateral load of 51.9 kips (231 kN) and drift angle of 0.3%, several diagonal cracks passing through the masonry units near the specimen's toes at the first and second brick courses occurred. As the applied lateral displacement increased, new diagonal cracks passing through the masonry blocks appeared in the bottom three masonry courses while the old cracks extended in length and width. The specimen reached its lateral strength of 57.1 kips (254 kN) while pushing the wall toward a drift angle of 0.38%. At a drift angle of 0.6% and lateral load of 48.7 kips (217 kN), minor masonry face shell spalling occurred in several places. At the first cycle at a drift angle of 0.88% and load of 38.17 kips (170 kN), vertical cracks were observed at the outermost blocks in the third through the fifth masonry courses. Such vertical cracks led to

a strength reduction of 40% of the measured specimen's peak strength when the specimen was subjected to the second and third cycle at a drift angle of 0.88%.

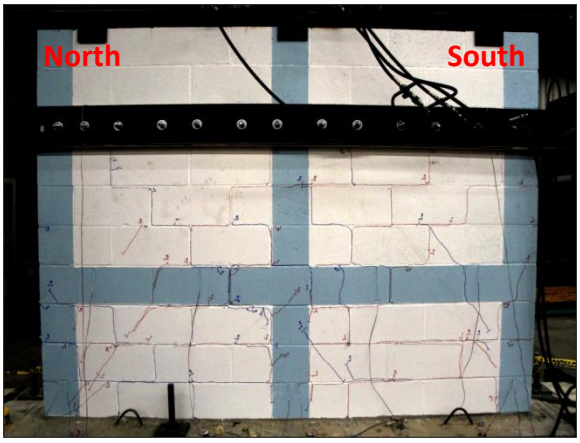

(a)

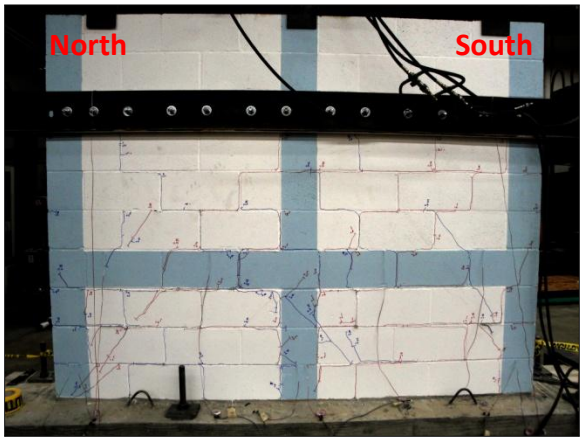

(b)

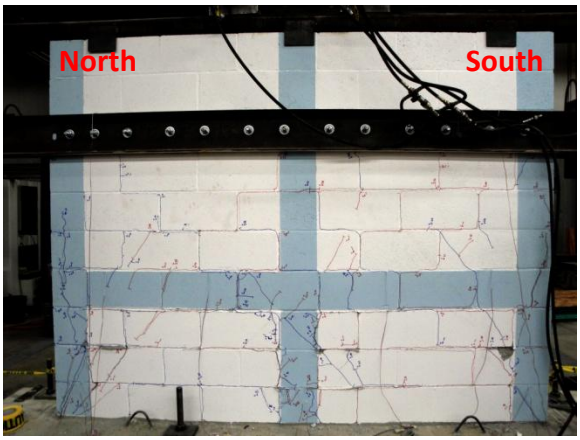

(c)

Figure 3. 4 Wall behavior at drift angles of : (a) 0.3%, (b) 0.4%,(c) 0.88%

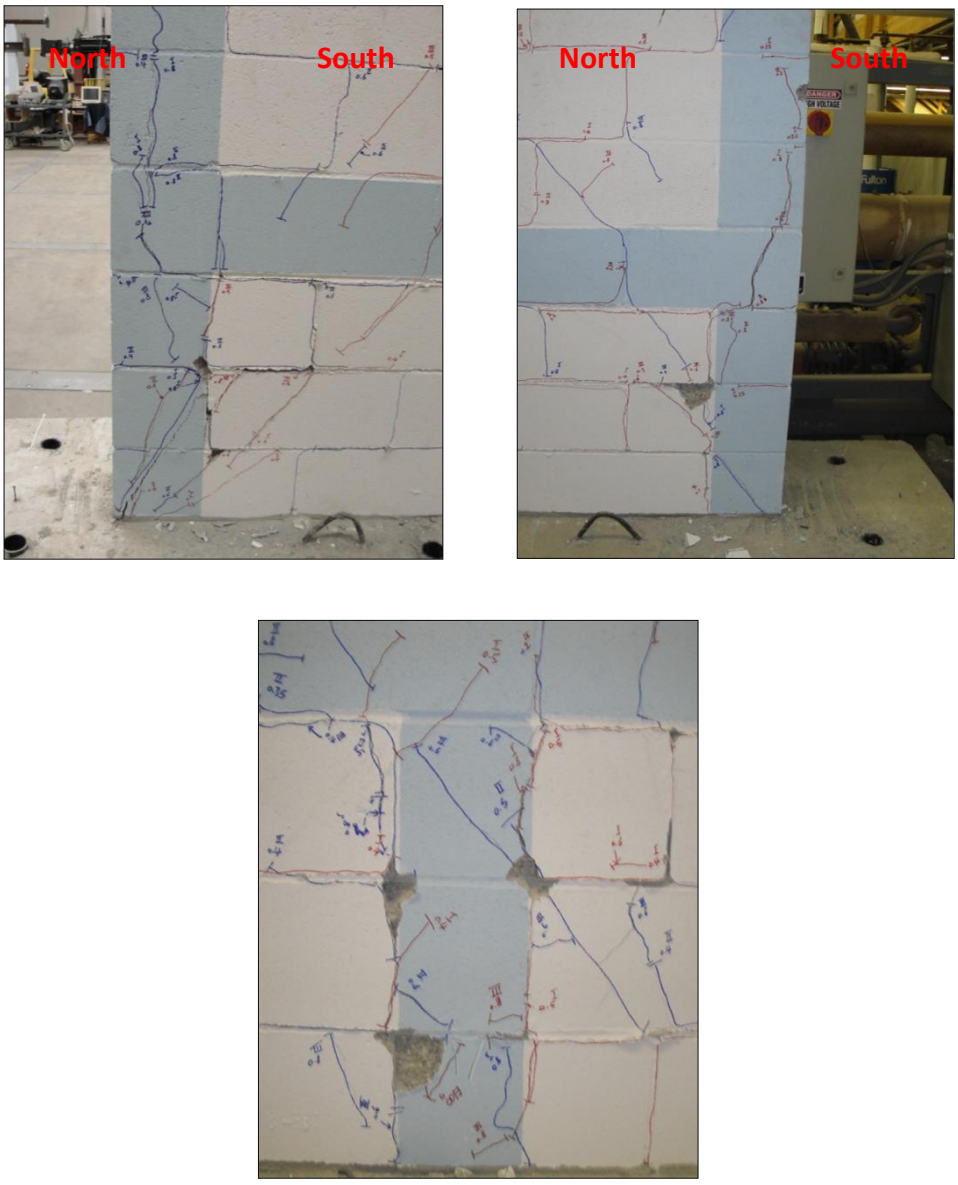

Figure 3. 5 Vertical cracks prior to the end of the test , mortar spalling, and limited face shell spalling at drift angle of 0.88%

Specimen PG180-48

This specimen had grouted vertical cells and flexural reinforcement at a horizontal spacing of 48 in (1219.2 mm). The flexural reinforcement consisted of 2 No. 6 (D 19) in

every grouted cell i.e. ρ_v= 0.33%. The wall was reinforced horizontally using 1 No. 6 (D 19) in courses No. 4, and 8 (ρ_h= 0.180%). Courses No. 9 and 10 were also reinforced using 1 No. 6, each, to act as rigid beam where the axial and the lateral loads were applied. Figure 3.6 and 3.7 show the damage in the wall at different drift angles.

The first observed crack was a stair-step crack and it appeared in the northern bottom masonry panel through the bottommost three brick courses at a drift angle of 0.09% and lateral load of 42.3 kips (188 kN). Another stair-step crack appeared in the same masonry panel when the lateral load was reversed. Several stair-step cracks occurred in all masonry panels by a drift angle of 0.25%. At a drift angle of 0.36% and lateral load of 59.1 kips (266 kN), diagonal cracks appeared in the CMUs at the toes of the wall. Each crack was approximately 2-block high long. Smaller diagonal cracks occurred also in the CMUs in the bond beam on the northern side. At a drift angle of 0.42% and a lateral load of 65.03 kips (289 kN), the specimen reached its ultimate strength. At a drift angle of 0.58% and a lateral load of 62.8 kips (279 kN), a significant diagonal crack approximately 2-block high long and having an angle of approximately 67^o with the vertical and passing through the bond beam and outermost grouted cells in the northern direction appeared through the fourth and fifth masonry courses. At a drift angle of 0.61%, vertical cracks appeared in the outermost grouted cells. Each crack was about 3-block high long. Cycling continued and at a drift angle of 0.72%, several stair-step cracks appeared and the width of a few of the existing cracks in the grouted cells reached about 3/8 in (9.5 mm).

Face shell spalling of the masonry blocks surrounding the toes of the wall occurred at a drift angle of 0.88% and a lateral load of 56.7 kips (252kN). By a drift angle of 0.91%, the lateral resistance of the specimen dropped by 40% and the test was stopped.

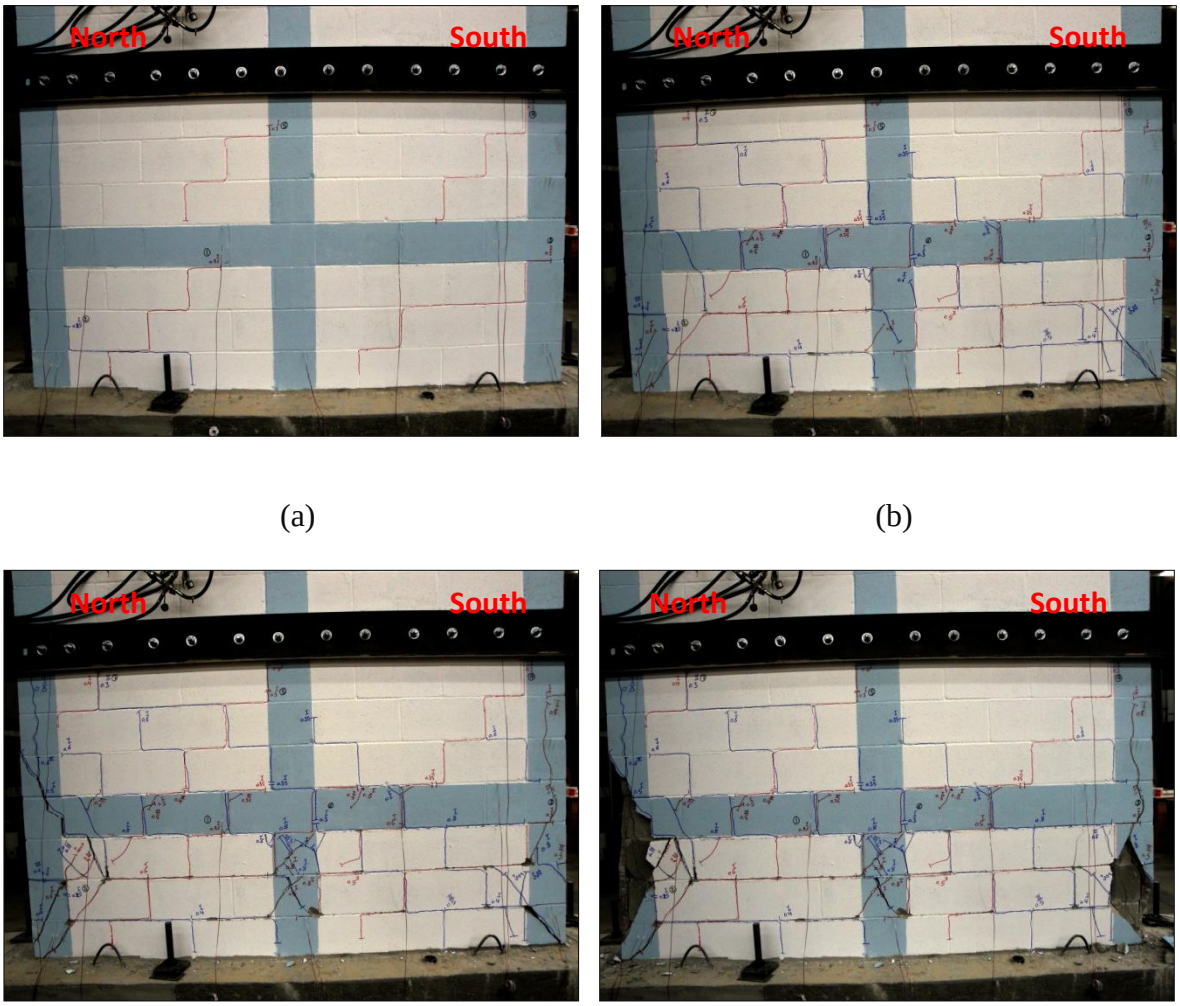

(a) (b)

(c) (d)

Figure 3.6 Specimen PG180-48 at drift angles of (a) 0.09%, (b) 0.36%, (c) 0.61%, and (d) 0.88%

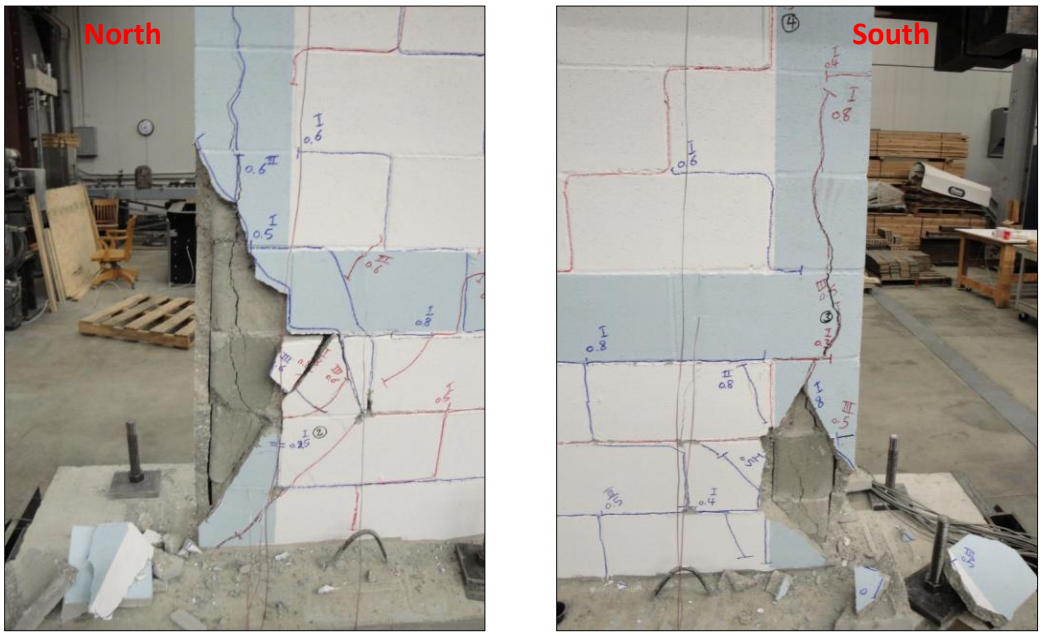

(a) (b)

Figure 3.7 Face shell crushing at both ends for (a) northern end, (b) southern end

3-5 Specimen PG254-48

This specimen had grouted vertical cells and flexural reinforcement at horizontal spacing of 48 in (1219.2 mm). The flexural reinforcement consisted of 2 No. 6 (D 19) in every grouted cell i.e. ρ_v= 0.33%. The wall was reinforced horizontally using 2 No. 5 (D 16) in courses No. 4 and 8 (ρ_h= 0.253%). Courses No. 9 and 10 were also reinforced using 2 No. 5, each, to act as a rigid beam where the axial and the lateral loads were applied. Figure 3.8 and 3.9 show the damage in the specimen at different drift angles.

The first observed crack was a stair-step crack which occurred in the top southern masonry panel through the 5th to 7th masonry courses during pulling to a drift angle of 0.06% corresponding to a lateral force of 41.75 kips (186 kN). A similar crack occurred at the top northern masonry panel when the load was reversed. In addition, while pushing to

the same drift angle, another stair-step crack occurred in the bottom southern masonry panel through the 1st to 3rd masonry courses. By a drift angle of 0.21% and lateral load of 54.3 kips (242 kN), several stair-step cracks appeared in all of the masonry panels. Diagonal cracks passing through the concrete masonry units in the bottom northern masonry panel appeared by a drift angle of 0.30% and a lateral load of 61 kips (271 kN). The number of these cracks increased significantly by a drift angle of 0.35%. In addition, minor face shell spalling occurred in the proximity of the wall's toes. The wall reached its ultimate strength of 65.5 kips (291 kN) at a drift angle of 0.42%. By a drift angle of 0.7%, vertical cracks were observed in the outermost vertical grouted cells through the 3rd to 7th masonry courses. Beyond that and at a drift angle of 0.8%, the lateral resistance of the wall dropped by 47% and the test was stopped.

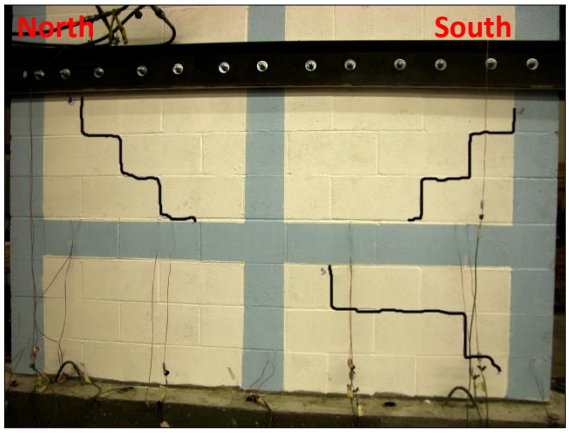

(a)

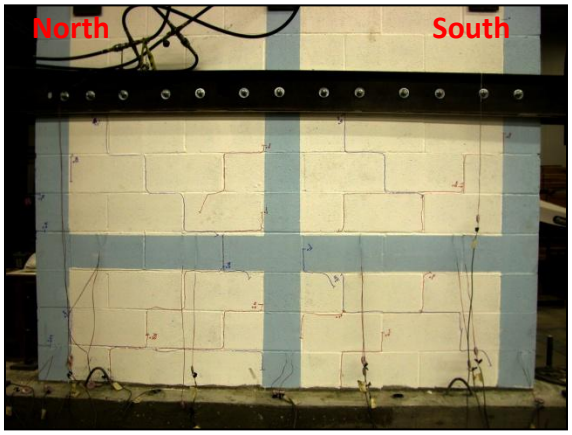

(b)

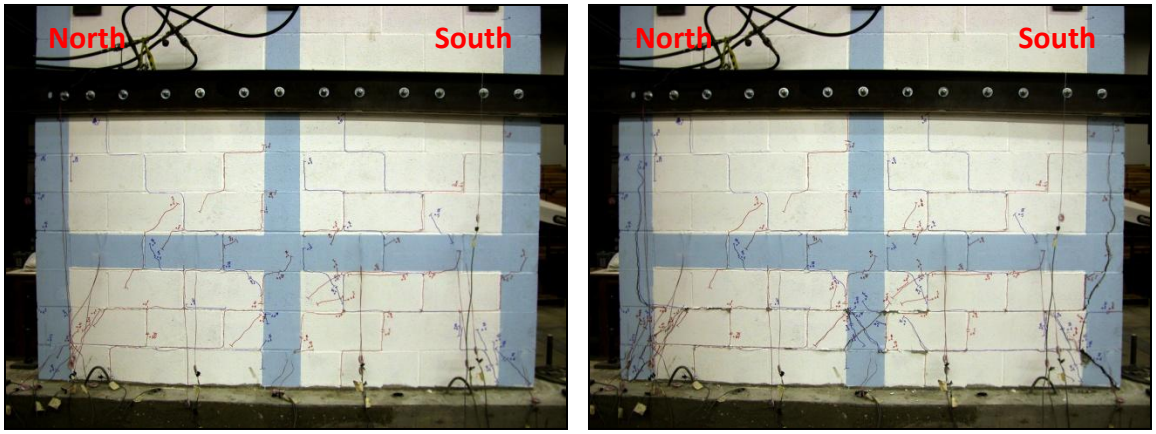

(c) (d)

Figure 3.8 Specimen PG254-48 at drift angles of: (a) 0.06%, (b) 0.21%, (c) 0.35%, and (d) 0.70%

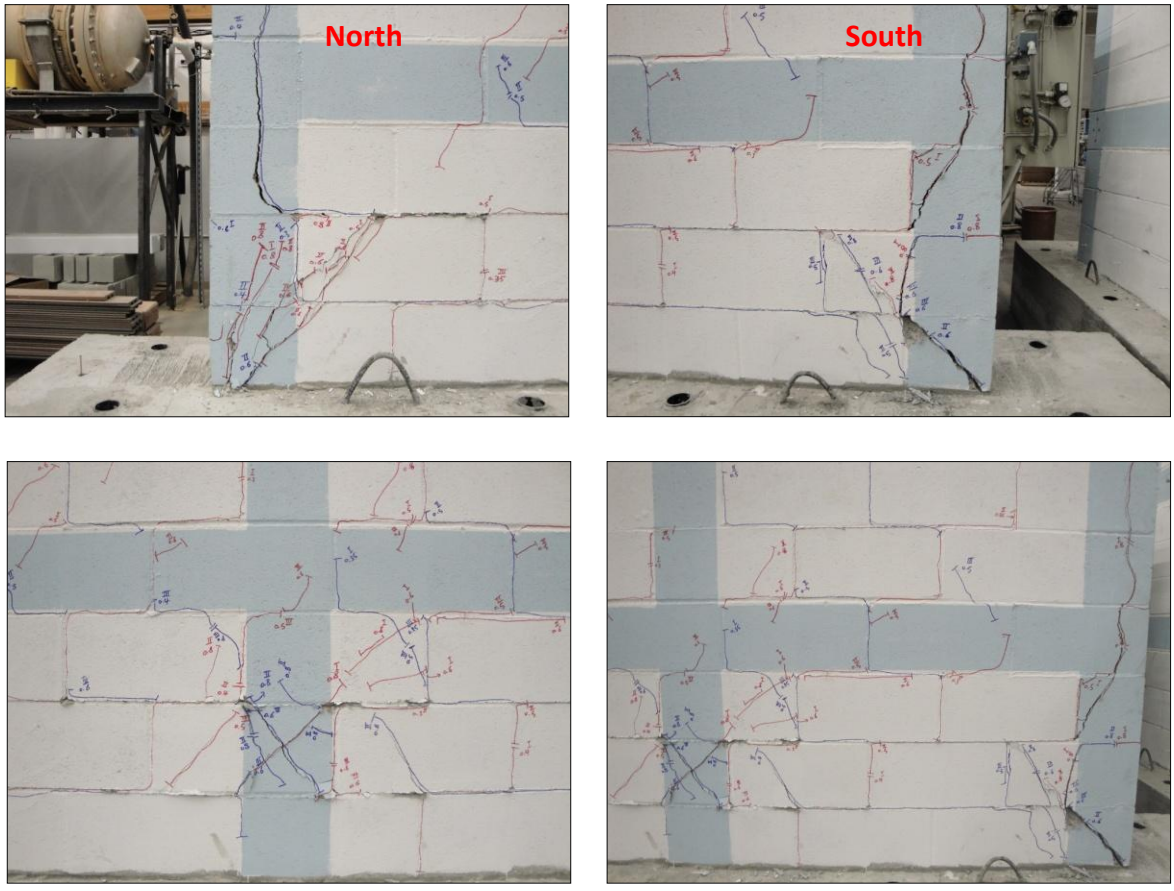

Figure 3.9 Vertical and diagonal cracks at drift angle of 0.70%

5.6 Specimen PG127-32

This specimen had grout and flexural reinforcement @ horizontal spacing of 32 in (1219.2 mm). The flexural reinforcement consisted of 2 No. 6 (D 19) in each grouted outermost cell while the rest of the vertical grouted cells were reinforced using 1 No 6 (D19) i.e. ρ_v= 0.33%. The wall was reinforced horizontally using 1 No. 5 (D 16) in courses No. 4, and 8 (ρ_h= 0. 127%). Courses No. 9 and 10 were also reinforced using 1 No. 5 each. Figure 3.10 and 3.11 show the damage of the test specimen at different drift angles.

The first observed crack was a stair-step crack passing through the 5th to 7th masonry courses in the top middle masonry panel which occurred while pulling the specimens to a drift angle of 0.08% and lateral load of 49.16 kips (219 kN). When the lateral load direction was reversed, another stair-step crack extending from the 1st masonry course through the 7th masonry course in the northern direction occurred. By a drift angle of 0.20% corresponding to a lateral force of 64.5 kips (287 kN), several stair-step cracks were propagated in the masonry panels. While pulling the specimen to a drift angle of 0.25% and load of 70.86 kips (315 kN), diagonal cracks started to form in the masonry units in the northern lower external masonry panel. Cycling continued and more diagonal cracks appeared in the CMUs in the bottom masonry panels. At a drift angle of 0.47% and lateral load 80.21 kips (357 kN), the specimen reached its peak resistance. Beyond that the strength of the specimen started to degrade. At a drift angle of 0.85% and lateral load of 77.5 kips (347kN), existing stair-steps and diagonal cracks significantly opened and new vertical cracks two-blocks long appeared in the southern outermost cells in the 4th and 5th

masonry course. In addition, similar but shorter vertical cracks appeared in the northern side in the 4th masonry course. Finally, at a drift angle of 1.29%, the resistance of the specimen dropped by 28% of its peak resistance and the test was stopped.

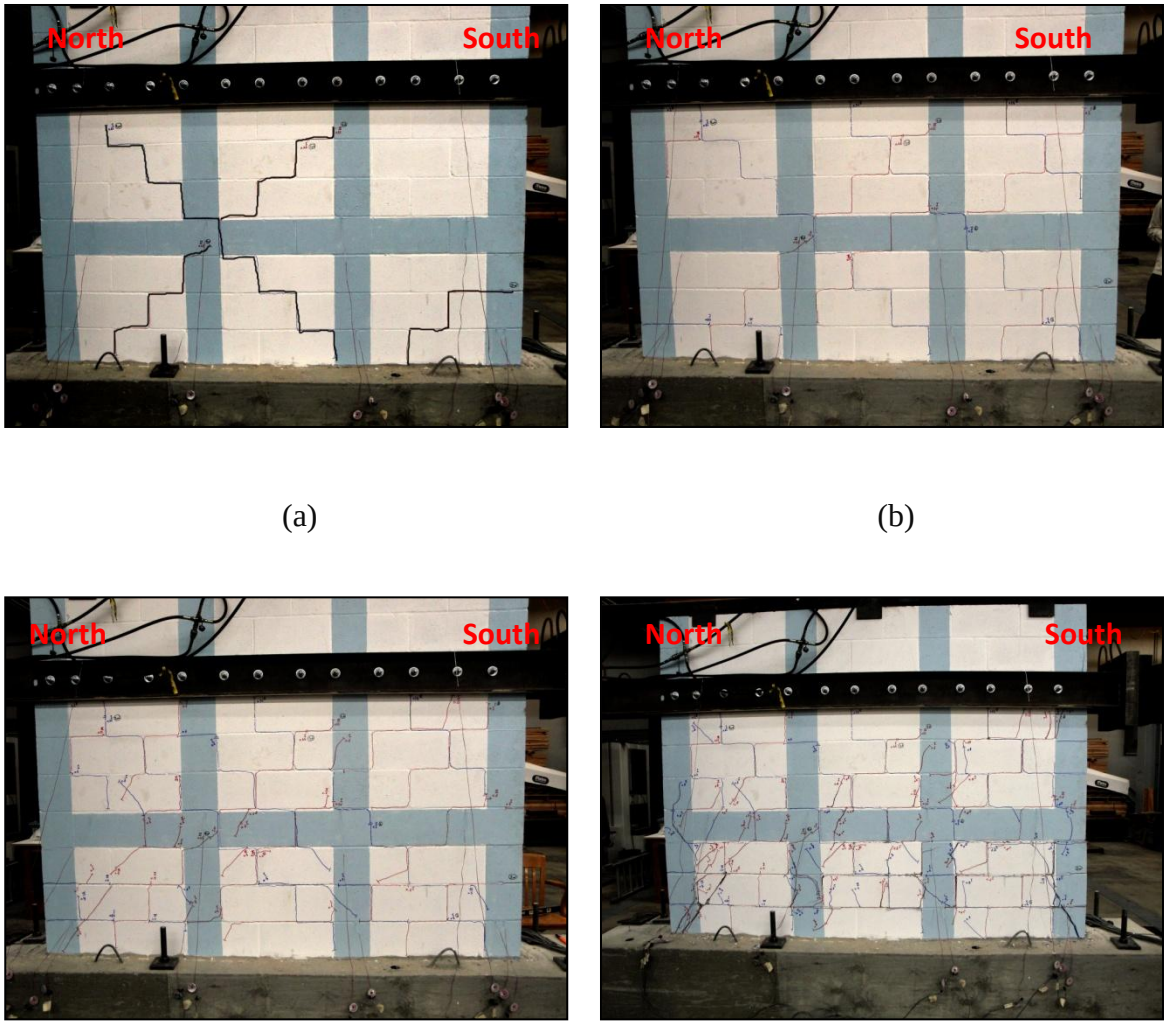

(a) (b)

(c) (d)

Figure 3.10 Specimens PG127-32 at drift angles of: (a) 0.084%, (b) 0.2%, (c) 0.25%, and (d) 0.85%

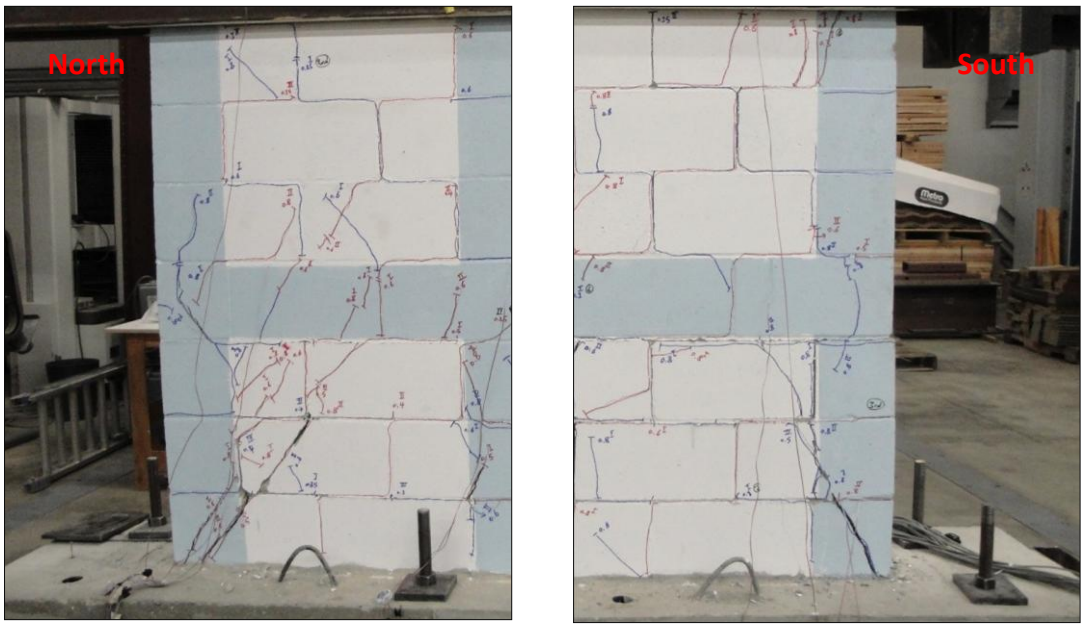

(a) (b)

Figure 3.11 Sliding in wall toes at: (a) northern masonry panel, (b) southern masonry panel

3.7 Specimen PG127-24

This specimen had grouted vertical cells and flexural reinforcement at horizontal spacing of 24 in (609.6 mm). The outer grouted cells were reinforced by 2 bars No. 6 (D 19) while the rest of the grouted cells were reinforced using one bar No. 5 (D16), each, i.e. ρv= 0.33%. The wall was reinforced horizontally using 1 No. 5 (D 16) in courses No. 4, and 8 (ρh= 0.127%). Courses No. 9 and 10 were also reinforced using 1 No. 5 each. Figures 3.12 to 3.14 show the damage in the tested specimen at different drift angles

Specimen PG135-24 behaved similar to the rest of the other specimens and had a dominant shear response, as indicated by the diagonal stair-step cracks. The wall exhibited symmetric responses for the loading in both push and pull directions. The first crack was a diagonal stair-step crack which was observed at the top internal northern and top southern

external masonry panels, while loading the specimen to a drift angle of 0.12% and a lateral load of 57.2 kips (254 kN). More stair-step cracks appeared while continuing to load the specimen. While pulling the specimen to a drift angle of 0.23% and lateral load of 69.5 kips (309 kN), a diagonal crack passing through the CMUs in the bottom four courses of the northern masonry panel occurred. A similar, but shorter, crack appeared in the bottom southern masonry panel at adrift angle of 0.31% and a load of 80.1 kips (356 kN). By a drift angle of 0.71%, diagonal cracks passing through CMUs were everywhere in the specimen and the specimen reached its ultimate strength of 96.8 kips (430 kN). At a drift angle of 1.00% and load of 67.3 kips (299 kN), vertical cracks appeared in the outermost grouted cells in the 4^{th} and 5^{th} masonry courses at the southern direction in the 2^{nd} to the 6^{th} masonry courses at the northern direction. At the second and third cycles of drift angle of 1.00%, vertical cracks appeared in the end-cells in the northern direction extending from the 1^{st} to 4^{th} masonry courses and in the southern direction through the 1^{st} masonry course. By this drift angle level, the toes were significantly damaged and the lateral resistance of the wall dropped by 30% of its ultimate strength.

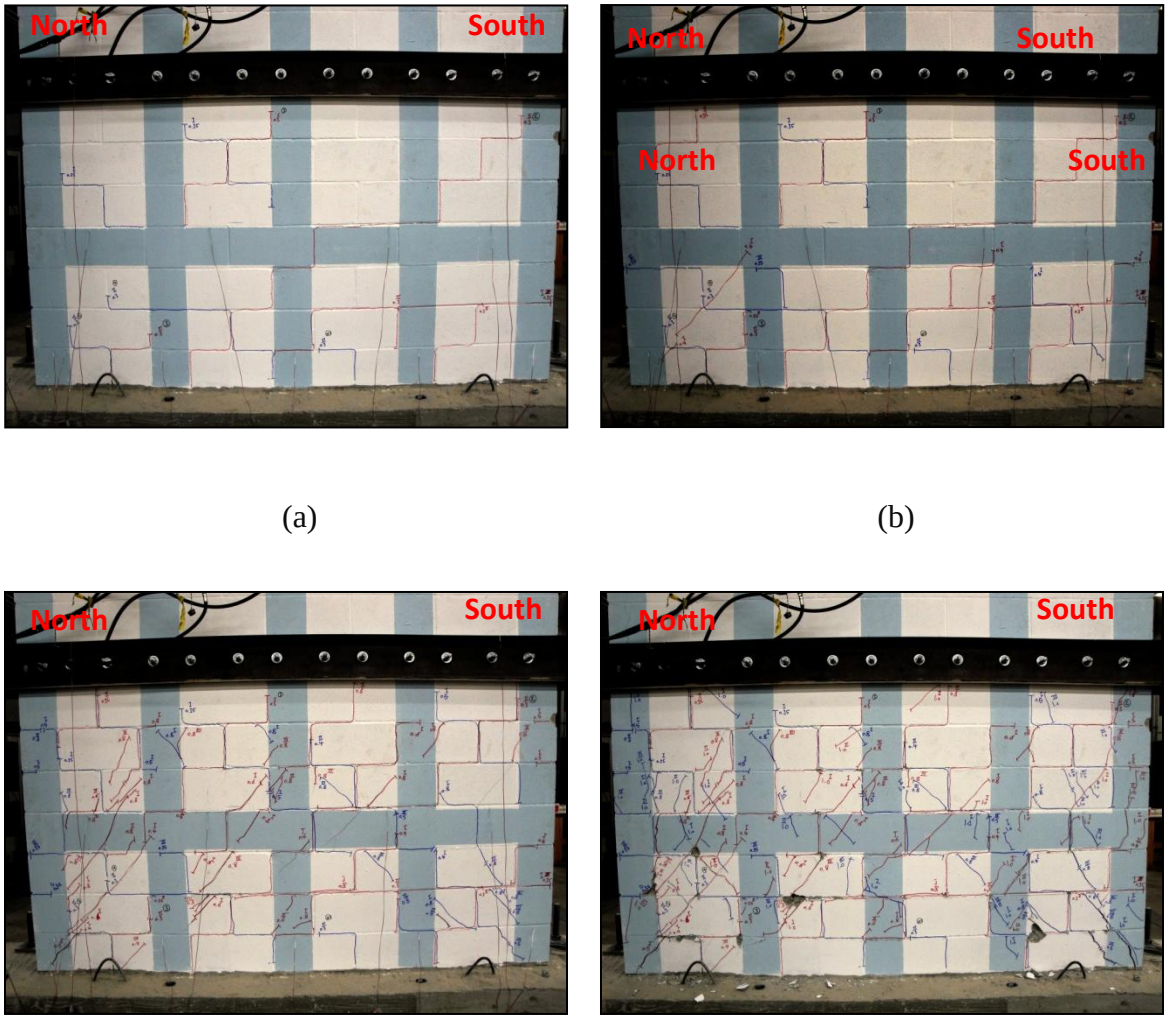

(a) (b)

(c) (d)

Figure 3.12 Specimen PG127-24 at drift angles of: (a) 0.17% , (b) 0.31% cycle one, (c) 0.71% cycle two, and (d) 1.00%

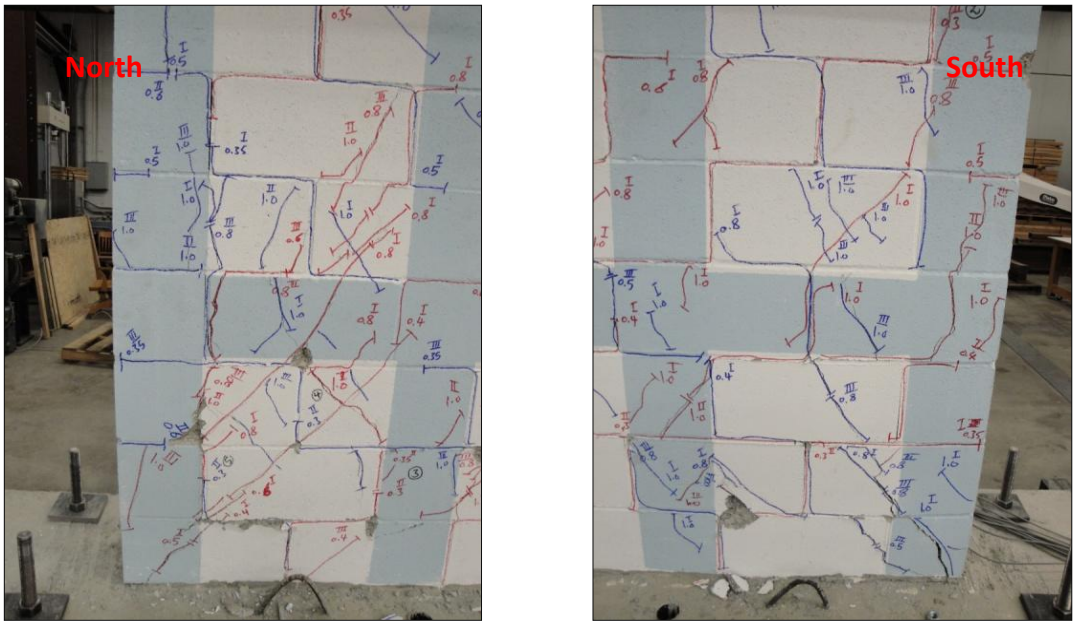

(a) (b)

Figure 3.13 Sliding in specimen PG127-24 at: (a) northern masonry panel, and (b) southern masonry panel

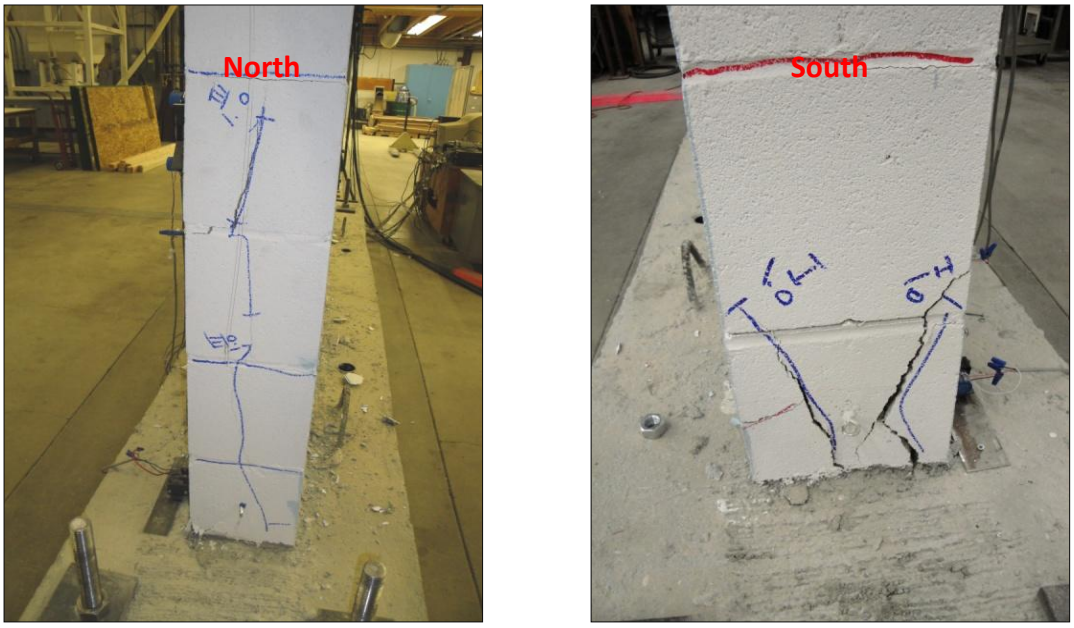

(a) (b)

Figure 3.14 Vertical cracks occurred at drift angle of 1.00% at: (a) northern masonry panel, (b) southern masonry panel

3.8 Load –Displacement Response

The load- displacement hysteresis curves for the full loading history range for loading in pull and push direction are presented in Figure 3.15.The hysteresis curves were plotted as a function of the applied lateral load and the resulting top displacement that was measured, using string potentiometers and independent frame, during the test of each specimen at the loading level course (course No. 8). Also are shown in the figure the peak strength in each direction (V_{exp}) and the strength at what deemed failure (i.e. 0.8 V_{exp}). The hysteresis cycles indicated linear elastic behavior and fairly symmetric narrow response to the applied force before cracking. Once the specimens started to crack, non linear response was observed with narrow hysteresis loops indicating a small amount of energy dissipation. By the end of the test and since significant cracking and spalling occurred, a significant non linear and energy dissipation occurred.

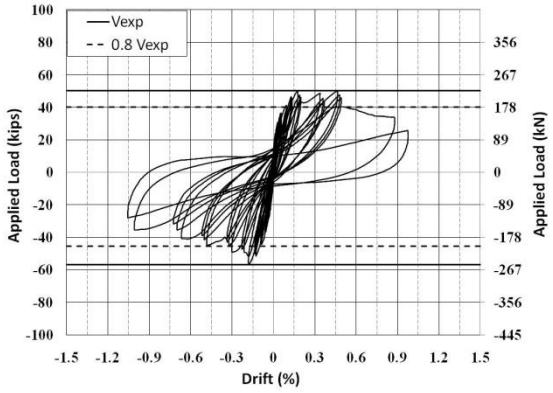

PG127-48

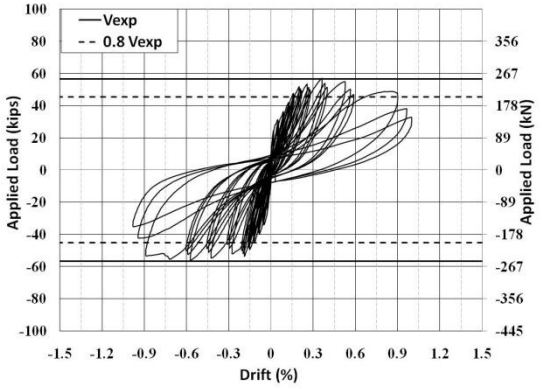

PG127-48I

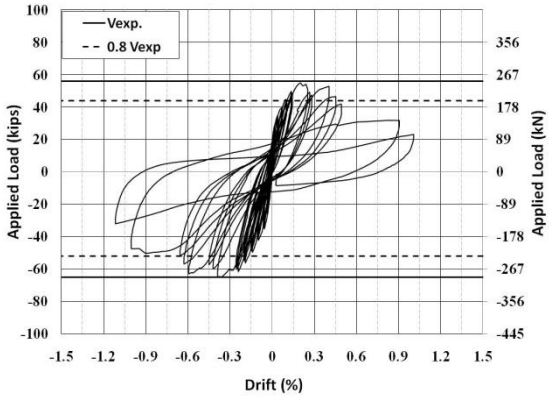

PG180-48

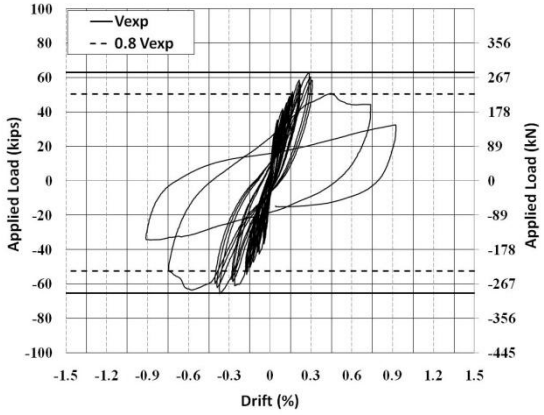

PG254-48

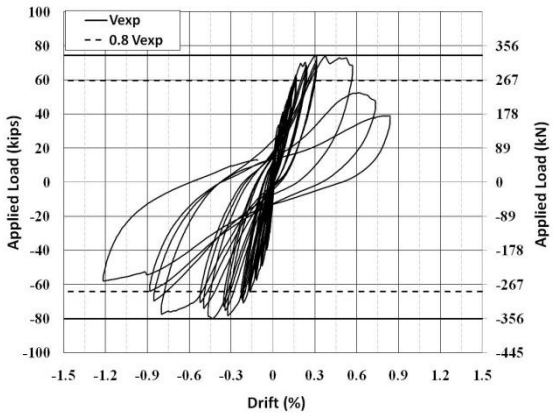

PG127-32

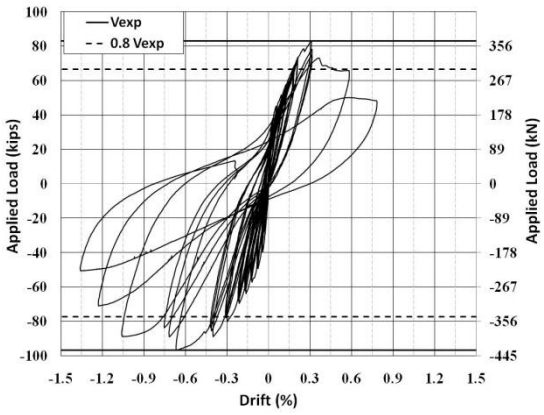

PG127-24

Figure 3.15 Load- displacement hysteresis loops

CHAPTER 4

ANALYSIS OF EXPERIMENTAL RESULTS

4.1 Introduction

An analysis and discussion of the test results of the test specimens is presented in this chapter. The effects of different parameters, including horizontal spacing of vertical grouted cells, and horizontal reinforcement ratio were investigated. In addition, the strengths of the walls were calculated using MSJC (2008) shear design equations, modified MSJC (Nolph (2010)) and strut and tie models. The envelopes of the load-displacement hysteresis curves of the tested shear walls are presented in Figure 4.1(a). Also, bilinearized backbone curves were prepared according to FEMA 356 (2000) and are presented in Figure 4.1(b).

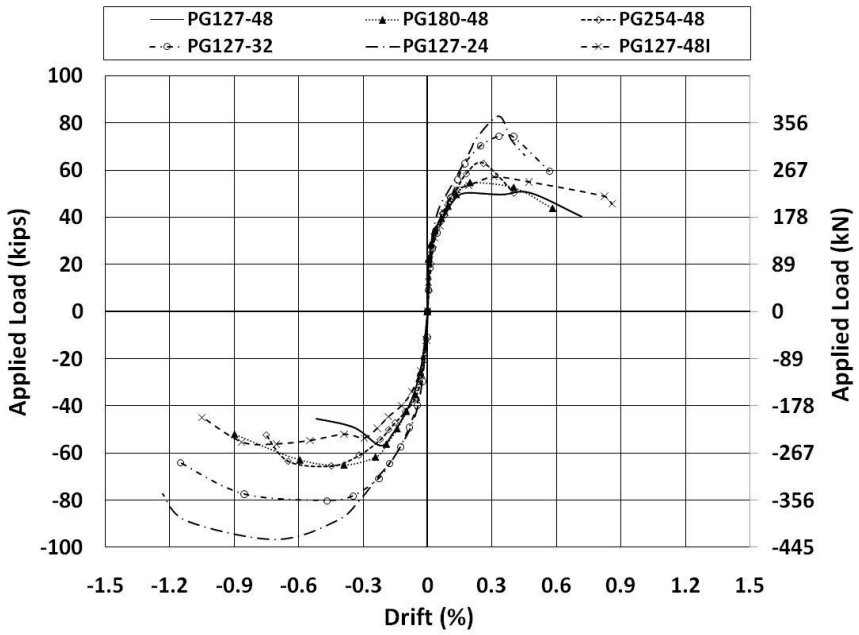

a) Backbone curves using load- displacement hysteresis loops envelopes

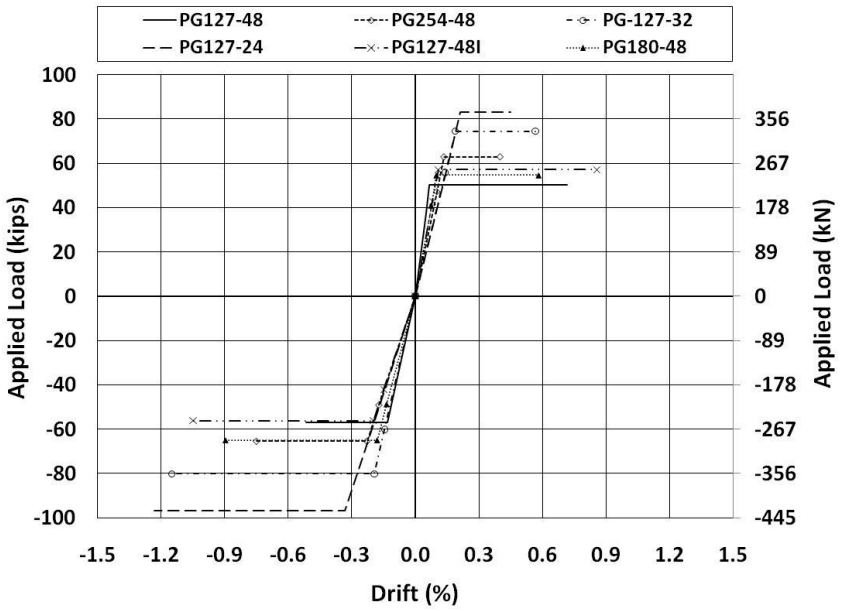

b) Backbone curves using bilinear approximation

Figure 4.1 Backbone curves for the tested specimens

4.2 Stiffness

The stiffness values of the tested walls are presented in this section. Table 4.1 shows the measured and the predicted initial stiffness (uncracked) of the specimens. The measured initial stiffness was calculated based on the first data point for each wall as average initial stiffness of both push and pull direction, while the predicted initial stiffness was calculated based on the estimated flexural and shear deformation using Eq. (4.1).

$$K = 1/(\frac{h^3}{3E_m I} + \frac{1.2h}{G_m A}) \qquad \text{Eq. (4.1)}$$

Where: h= Height of the wall

f'_m= Masonry compressive strength = 2530 psi (17.43 Mpa)

E_m= Masonry modulus of elasticity ($E_m = 900f'_m$)

G_m= Shear modulus ($G_m = 0.4E_m$)

I= Moment of inertia

A= Cross section area

Table 4.2 shows the measured yield and ultimate stiffness of each specimen. The yield stiffness was defined as the stiffness at the maximum lateral load. The ultimate displacement is defined as the stiffness at ultimate displacement.

Table 4.1 Measured and calculated initial stiffness for specimens

Wall ID	Measured initial stiffness			Calculated stiffness Kips/in (KN/mm)	Displacement ductility ($\mu\Delta$)		
	Pull Kips/in (KN/mm)	Push Kips/in (KN/mm)	Ave Kips/in (KN/mm)		Pull	Push	Average
PG127-48	1509 (264)	7900 (1383)	4705 (823)	3676 (643)	1.5	2.3	1.90
PG180-48	1338 (234)	6446 (1128)	3892 (681)	3676 (643)	2.8	2.3	2.55
PG254-48	2180 (382)	2830 (495)	2505 (438)	3676 (643)	1.6	1.7	1.65
PG127-32	3802 (665)	7782 (1362)	5792 (1013)	3957 (692)	1.8	2.3	2.10
PG127-24	7637 (1336)	3234 (566)	5436 (951)	4248 (743)	1.5	1.6	1.55
PG127-48I	5228 (915)	3891 (681)	4560 (798)	3676 (643)	1.7	1.5	1.60

Table 4.2 Measured yield and ultimate stiffness for specimens

Wall ID	Measured yield stiffness			Measured ultimate stiffness		
	Pull Kips/in (KN/mm)	Push Kips/in (KN/mm)	Ave Kips/in (KN/mm)	Pull Kips/in (KN/mm)	Push Kips/in (KN/mm)	Ave Kips/in (KN/mm)
PG127-48	1256 (220)	710 (124)	983 (172)	117 (20)	183 (32)	150 (26)
PG180-48	910 (160)	602 (105)	756 (132)	156 (27)	121 (21)	139 (24)
PG254-48	777 (136)	478 (84)	628 (110)	262 (46)	146 (26)	204 (36)
PG127-32	657 (115)	691 (121)	674 (118)	219 (38)	116 (20)	168 (29)
PG127-24	648 (113)	484 (85)	566 (99)	307 (54)	131 (23)	219 (38)
PG127-48I	878 (154)	472 (83)	675 (118)	111 (19)	89 (16)	100 (18)

4.3 Effects of Parameters Based on Test Results

4.3.1 Effects of the horizontal reinforcement ratio

Specimens PG127-48, PG180-48, and PG254-48 were identical in every aspect, except the shear reinforcement ratio. Figure 4.2 shows the backbone curves for the three specimens.

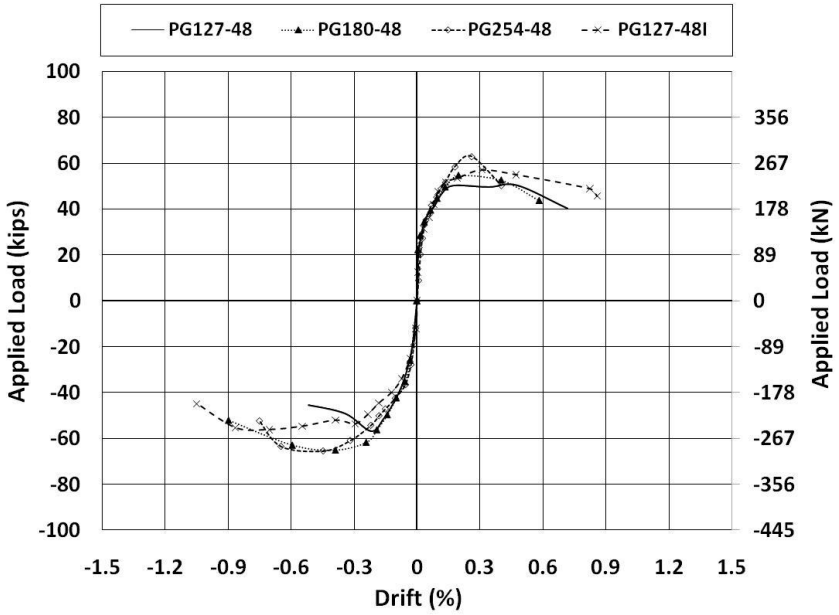

Figure 4.2 Backbone curve for specimens PG127-48, PG180-48, and PG254-48

Figure 4.3 shows the average shear strength of each wall versus the provided reinforcement ratio. As shown in the figure, by increasing the horizontal reinforcement ratio, the measured shear strength increased. However, the increase was quite modest. By increasing the reinforcement ratio from 0.127% to 0.180% the shear strength remained approximately constant at 53.5 kips (238 kN). However, doubling the reinforcement ratio in specimen PG254-48, i.e. increasing the shear reinforcement ratio from 0.127% to

0.254%, increased the shear strength by 20% from 53.5 kips (238 kN) to 64.2 kips (286 kN).

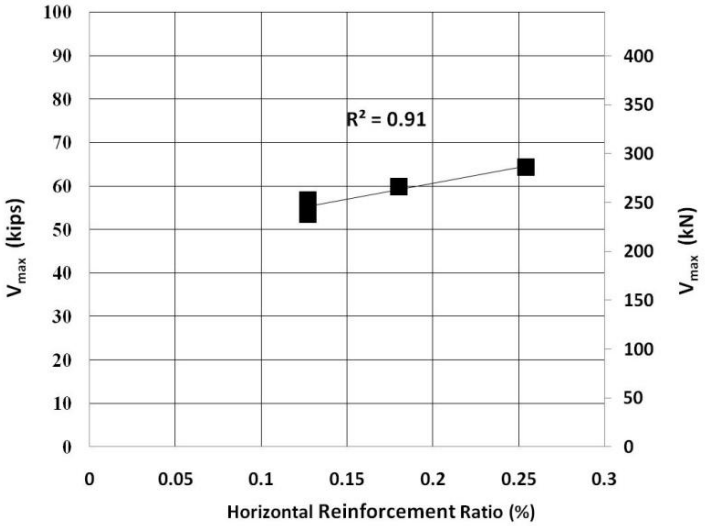

Figure 4.3 Effect of horizontal reinforcement ratio on the measured shear strength

The values of the measured maximum strains in the shear reinforcement of the middle bond beam in specimens PG127-48, PG127-48I, PG180-48, and PG254-48 are presented in Figure 4.4. As shown in the figure, increasing the reinforcement ratio from 127% to 180% had an insignificant effect on the measured maximum steel strains. However, increasing the shear reinforcement ratio from 127% to 254% resulted in a decrease in the measured maximum steel strain. Similar observations were reported by Nolph (2010) for walls having an aspect ratio of 1. Nolph (2010) proposed using equation 4.2 to predict the maximum strain in the shear reinforcement in partially grouted walls. Equation 4.2 is presented in Figure 4.4. As shown in the figure, equation 4.2 is in general agreement with the measured strains. The calculated strains ranged from 87% to 97% of measured strains with an average of 92%.

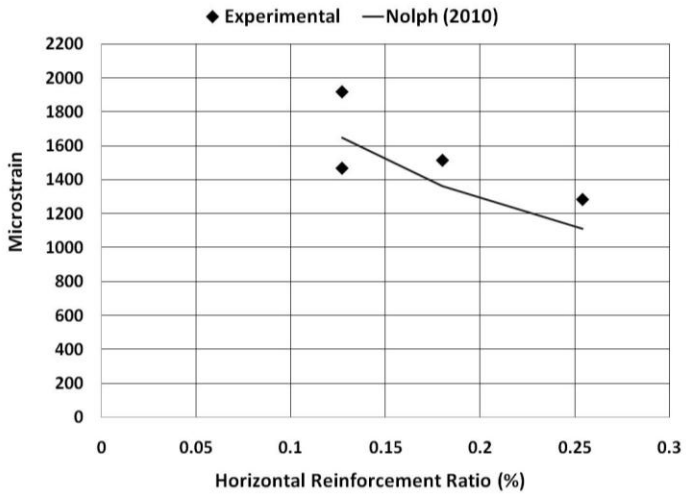

Figure 4.4. Axial strains in shear reinforcement vs. shear reinforcement ratio

Figure 4.5 shows the backbone curves of each test specimen of the three specimens, namely PG127-48, PG180-48, and PG254-48. Also, shown in each figure is the force developed in the shear reinforcement in the middle bond beam. The forces in the reinforcement were calculated using the measured strains times a steel Young's Modulus of 29,000,000 psi (200000 MPa) times the cross sectional area of the rebar in the bond beam. As shown in the figures, the peak forces in the reinforcement developed at lateral drift angle greater than those corresponding to the peak lateral resistance of the walls suggesting that the simple addition of the masonry strength component (V_{nm}) to the shear strength component (V_{ns}) as proposed by the current MSJC(2008) is not correct. There should be an interaction between the amount of the horizontal reinforcement, the mobilized force in the shear reinforcement, and the masonry contribution to the shear strength of partially grouted masonry walls. In addition, increasing the shear reinforcement rebar from 1#5 (D 16) to 1#6 (D 19) increased the force in the steel from 13.2kips (58.7 kN) to 18 kips (80 kN). However, increasing the reinforcement rebar from

1#6 to 2#5 did not have a significant effect on the contribution of the shear reinforcement on the shear strength of the walls. It seems that the contribution of the shear reinforcement to the shear strength of the walls has an upper limit of approximately 20 kips (89 kN).

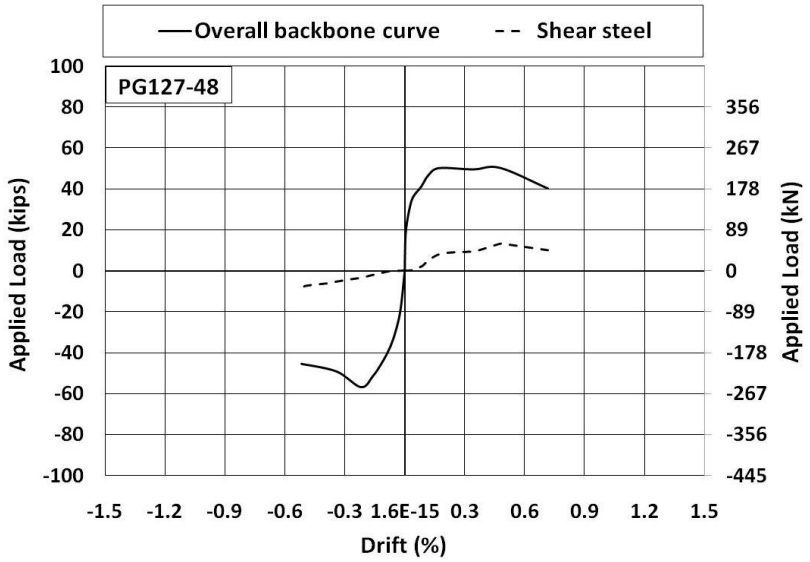

a) Drift vs. force in shear reinforcement in specimen PG127-48

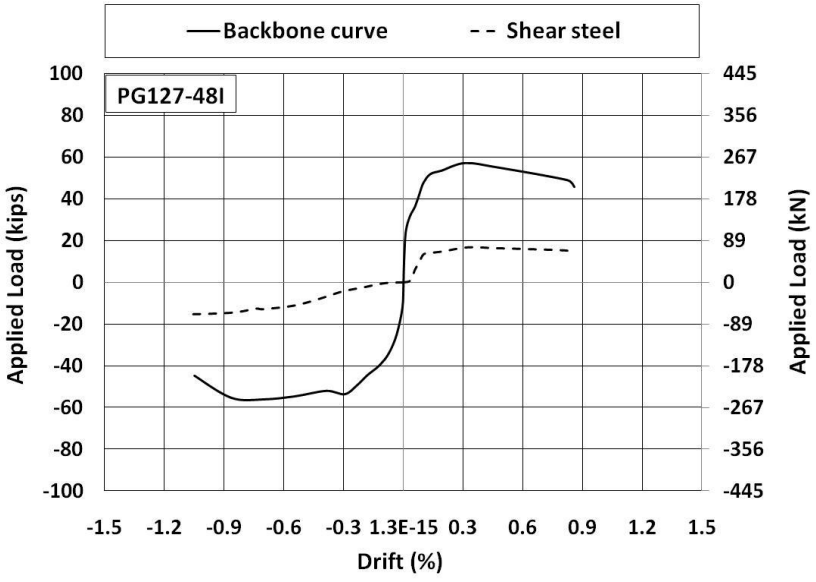

b) Drift vs. force in shear reinforcement in specimen PG127-48I

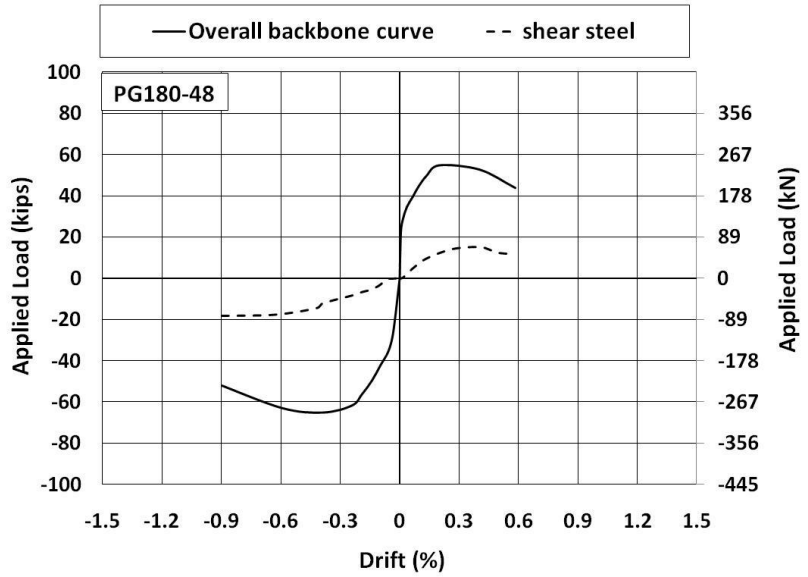

c) Drift vs. force in shear reinforcement in specimen PG180-48

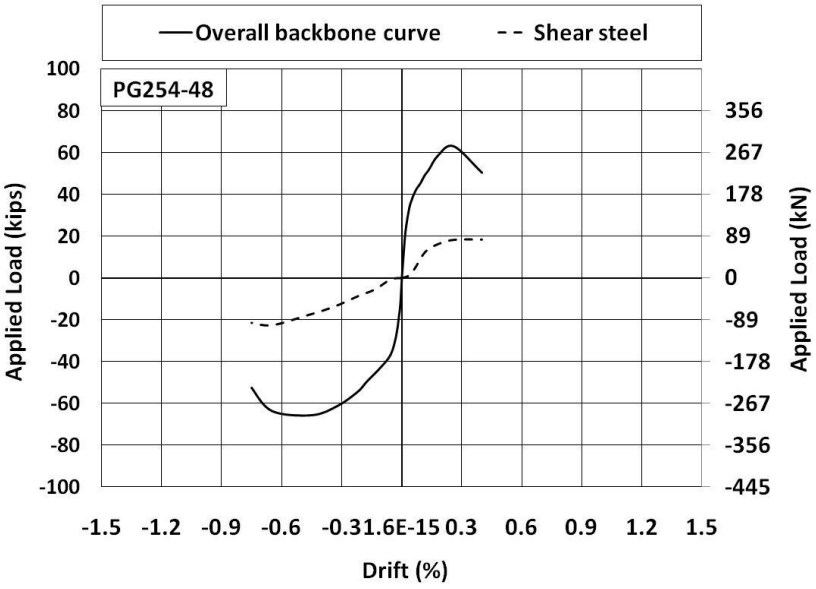

d) Drift vs. force in shear reinforcement in specimen PG254-48

Figure 4.5. Axial force in the shear rebar vs. lateral drift angle and the backbone curves

Figure 4.6 shows the net shear stresses vs. the lateral drift angles of specimens PG127-48, PG127-48I, PG180-48, and PG254-48. The net shear stresses were calculated by dividing the average lateral resistance in the push and pull directions at each drift angle by the net cross sectional area. The net cross sectional area was calculated as the sum of the mortared face shells, external webs only and the area of grouted cells. As shown in the figure, the shear stresses in the four walls reached a net shear strength of 150 psi (1.03 MPa), 155 psi (1.07 MPa), 165 psi (1.14 MPa), and 168 psi (1.16 MPa) corresponding to approximately $2.9\sqrt{f'm}$, $3.1\sqrt{f'm}$, $3.3\sqrt{f'm}$, and 3.5 $\sqrt{f'm}$ for specimens PG127-48, PG127-48I, PG180-48, and PG254-48 respectively, where f'_m is the compressive strength of the un-grouted masonry.

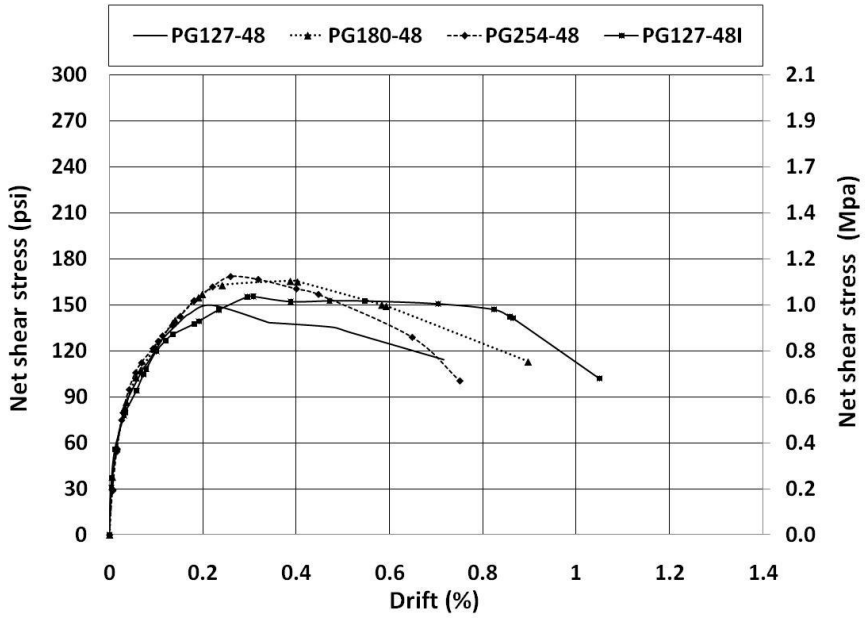

Figure 4.6 Net shear stress for PG127-48, PG180-48, and PG254-48

It is worth noting that the MSJC (2008) recommends a value of 5.1 $\sqrt{f'm}$ as an upper limit of the shear stress for masonry walls having an aspect ratio of 0.58

The effect of increased shear reinforcement on initial, yield, and ultimate stiffness are presented in Table 4.3; from the table, increased horizontal reinforcement led to a decrease in the measured initial, yield, and ultimate stiffness for specimens PG127-48, 127-48I, PG180-48, and PG254-48.

Table 4.3 Initial, yield and ultimate stiffness for specimens PG127-48, 127-48I, PG180-48 and PG254-48

Wall ID	Measured initial stiffness			Measured yield stiffness			Measured ultimate stiffness		
	Pull Kips/in (KN/mm)	Push Kips/in (KN/mm)	Ave Kips/in (KN/mm)	Pull Kips/in (KN/mm)	Push Kips/in (KN/mm)	Ave Kips/in (KN/mm)	Pull Kips/in (KN/mm)	Push Kips/in (KN/mm)	Ave Kips/in (KN/mm)
PG127-48	1509 (264)	7900 (1383)	4705 (823)	1256 (220)	710 (124)	983 (172)	117 (20)	183 (32)	150 (26)
PG180-48	1338 (234)	6446 (1128)	3892 (681)	910 (160)	602 (105)	756 (132)	156 (27)	121 (21)	139 (24)
PG254-48	2180 (382)	2830 (495)	2505 (438)	777 (136)	478 (84)	628 (110)	262 (46)	146 (26)	204 (36)
PG127-48I	5228 (915)	3891 (681)	4560 (798)	878 (154)	472 (83)	675 (118)	111 (19)	89 (16)	100 (18)

4.3.2 Effect of grout horizontal spacing

Different grout horizontal spacing of 48 in. (1219 mm), 32 in. (813 mm) and 24 in. (610 mm) were used for the construction of the test specimens. These walls had a reinforcement ratio of 127% in the form of 1#5 (D 16). Figure 4.7 shows the backbone curves of the four specimens. As shown in the figure, the measured shear strength capacity increased significantly by increasing the number of grouted flues and by decreasing grout

horizontal spacing. Specimens PG127-48 and PG127-48 had grout horizontal spacing of 48 in. (1219 mm) reached ultimate lateral shear strength of 53.5 kips (238 kN) and 56.7 kips (252 kN) respectively. Reducing the grout horizontal spacing from 48 in. (1219 mm) to 32 in. (813 mm) in specimen PG180-32 increased the average shear strength by 40% and the specimen reached an ultimate shear strength of 77.3 kips (344 kN). Finally, reducing the grout horizontal spacing to 24 in. (610 mm) bumped up the ultimate shear strength by 63% compared to specimens PG127-48 and PG127-48I, and the specimen reached an ultimate strength of 89.9 kips (400 kN). Figure 4.8 shows the relationship between the grout horizontal spacing and the ultimate shear strength of the four test specimens. As shown in the figure, the shear strength decreased linearly with increasing grout horizontal spacing.

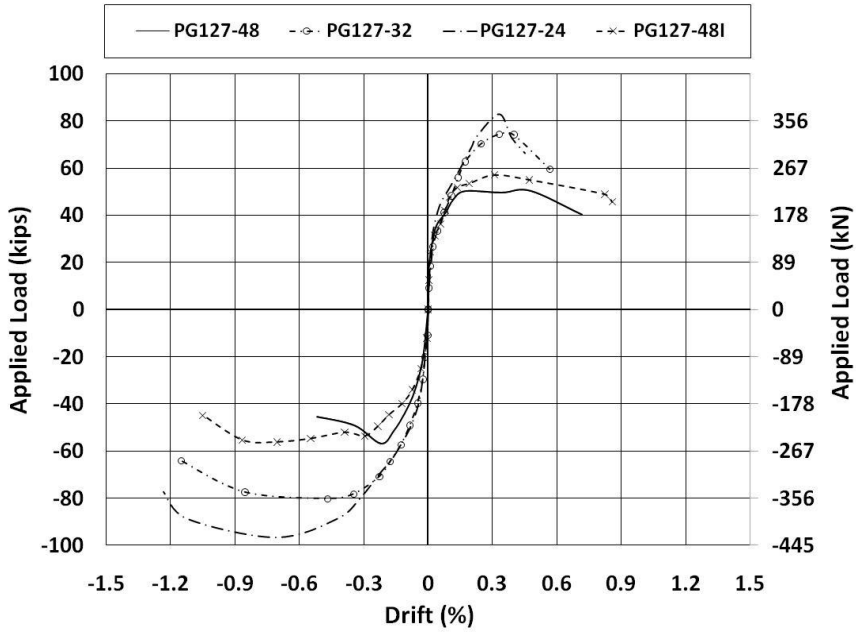

Figure 4.7 Backbone curves for specimens having different grout horizontal spacing

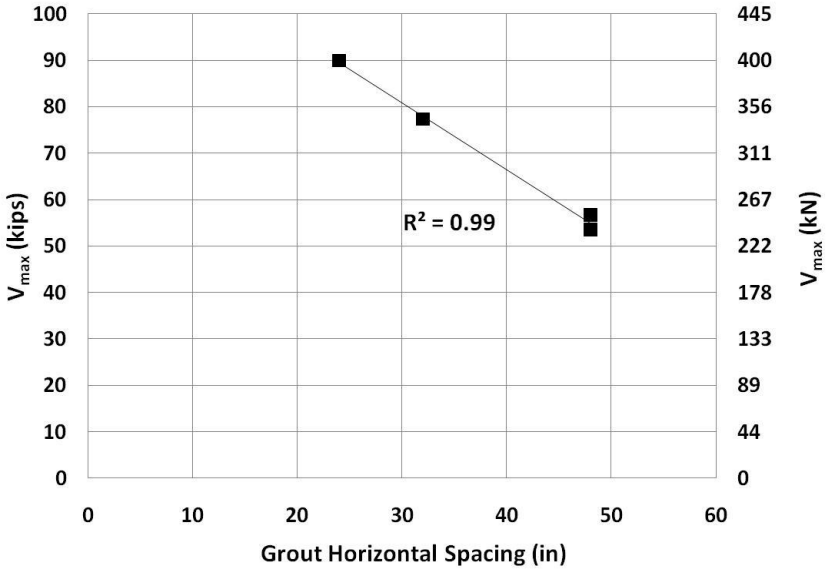

Figure 4.8 Effect of horizontal grout spacing on the measured shear strength for specimens PG127-48, PG127-48I, PG127-32, and PG127-24

Figure 4.9 shows the net area shear stresses of the four specimens having different horizontal spacing between vertical grouted cells. As shown in the figure, specimens having grout horizontal spacing of 32 in. (813 mm) and 24 in. (610 mm) have approximately the same peak value of the net area shear stresses of 197 psi (1.35 MPa) corresponding to $4.1\sqrt{f'm}$, while specimens PG127-48 and PG127-48I with grout horizontal spacing of 48 in. (1219 mm) have a peak net area shear stresses of 150 psi (1.03 MPa) and 155 psi (1.07 MPa). These values correspond to $2.9\sqrt{f'm}$, and $3.1\sqrt{f'm}$, respectively.

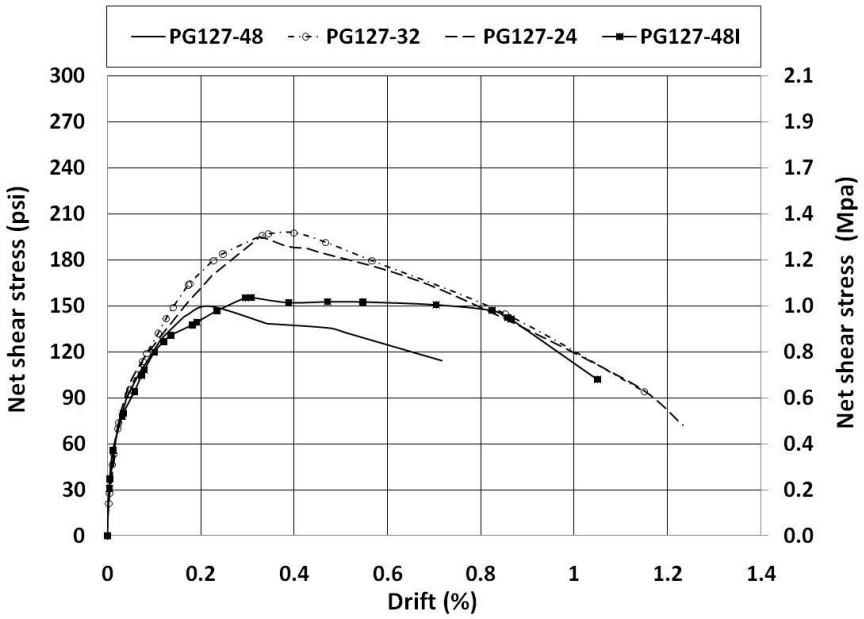

Figure 4.9 Net shear stress for specimens PG127-48, PG127-48I, PG127-32, and PG127-24

Figure 4.10 shows the backbone curves and the axial force in the shear reinforcement vs. the lateral drift angle for specimens PG127-48, PG127-48I, PG127-32, and PG127-24. As shown in the figure, decreasing the grout horizontal spacing from 48 in. (1219 mm) to 32 in. (813 mm) and 24 in. (610 mm) resulted in yielding of the horizontal rebar. In addition, the engagement of the shear reinforcement in the lateral resistance started approximately at the same drift angle of approximately 0.05%. In addition, specimens PG127-32 and PG127-24 reached their peak strengths at a drift angle similar to those corresponding to yielding of the horizontal rebar. Yielding of the rebar occurred at drift angles ranged from 0.3 to 0.6%.

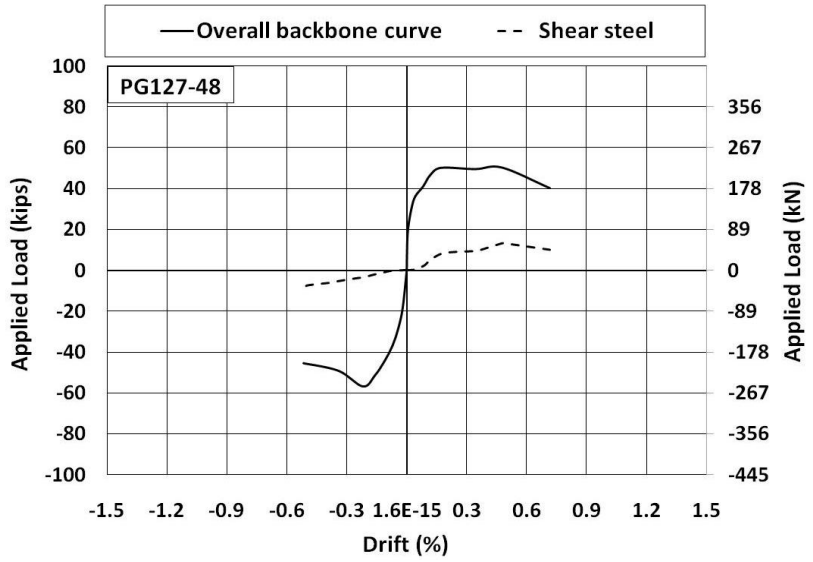

a) Drift vs. force in shear reinforcement in specimen PG127-48

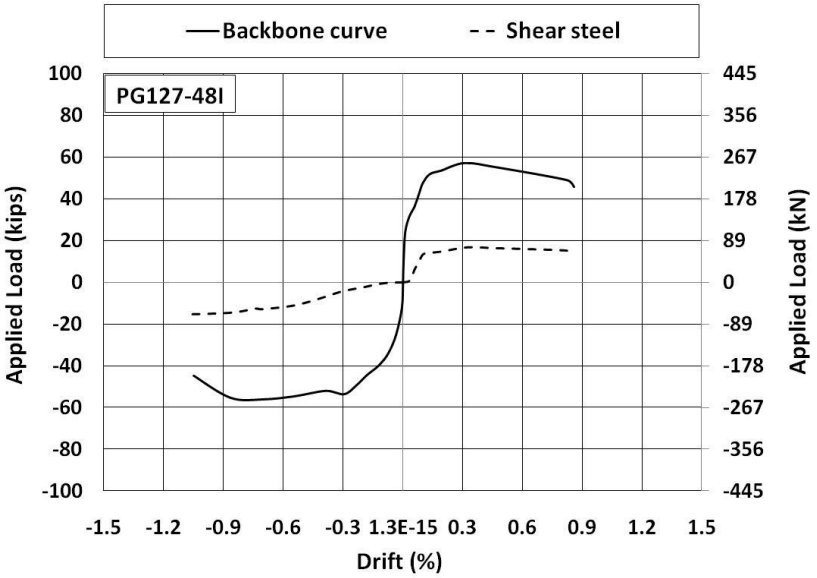

b) Drift vs. force in shear reinforcement in specimen PG127-48I

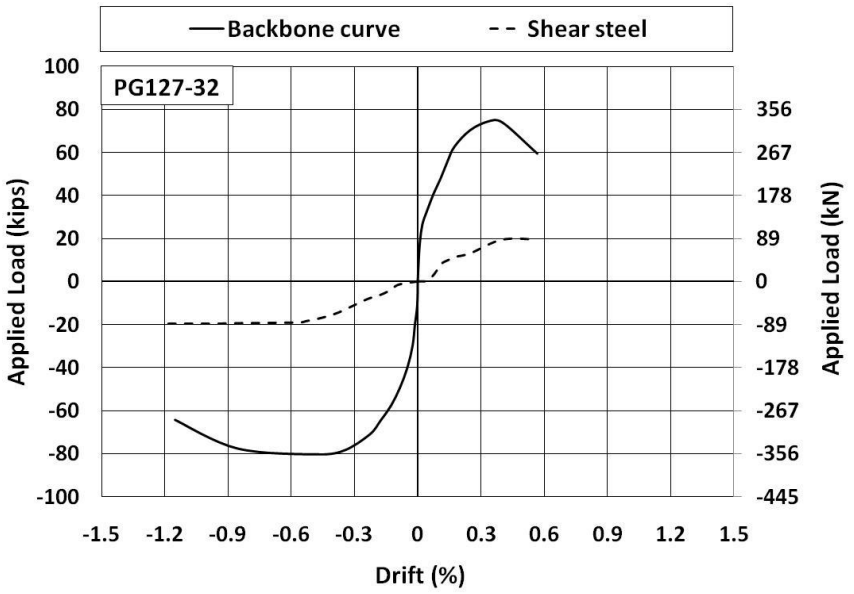

c) Drift vs. force in shear reinforcement in specimen PG180-32

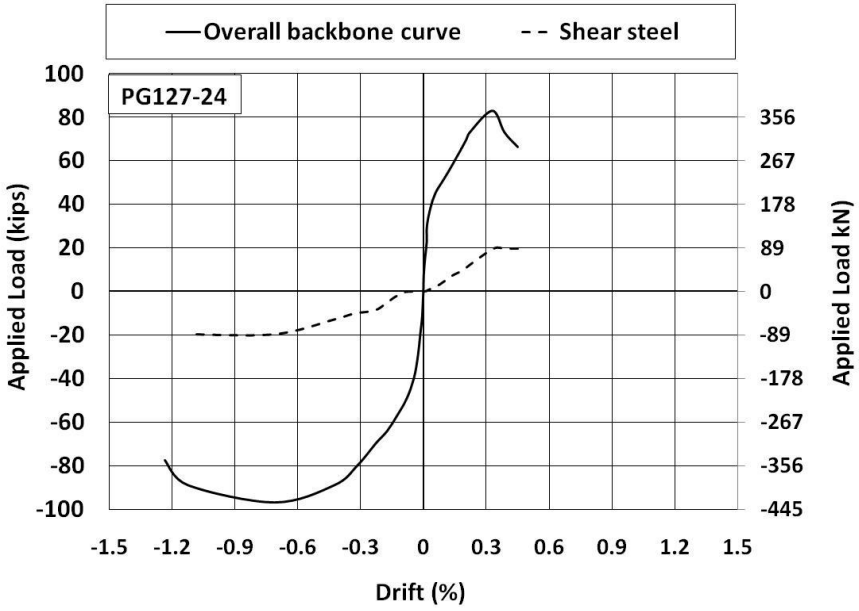

d)Drift vs. force in shear reinforcement in specimen PG180-32

Figure 4.10 Axial force in shear rebar vs. lateral drift angle and backbone curves for specimens have different grout horizontal spacing

In terms of stiffness, decrease the grout spacing from 48 in. (1219 mm) to 32 in. (813 mm) and 24 in. (610 mm) led to an increase in the initial stiffness, as shown in Table 4.4. However, decreasing in the grout spacing led to a decrease in the yield stiffness, while it had insignificant effect on the ultimate stiffness.

Table 4.4 Effect of grout spacing on initial, yield, and ultimate stiffness for specimens PG127-48, PG127-48I, PG180-32, and PG254-24

Wall ID	Measured initial stiffness			Measured yield stiffness			Measured ultimate stiffness		
	Pull Kips/in (KN/mm)	Push Kips/in (KN/mm)	Ave Kips/in (KN/mm)	Pull Kips/in (KN/mm)	Push Kips/in (KN/mm)	Ave Kips/in (KN/mm)	Pull Kips/in (KN/mm)	Push Kips/in (KN/mm)	Ave Kips/in (KN/mm)
PG127-48	1509 (264)	7900 (1383)	4705 (823)	1256 (220)	710 (124)	983 (172)	117 (20)	183 (32)	150 (26)
PG127-48I	5228 (915)	3891 (681)	4560 (798)	878 (154)	472 (83)	675 (118)	111 (19)	89 (16)	100 (18)
PG127-32	3802 (665)	7782 (1362)	5792 (1013)	657 (115)	691 (121)	674 (118)	219 (38)	116 (20)	168 (29)
PG127-24	7637 (1336)	3234 (566)	5436 (951)	648 (113)	484 (85)	566 (99)	307 (54)	131 (23)	219 (38)

4.4 Experimental vs. Calculated Shear Strength Using MSJC (2008) Shear Equation

The MSJC (2008) predicts the shear strength for partially grouted masonry shear walls (V_n), equation (4.2) as the summation of the nominal shear strength provided by shear reinforcement (V_{ns}), given by equation (4.3) and the nominal shear strength provided by masonry panel (V_{nm}), given by equation (4.4). The only distinction between partially and fully grouted masonry walls is that, in partially grouted walls the MSJC (2008) uses the net grouted area (A_n) instead of the cross sectional area (A_g), as is in fully grouted masonry walls. Table 4.5 presents the parameters that were used to calculate the shear strength for the tested specimens.

$$V_n = V_{nm} + V_{ns} \qquad \text{Eq. (4.2)}$$

$$V_{ns} = 0.5\left(\frac{A_v}{s}\right)\cdot f_y \cdot d_v \qquad \text{Eq. (4.3)}$$

$$V_{nm} = \left[4.0 - 1.75\left(\frac{M_u}{V_u \cdot d_v}\right)\right]\cdot A_n \cdot \sqrt{f'_m} + 0.25P_u \qquad \text{Eq. (4.4)}$$

Where:

A_n = Net area, d_v = Effective depth in the direction of shear, P_u = Axial load, f'_m =Compressive strength of un-grouted masonry, F_y = Yield strength of horizontal reinforcement, S = Spacing of horizontal steel, and A_v =Area of horizontal steel.

Table 4.5 Parameters used for MSJC (2008) shear calculations

Wall ID	PG127-48	PG127-48I	PG180-48	PG254-48	PG127-32	PG127-24	Units
A_n	356 (229,677)	356 (229,677)	356 (229,677)	356 (229,677)	388 (250,322)	421 (271,612)	In^2 (mm^2)
A_v	0.31 (200)	0.31 (200)	0.44 (284)	0.62 (400)	0.31 (200)	0.31 (200)	In^2 (mm^2)
V_{nm}	56.2 (250)	56.2 (250)	56.2 (250)	56.2 (250)	61 (271)	66 (294)	kips (kN)
V_{ns}	32.9 (146)	32.9 (146)	44 (196)	65.8 (293)	32.9 (146)	32.9 (146)	kips (kN)
V_n	89.1 (396)	89.1 (396)	100.2 (446)	122 (543)	93.8 (424)	99 (440)	kips (kN)
$V^*_{n\ final}$	89.1 (396)	89.1 (396)	91.7 (408)	91.7 (408)	93.8 (424)	99 (440)	kips (kN)
f_y	61.5 (424)	61.5 (424)	65.6 (452)	61.5 (424)	61.5 (424)	61.5 (424)	ksi (Mpa)

For all specimens: h_w=60 in. (1524 mm), d_v=103.7 in. (2634 mm), P_u=11000 Ib (48928 N), f'_m= 2530 ksi

* Smaller of $V_{n,\,max}$ and V_n

Where :

$$\begin{cases} V_{n,\max} \le 6A_n\sqrt{f'm} & for \quad \dfrac{M_u}{V_u d_v} \le 0.25 \\ V_{n,\max} \le 4A_n\sqrt{f'm} & for \quad \dfrac{M_u}{V_u d_v} \ge 1.00 \end{cases}$$

The experimental shear strengths, the calculated shear strengths using MSJC (2008) for all specimens, as well as the differences between the calculated and measured strength values are presented in Table 4.6. Figure 4.11 shows load-drift hysteretic loops for each specimen at the top course (course No. 8) and the predicted strengths using MSJC (2008). Also, in the figure, ϕVn was shown where ϕ is the shear strength reduction factor (ϕ= 0.8). As shown in the figure and the table, the MSJC (2008) shear design equations are highly un-conservative and over-estimated the shear strength capacity for the tested walls. The measured shear strengths ranged from 60% to 91% of the predicted values.

Figure 4.12 shows the relationship between the horizontal reinforcement ratio and V_{exp}/ V_n which represents the ratio between the measured and the predicted shear strength. As shown in the figure, increasing the horizontal reinforcement ratio from 0.127% to 0.180% showed an insignificant effect on the over-estimation ratio of the shear strength, while increasing the horizontal reinforcement from 0.127% (i.e. specimen PG127-48) to 0.254% (i.e. specimen PG254-48), which represents doubling amount of reinforcement, decreased the over-estimation of the MSJC code shear equations by only 10%. As explained earlier, increasing the shear reinforcement prevented the shear rebar from reaching its yield strength prior to the specimen's failure. In addition, the strain in the shear rebar decreased with increasing the shear reinforcement ratio. The MSJC (2008) shear design equations assume yielding of shear rebar.

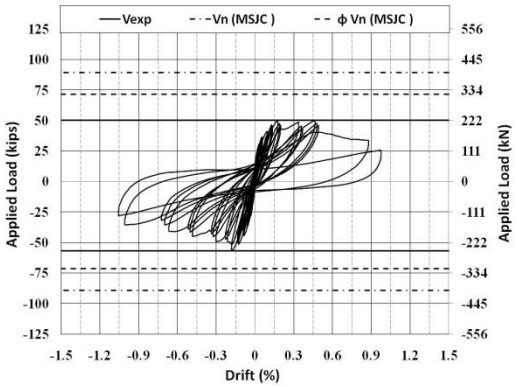

PG127-48

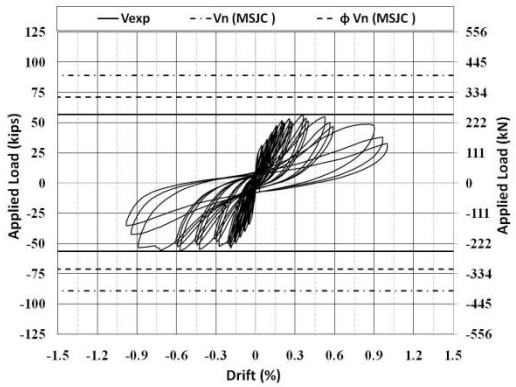

PG127-48I

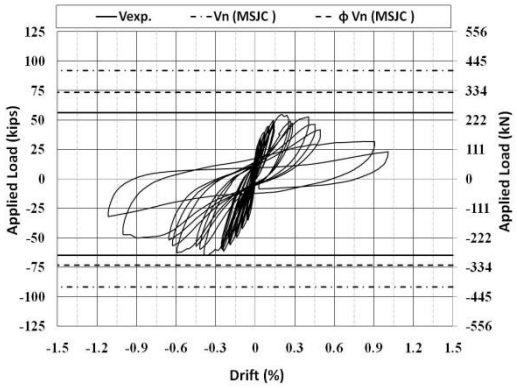

PG180-48

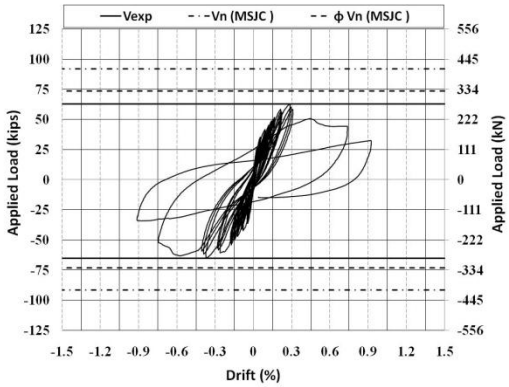

PG254-48

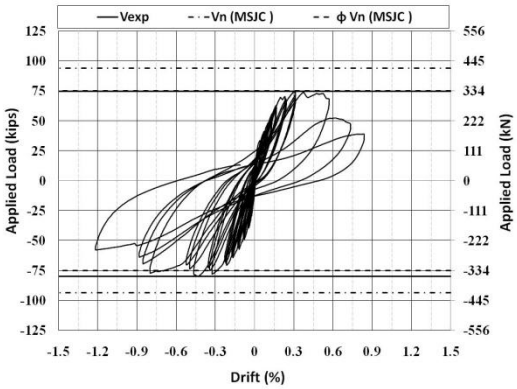

PG127-32

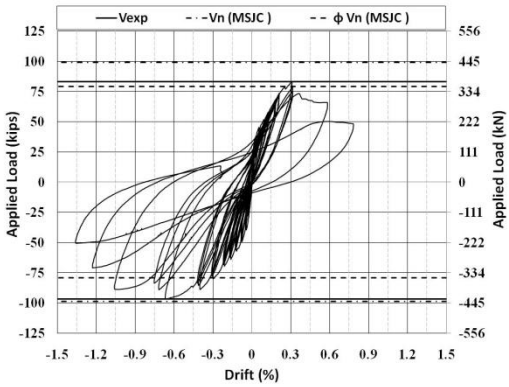

PG127-24

Figure 4.11 Load-drift hysteresis for the test specimens

Table 4.6 MSJC calculated shear strength, measured shear strength and error percentage

Wall ID	PG127-48	PG127-48I	PG180-48	PG254-48	PG127-32	PG127-24
MSJC (V_n)	89.1 kips (396) kN	89.1 kips (396) kN	91.7 kips (408) kN	91.7 kips (408) kN	93.8 kips (424) kN	99 kips (440) kn
Measured strength (V_{exp})	53.5 kips (238) kN	56.7 kips (252) kN	59.8 kips (246) kN	64.2 kips (286) kN	77.3 kips (344) kN	89.9 kips (400) kN
V_{exp}/V_n	60%	63%	65%	70%	82%	91%

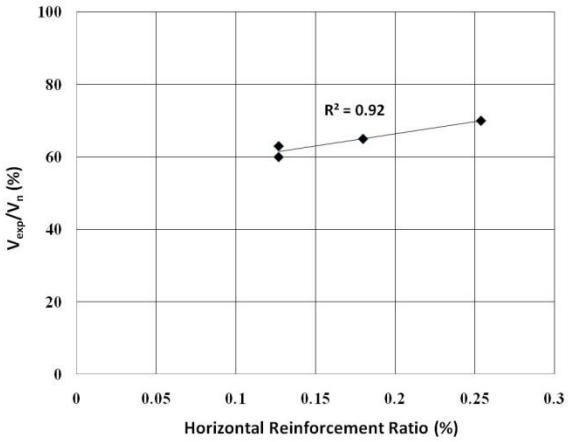

Figure 4.12 Effect of horizontal reinforcement on the predictions using MSJC (2008) shear equation for specimens with grout horizontal spacing of 48 in

Specimens PG127-48, PG127-48I, PG127-32, and PG127-24 have constant horizontal reinforcement ratio of 0.127%, but different grout horizontal spacing of 48 in. (1219 mm), 32 in. (813 mm), and 24 in. (610 mm), respectively. Figure 4.13(a) shows the relationship between the net cross sectional area and the measured shear strengths. Also, the figure shows predictions using MSJC (2008) shear design equations. As shown in the figure, by decreasing the grouted cross sectional area, the difference between the MSJC (2008) shear design equations and the measured shear strengths increased. Similarly,

Figure 4.13(b) shows the measured and predicted shear strengths versus the grout horizontal spacing. As shown in the figure, the MSJC (2008) shear predictions became more accurate by decreasing the grout horizontal spacing. Also, the shear strength was linearly proportional to the grout horizontal spacing with an R^2 of 1. Figure 4.14 summarizes the effect of the horizontal spacing on the percentage of the over-estimation.

This finding indicates the need to modify the shear strength of partially grouted masonry shear walls with respect to grout horizontal spacing and net cross sectional area.

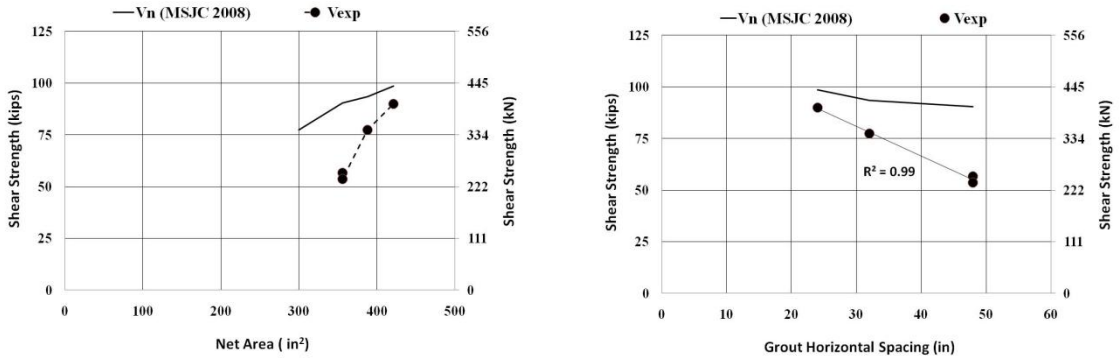

(a) (b)

Figure 4.13 Specimens with horizontal reinforcement of 0.127%: (a) Net area vs. V_{exp} and V_n, and (b) Grout horizontal spacing vs. V_{exp} and V_n

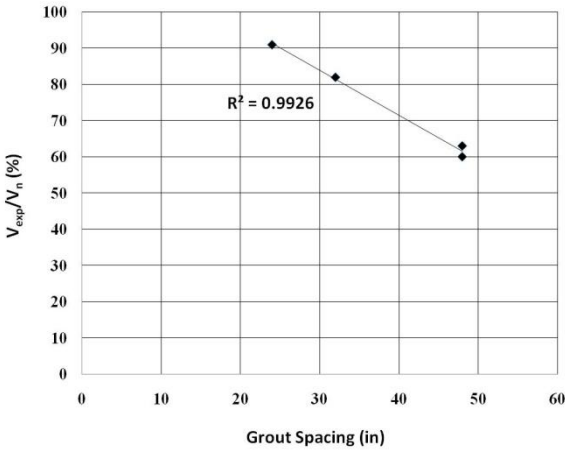

Figure 4.14 Effect of grout spacing on V_{exp}/ V_n for specimens having ρ_h of 0.127%

4.5 Nolph's Proposed Modifications to the Shear Design Equations of MSJC (2008)

As mentioned in section (4.4), the MSJC (2008) over-estimated the shear strengths for partially grouted masonry shear walls tested during the course of this study. Nolph (2010) suggested a few modifications in order to increase the accuracy of the shear design equation presented by MSJC (2008). The first modification was to replace (d_v/s) in equation (4.3), which represents the number of provided stirrups, by (d_{45}/s) as shown in equation (4.5), where d_{45} is the smaller of the wall length (d_v) or height (h_w). Using (d_v/s) for squat shear walls results in an incorrect number of stirrups that resist a shear crack at 45°. Table 4-7 presents (V_{exp}) and the calculated shear strengths (V_n) using the shear equations of MSJC (2008) (i.e. equation (4.2) to (4-4)) as well as the shear strengths calculated after the first modification of Nolph (2010) ($V_{n,n1}$). As shown in the table, introducing the d_{45} term significantly improved the shear strength predictions of all specimens.

$$V_{ns} = \left(\frac{1}{2}\right) \cdot \left[A_v \cdot f_y\right] \cdot \left(\frac{d_{45}}{s}\right) \qquad \text{Eq. (4.5)}$$

Table 4.7 Experimental results vs. V_n and ($V_{n,n1}$)

Wall ID	PG127-48	PG127-48I	PG180-48	PG254-48	PG127-32	PG127-24
V_{exp} / V_n	0.60	0.63	0.65	0.70	0.82	0.91
$V_{exp} / V_{n,n1}$	0.71	0.75	0.67	0.70	0.96	1.05

The second modification developed by Nolph (2010) was a reduction factors α applied to the V_{nm} term, i.e. equation (4.4) as shown in equation (4.6) .The α factor can be calculated using equation (4.7) and it reflects that partially grouted masonry walls are able

to resist smaller shear stresses compared to a counterpart of fully grouted shear walls. The α factor ranges from 0.75 for specimens having horizontal grout spacing of 48 in. (1219 mm) to 1.00 for horizontal grout spacing of 24 in. (610 mm). Table 4.8 presents the comparison between the measured shear strengths (V_{exp}) and the calculated shear strengths (V_n) using the shear equations of MSJC (2008) (i.e. equation (4.2) to (4.4) as well as the shear strengths calculated after applying the first and second modifications of Nolph (2010)$V_{n,n2}$. As shown in the table, introducing the α factor term significantly improved the shear strength predictions of all specimens.

$$V_{nm} = \alpha \cdot \left[4.0 - 1.75 \left(\frac{M_u}{V_u \cdot d_v} \right) \right] \cdot A_n \cdot \sqrt{f'_m} + 0.25 P_u \qquad \text{Eq. (4-6)}$$

$$\propto = 3.6 \left(\frac{A_n}{A_g} \right) - 0.8 \geq 0 \qquad \text{Eq. (4-7)}$$

where: $\alpha = 1.0$ for $A_n / A_g \geq 0.5$

Table 4.8 Experimental results vs. V_n and ($V_{n,n2}$)

Wall ID	PG127-48	PG127-48I	PG180-48	PG254-48	PG127-32	PG127-24
V_{exp} / V_n	0.60	0.63	0.65	0.70	0.82	0.91
$V_{exp} / V_{n,n2}$	0.86	0.91	0.81	0.79	1.05	1.06

The third modification proposed by Nolph (2010) was developed based on investigating the axial strains in shear reinforcement of partially grouted shear walls having different reinforcement ratios. It was found that by increasing the horizontal reinforcement ratio, there is a reduction in the ultimate axial strains in the shear

reinforcement. Based on that finding, a reduction factor, β, was proposed and applied to V_{ns} term, as shown in equation (4.8).

$$V_{ns} = \beta \cdot \left(\frac{1}{2}\right) \cdot \left[A_v \cdot f_y\right] \cdot \left(\frac{d_{45}}{s}\right) \qquad \text{Eq. (4.8)}$$

where: $\beta = 1.0$ for $\rho_h < 0.001$, else

$$\beta = 1 - 200\,\rho_h \geq 0 \qquad \text{Eq. (4.9)}$$

Table 4.9 presents compressions between the measured shear strengths (V_{exp}) and the calculated shear strengths (V_n) using the shear equations of MSJC (2008) (i.e. equation (4-2), to (4-4)), as well as the shear strengths calculated after applying the three modifications proposed by Nolph (2010)$V_{n,n3}$. As shown in the table, these modifications significantly improved the predictions of the shear strengths. Using the MSJC (2008) shear design equations, V_{exp}/V_n ranged from 60 to 91%, with an average of 70%. Implementing the proposed modification resulted in V_{exp} /$V_{n,n3}$ ranging from 0.93% to 112%, with an average of 102%

Table 4.9 Experimental results vs. V_n and ($V_{n,n3}$)

Wall ID	PG127-48	PG127-48I	PG180-48	PG254-48	PG127-32	PG127-24
V_{exp} / V_n	0.60	0.63	0.65	0.70	0.82	0.91
V_{exp} / $V_{n,n2}$	0.94	0.99	0.93	1.04	1.12	1.12

4.6 Strut and Tie Model

The strut and tie model (STM) is a helpful approach to predict the strength of masonry shear walls. The model involves formulating the masonry shear walls into appropriate simplified truss models. This truss consisted of struts and ties in which the compressive forces in the struts are resisted by masonry blocks, and the tensile forces in the ties are resisted by steel rebar. All the struts and ties are interconnected at nodes in both member ends.

4.6.1 ACI 318-08 code provisions

In this study, ACI 318-08 appendix A was used to analyze the masonry shear walls using prismatic struts with constant cross section. The nominal compressive strength of the strut is given by equation. (4.10).

$$F_{ns} = f_{ce} \cdot A_{cs} \qquad \text{Eq. (4.10)}$$

where the (A_{cs}) is the cross section area of the strut, and (f_{ce}) is the smaller value of the effective compressive stress of the strut and node which can be calculated from equations.(4.11) and (4.12) for struts and nodes, respectively.

$$f_{ce} = 0.85\beta_s \cdot f'_m \qquad \text{Eq. (4.11)}$$

$$f_{ce} = 0.85\beta_n \cdot f'_m \qquad \text{Eq. (4.12)}$$

where β_s= 1.00 for a strut of uniform cross-sectional area over its length, f'_m= specified masonry compressive strength, β_n= 0.8 when nodes anchor only one tie, and β_n= 0.6 when nodes anchor more than one tie.

In order to calculate the net cross section area of the strut (A_{cs}) from equation (4.14) the width of the strut (w_s) must be calculated first from equation (4.13).

$$w_s = cd = ca / \text{Cos}\ \phi \quad (4\text{-}13)$$

$$A_{cs} = w_s \,.\, 2.t \quad (4\text{-}14)$$

where ϕ= the strut angle (the angle between the strut and the horizontal), ca= the bond beam depth, and t= the face shell thickness of the concrete masonry blocks (1.25 in. (32 mm)

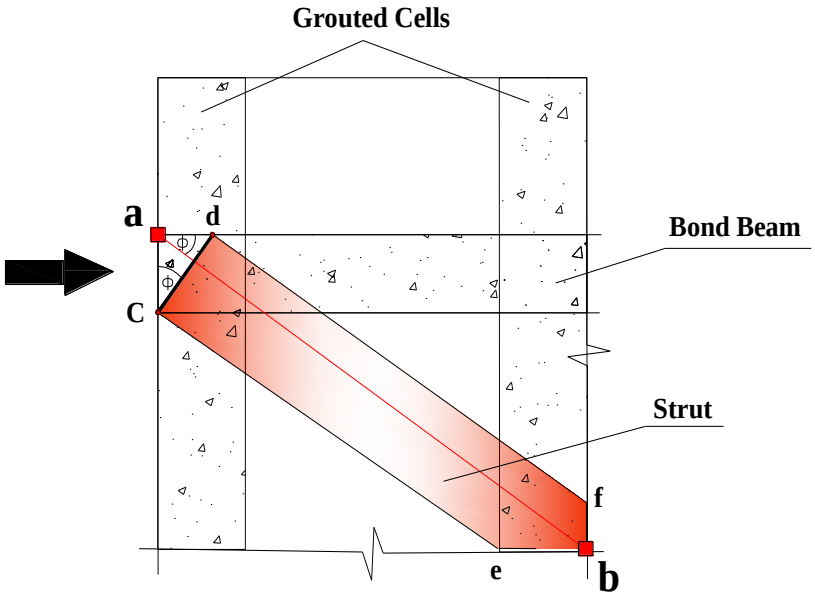

Figure 4.15 Calculation of strut width in masonry shear walls

According to ACI 318-05 Appendix A, the strut angle (ϕ) should not be taken less then 25° and not greater than 65° (i.e. $25° \leq \phi \leq 65°$). The strut and tie models for the masonry shear walls in this section were analyzed using Sap2000 software. The force was equally applied to the nodes at course No. 8. However, the nodes furthest from the applied lateral load gets zero force (i.e. if the load was applied from north to south direction, the node at the south most direction gets zero load). The applied load was increased gradually

until either failure occurred in strut or yielding of rebar occurred. In the case where the tie failed before compression failure occurred in the strut, the tie member was removed and substituted with the tie yield strength and the applied force was increased until compression failure was obtained in the strut. This process was used in all specimens during the analysis of strut and tie models.

4.6.2 Strut and tie model for specimens PG127-48, PG127-48I, PG180-48, and PG254-48

Specimens PG127-48, PG127-48I, PG180-48, and PG254-48 had a horizontal spacing of 48 in (1219 mm) between the vertical grouted cells. All the specimens had the same vertical reinforcement ratio but different horizontal reinforcement ratios. Specimens PG127-48 and PG127-48I had similar shear reinforcement of 1 rebar No. 5 (D 16) in each bond beam. Specimen PG180-48 was horizontally reinforced using 2 rebar #5 (D 16) while specimen PG254-48 had 1 rebar No.6 (D 19) in each bond beam.

Figures 4.16 and 4.17 show the strut and tie model for specimens PG127-48, PG127-48I, PG180-48, and PG254-48. The angle of the diagonal strut in this model is 32^{o}. According to the ACI 318-05 Appendix A, the maximum strut compressive strength was calculated to be 50.7 kips (226 kN), while the node compressive strength was about 110 kips (490 kN). For ties having reinforcement consisting of 1 #5, 1 #6, and 2 #5, yield strengths of 20.33 kips (90 kN), 27.2 kips (121 kN), and 40.7 kips (181 kN) were estimated, respectively. In specimens PG127-48, PG127-48I, PG180-48, and PG254-48, the lateral forces were applied equally to the first and second nodes in course No. 8.

Table 4.10 Calculated values according to ACI 318-05 Appendix A at strut angle of 32^o

Strut angle	f'_m (strut)	f'_m (node)	β_s	β_n	f_{ces}	f_{cen}	A_{css}	A_{csn}	F_{ns}	F_{nn}
	psi (MPa)	psi (MPa)			psi (MPa)	psi (MPa)	in^2 (mm^2)	in^2 (mm^2)	kips (kN)	kips (kN)
32^o	2530 (17.7)	3540 (24.4)	1.0	0.6	2151 (19)	1805 (12.4)	23.6 (15226)	70.4 (45443)	50.7 (226)	127 (565)

For specimens PG127-48 and PG127-48I, ties No. 8 and 9, representing the middle bond beam, reached their yield strength at an applied lateral load of 54.3 kips (242 kN). At that lateral load, the ties were replaced by horizontal tensile loads equal to their yield loads (i.e. 20.33 kips (90 kN)) and applied to the middle bond beam joints, as shown in Figure 4.16; then, the lateral load was increased step by step until strut No. 4 reached its ultimate strength at an applied lateral load of 62.5 kips (278 kN). This lateral load represents 113% of the average peak strengths of two specimens measured during the experimental work.

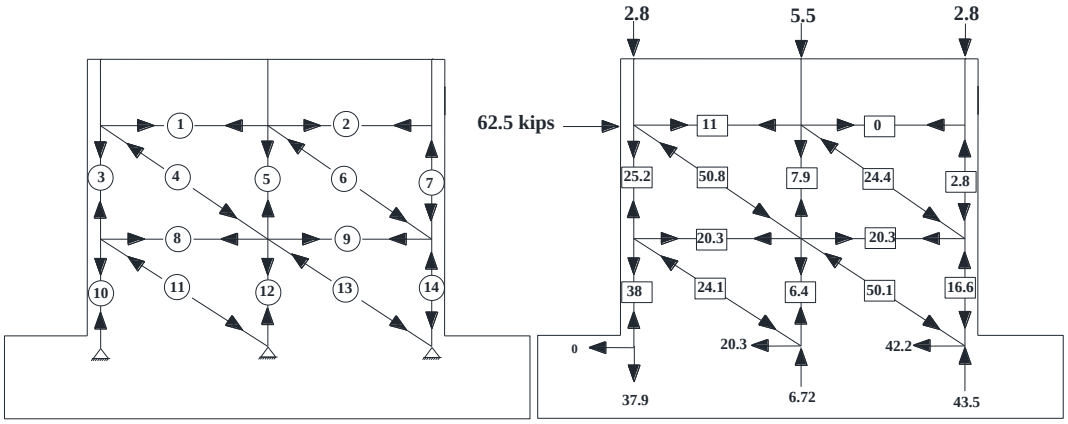

Figure 4.16 Strut and tie model for specimens PG127-48 and PG127-48I

For specimens PG180-48 and PG254-48 with maximum ties strength of 27.2 kips (121 kN) and 40.7 kips (181 kN), respectively, a compression failure occurred in strut No.

13 at a lateral load of 66 kips (294 kN) in both specimens. Yielding of tie No. 9 was achieved at a lateral load of 58.2 kips (259 kN) while in the case of specimen PG253-48 no yielding of the rebar was observed. The calculated strengths using the strut and tie model for specimen PG180-48 and PG253-48 represent 119% and 103% of the average measured peak strengths, respectively.

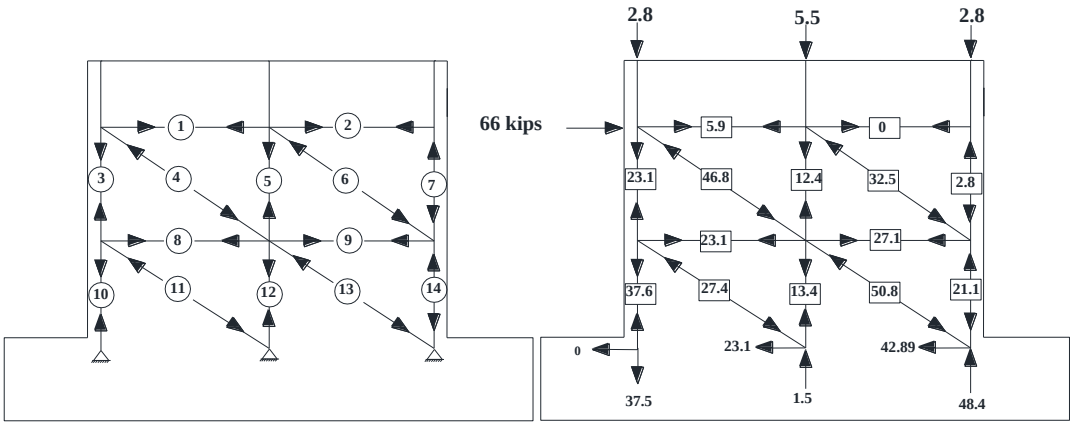

Figure 4.17 Strut and tie model for specimens PG180-48 and PG254-48

While the model presented in Figure 4.17 predicted the minimum lateral force that the wall can resist using a strut and tie model, the model has one shortcoming, it over-predicted the force in the steel reinforcement in bond beam. At lateral forces of 53.5 kips(238 kN), 56.7 kips (252 kN), 55.3 kips (246 kN), and 64.2 kips (286 kN), which represent the average peak lateral forces measured during the experimental forces for specimens PG127-48, PG127-48I, PG180-48, and PG254-48, the strut and tie model indicated that the maximum axial forces in the middle bond beams were approximately 20.3 kips (90 kN) for specimens PG127-48 and PG127-48I, and about 27.1 kips for specimens PG180-48 and PG254-48, respectively. However, the measured axial strains in

the bond beams during the experimental work were 1469 με, 1830 με, 1515 με, and 1284 με corresponding to an axial force of 12.7 kips (57 kN), 16.5 kips (73 kN), 19.33 kips (86 kN), and 23.1 kips (103 kn) for specimens PG127-48, PG127-48I, PG180-48, and PG254-48, respectively. The values indicate that the proposed strut and tie model predicted 62%, 81%, 71%, and 85% of the measured axial force in the bond beam reinforcement.

Other strut and tie models were developed, as shown in Figure 4.18 for specimens PG127-48, PG127-48I, PG1180-48, and PG254-48. In these models, the strut in member No. 4 achieved compression failure at a lateral load of 68 kips (302 kN) without yielding occurring in the ties. This behavior matches the observed behavior during the experimental work. These axial forces in the middle bond beam corresponded to axial forces in the middle rebar of 14.6 kips (65 kN), for specimens PG127-48, PG127-48I, PG1180-48, and PG254-48. These values represent 87%, 113%, 132%, and 158% of the measured axial strains in the rebar during the experimental work, respectively. Finally, a lateral force of 68 kips (302 kN) represents 127%, 119%, 113%, and 106% of the measured peak strengths of specimens PG127-48, PG127-48I, PG1180-48, and PG254-48, respectively.

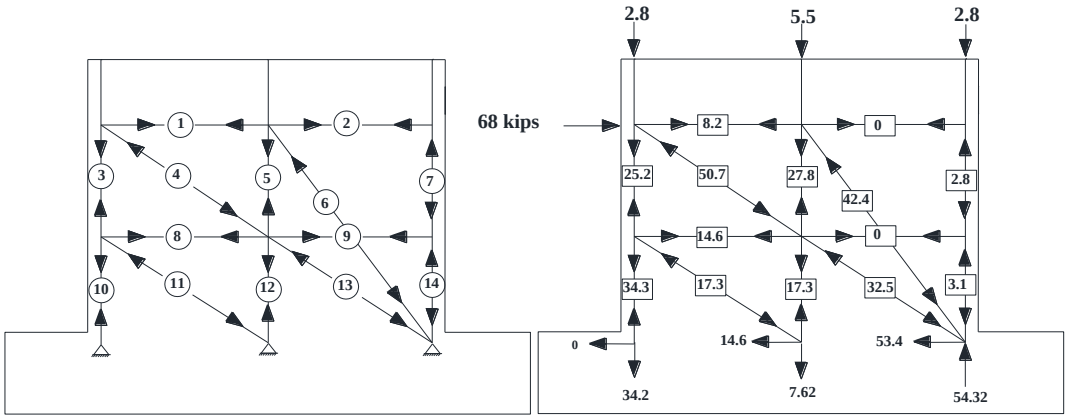

Figure 4.18 Alternative strut and tie model for specimens PG127-48, PG127-48I, PG180-48, and PG254-48

4.6.3 STM for specimen PG127-32

Figure 4.19 shows a strut and tie model for specimen PG127-32. The struts in this model have angles of 44° and 25° with the horizontal bond beam. Table 4.11 shows the predicted ultimate compression force in these struts. The lateral force was applied equally to the first three nodes at the top bond beam. By applying a lateral force of 54.7 kips (243 kN), tie No. 12 reached its yield strength of 20.3 kips (90 kN). Then, this member was removed and replaced with a force equal to the horizontal rebar yield strength of 20.33 kips (90 kN). The analysis was stopped at an applied lateral force of 63.8 kips (284 kN) when strut No. 19 reached its ultimate strength. This applied lateral load represents 83% of the peak strength measured during the experimental load. During the experimental work, yielding of the rebar in the model bond beam was observed as indicated by the strut and tie model.

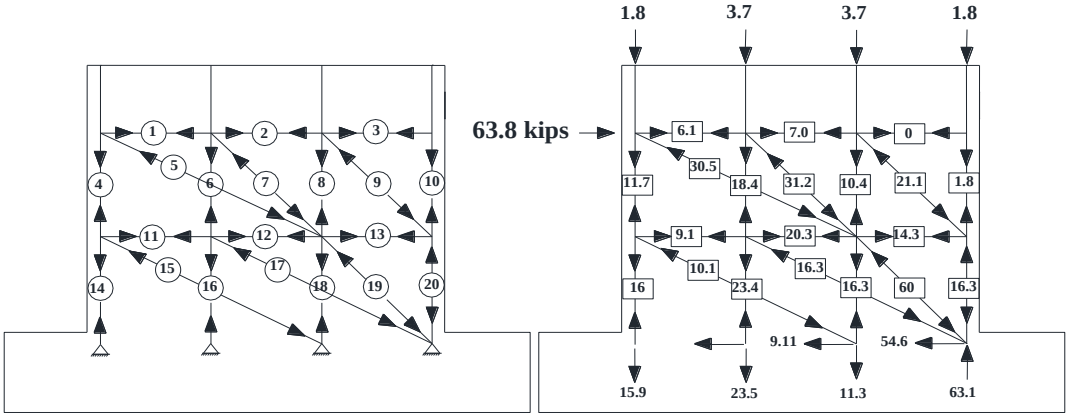

Figure 4.19 Strut and tie model for specimen PG127-32

Table 4.11 Calculated STM values for specimen PG127-32

Strut angle	**f'_m (strut)**	**f'_m (node)**	**β_s**	**β_n**	**f_{ces}**	**f_{cen}**	**A_{css}**	**A_{csn}**	**F_{ns}**	**F_{nn}**
	psi (MPa)	psi (MPa)			psi (MPa)	psi (MPa)	in^2 (mm^2)	in^2 (mm^2)	kips (kN)	kips (kN)
44	2530 (17.7)	3540 (24.4)	1.0	0.6	2151 (19)	1805 (12.4)	27.6 (701)	84.2 (2139)	59.4 (264)	153 (681)
25	2530 (17.7)	3540 (24.4)	1.0	0.6	2151 (19)	1805 (12.4)	22.1 (561)	67.5 (1715)	47.65 (212)	124 (550)

A second strut and tie model was investigated, as shown in Figure 4.13. However, this strut and tie model yielded significantly higher lateral loads of 95 kips (423 kN).

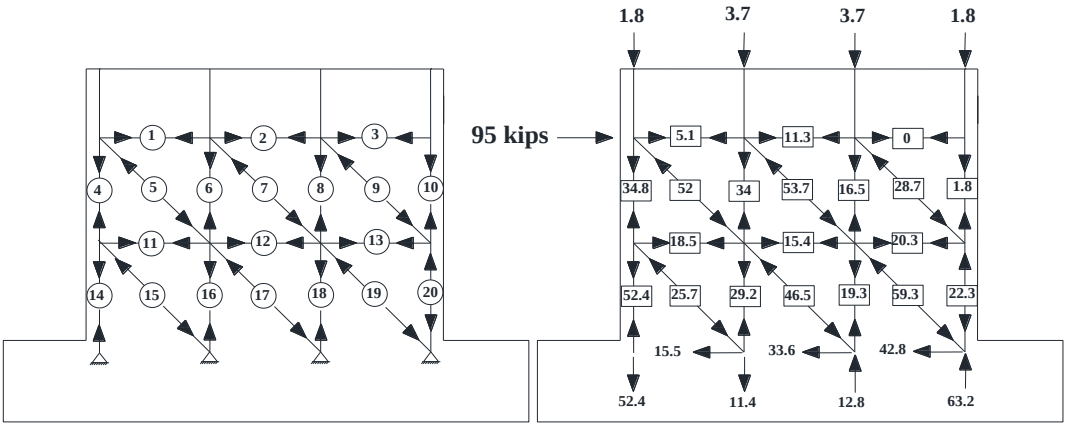

Figure 4.20 Alternative strut and tie model for specimen PG127-32

4.6.4 STM for specimen PG127-24

The lateral force in this model was applied equally to the first four nodes. The compressive strengths of the struts of this model are shown in Table 4.12. At a lateral force of 86.3 kips (384 kN), tie No. 15 reached its yield strength of 20.33 kips (90 kN). This member was then replaced by two forces equal to its yield strength. As the applied load was increased to 96 kips (427 kN), strut No. 25 reached its maximum compression strength and the analysis was stopped.

Table 4.12 Calculated STM values for specimen PG127-24

Strut angle	**f'_m (strut)**	**f'_m (node)**	**β_s**	**β_n**	**f_{ces}**	**f_{cen}**	**A_{css}**	**A_{csn}**	**F_{ns}**	**F_{nn}**
	psi (MPa)	psi (MPa)			psi (MPa)	psi (MPa)	in^2 (mm^2)	in^2 (mm^2)	kips (kN)	kips (kN)
52	2530 (17.7)	3540 (24.4)	1.0	0.6	2151 (19)	1805 (12.4)	32.3 (820)	99 (2504)	69.5 (309)	179 (796)
32	2530 (17.7)	3540 (24.4)	1.0	0.6	2151 (19)	1805 (12.4)	23.7 (602)	72.2 (1834)	50.9 (226)	132 (587)

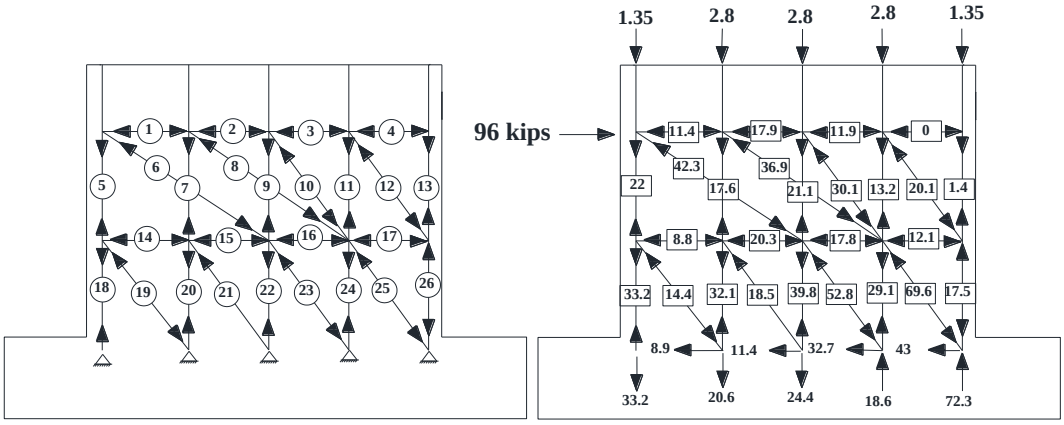

Figure 4.21 Strut and tie model for specimens PG127-24

4.7 STM vs. Experimental Results.

The comparison between the strut and tie model and the experimental results are shown in Table 4.13. As shown in the table, the strut and tie model predicted the peak strengths of the test specimens within approximately ±20% of the measured average peak strengths.

Table 4.13 Strut and tie models vs. experimental results

Wall ID	**PG127-48**	**PG127-48I**	**PG180-48**	**PG254-48**	**PG127-32**	**PG127-24**
V_{exp}/ V_{STM}	0.79	0.83	0.81	0.94	1.2	0.95

CHAPTER 5

CONCLUSION

5.1 Summary

The general purpose of this research was to examine and better understand the seismic behavior of partially grouted masonry shear walls. Effects of grout horizontal spacing and horizontal reinforcement ratio were investigated. The objectives of this research were achieved through experimentally testing six partially grouted masonry shear walls under in-plane lateral cyclic loading. The walls had an aspect ratio of 0.58, the grout horizontal spacing ranged from 24 in. (610 mm) to 48 in. (1219 mm), and the horizontal reinforcement ratio ranged from 0.127% to 0.254%. The test results were analyzed and compared to the shear strengths predicted by the MSJC (2008). In addition, the measured shear strengths were compared to the design equations proposed by Nolph (2010). Finally, strut and tie models were developed for the test specimens.

5.2 Conclusion

The experimental and analytical work presented in this thesis revealed that:

- There seems to be a threshold horizontal reinforcement ratio beyond which any increase in the shear reinforcement does not yield any increase in the strength of the shear walls since failure occurred due to compression strut failure.
- Decreasing the grout horizontal spacing significantly improved the strength of the investigated shear walls.

- The current MSJC (2008) shear design equation for partially grouted masonry shear walls is highly un-conservative and over-estimated the shear strength capacity for the tested walls. The over-estimation in the predicted shear strengths using the current MSJC (2008) ranged from 60 to 91%.
- Using the shear design equations proposed by Nolph (2010) led to better estimation of the shear strengths of the test specimens. Nolph's equations predicted 93% to 112% of the measured peak strengths.
- Strut and tie models were able to predict the shear strength of the tested specimens within ±20%.

Figure 5.1 shows a comparison between the measured average peak strength of each specimen and the predicted strength using the MSJC (2008) equations, Nolph's equations, and strut and tie models.

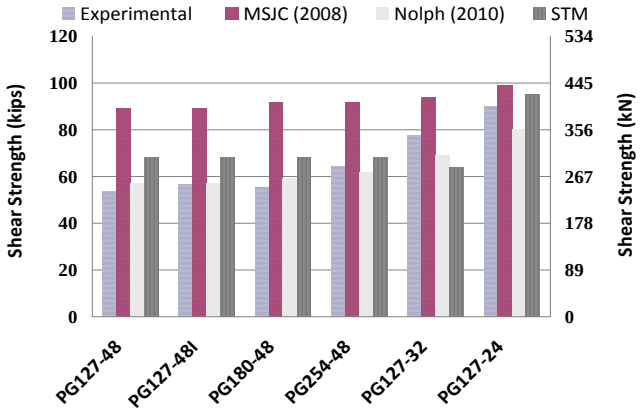

Figure 5.1 Compression between V_{exp}, V_n, $V_{n,n3}$, and V_{STM}

REFERENCES

American Concrete Institute: 2005, *Building Code Requirements for Structural Concrete (ACI 318-05) and Commentary (ACI 318R-05)*, Farmington Hills, MI.

ASTM Standard C 140, "Standard Test Methods for Sampling and Testing Concrete Masonry Units and Related Units," ASTM International, West Conshohocken, PA, www.astm.org

ASTM Standard C 270, "Standard Specification for Mortar for Unit Masonry," ASTM International, West Conshohocken, PA, www.astm.org

ASTM Standard C 476, "Standard Specification for Grout for Masonry," ASTM International, West Conshohocken, PA, www.astm.org

Brandow, G.E., Ekwueme, C.G., Hart G.C., *2006 Design of Reinforced Masonry Structures*, Concrete Masonry Association of California and Nevada, Citrus Heights, CA, 2007.

Davis, C.L. "Evaluation of Design Provisions For In-Plane Shear In Masonry Walls", Washington State University, Masters Thesis, Dec 2008.

Elmapruk, J.H., ElGawady, M.A., "Evaluation of the MSJC 2008 Shear Strength Equations For Partially Grouted Masonry Shear Walls." 11th Canadian Masonry Symposium, Toronto, Ontario, May 31-June 3, 2009.

Fattal, S. G. (1993a) "Strength of partially-grouted masonry shear walls under lateral loads," NISTIR 93-5147, Gaithersburg, MD.

Fattal, S. G. (1993b) "The effect of critical parameters on the behavior of partially grouted masonry shear walls under lateral loads," NISTIR 93-5147, Gaithersburg, MD

FEMA 356: Prestandard and Commentary for the Seismic Rehabilitation of Buildings, Federal Emergency Management Agency, Washington, D.C., Nov 2000

Maleki, Majid "Behaviour of Partially Grouted Reinforced Masonry Shear Walls Under Cyclic Reversed Loading" University of McMaster, PhD Thesis, June 2008.

Masonry Standards Joint Committee: 2008, *Building Code Requirements for Masonry Structures*, TMS 402-08, The Masonry Society, Boulder, CO, ACI 530-08, American Concrete Institute, Farmington Hills, MI, ASCE 5-08, American Society of Civil Engineers, Reston, VA.

Matsumura, A. (1985) "Effect of Shear Reinforcement in Concrete Masonry Walls," First Joint Technical Coordinating Committee on Masonry Research, U.S.-Japan Coordinated Earthquake Research Program, Tokyo, Japan, August 26 - 27, 1985

Matsumura, A. (1986) "Shear strength of reinforced hollow unit masonry walls," Second Meeting of the U.S.-Japan Joint Technical Coordinating Committee on Masonry Research, Keystone, Colorado

Minaie, Ehsan 'Behavior and Vulnerability of Reinforced Masonry Shear Walls' Drexel University, PhD Thesis, August 2009.

New Zealand Standard 4230:2004, *Design of Reinforced Concrete Masonry Structures*, Standards Association of New Zealand, Wellington.

Nolph, Shown 'IN-PLANE SHEAR PERFORMANCE OF PARTIALLY GROUTED MASONRY SHEAR WALLS' Washington State University, M.Sc. Thesis, August 2010.

Priestley, M.J.N., Calvi, G.M., Kowalsky, M.J., *Displacement-Based Seismic Design of Structures*, IUSS Press, Italy, 978-88-6198-000-6, 2007.

Priestley, M.J.N., Seible, F., Calvi, G.M., *Seismic Design and Retrofit of Bridges*, Wiley, New York, NY, 0-471-57998-X, 1996.

Voon, K.C. and Ingham J. M. (2006) “Experimental In-Plane Shear Strength Investigation of Reinforced Concrete Masonry Walls”, Journal of Structural Engineering, Vol. 132, No. 3, pp. 400-408

Voon, K.C. "In-Plane Seismic Design of Concrete Masonry Structures", University of Auckland, PhD Thesis, June 2007.

Wight, G.D., Kowalsky, M.J., Ingham, J.M., "Direct Displacement-Based Seismic Design of Unbonded Post-Tensioned Masonry Walls." *ACI Structural Journal*, Sept-Oct 2007, pp560-569.

Appendix A
The hysteresis loops for the tested specimens

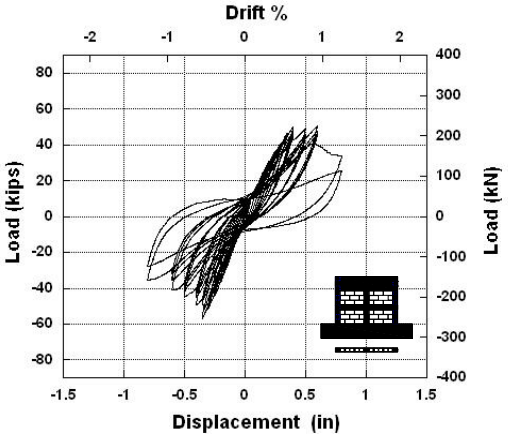

Actuator vs. Load

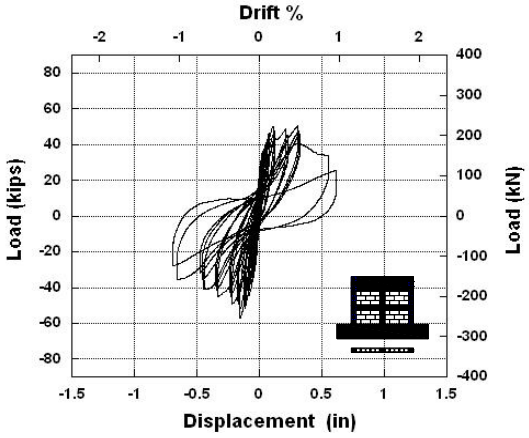

Main jack vs. Load

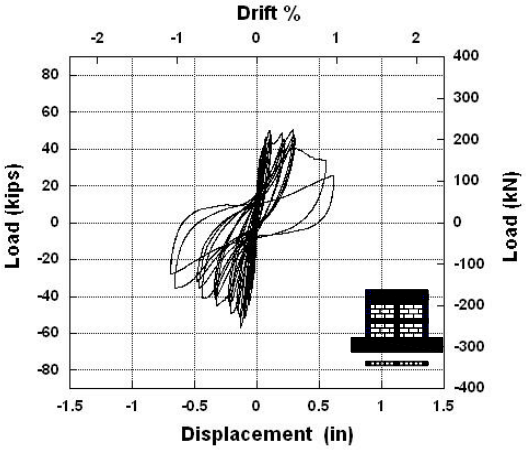

Top of the wall vs. load

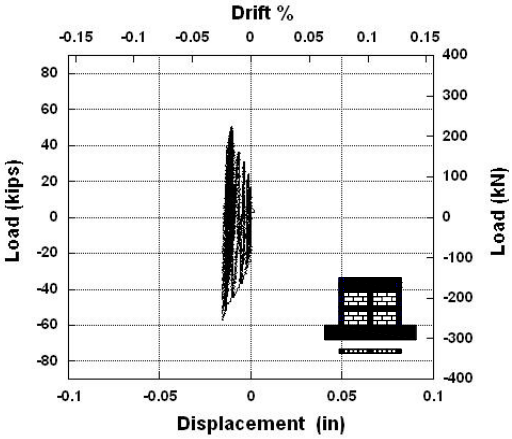

Foundation vs. Load

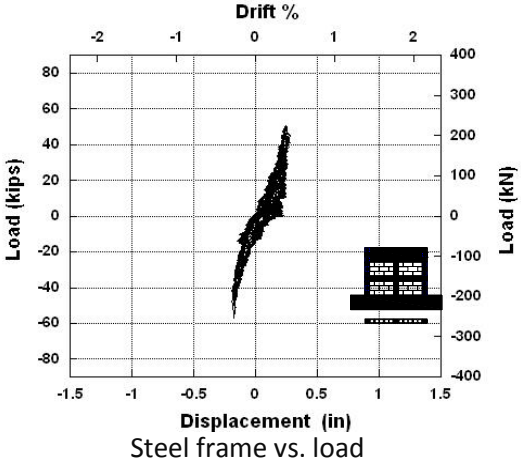

Steel frame vs. load

Figure A.1 Hysteresis loops for Specimen PG127-48

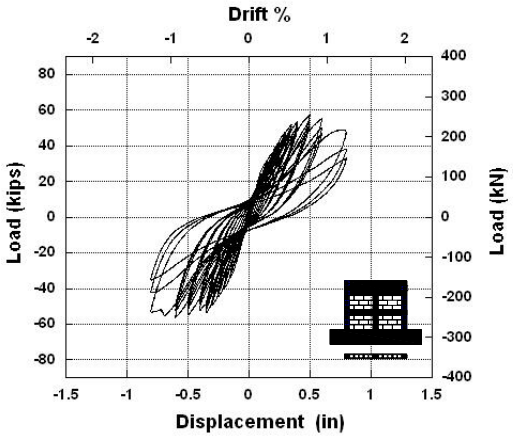

Actuator vs. Load

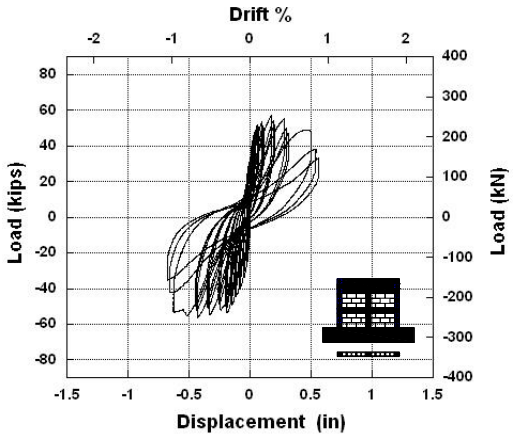

Main jack vs. Load

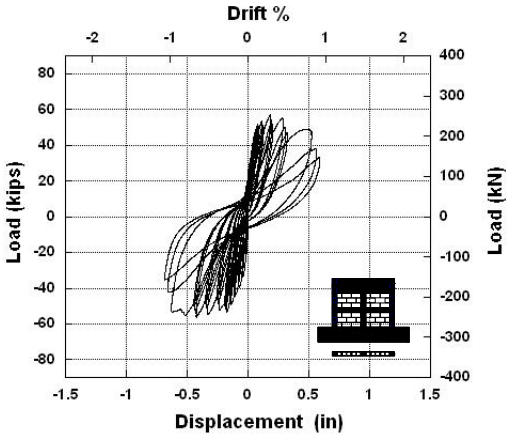

Top of the wall vs. load

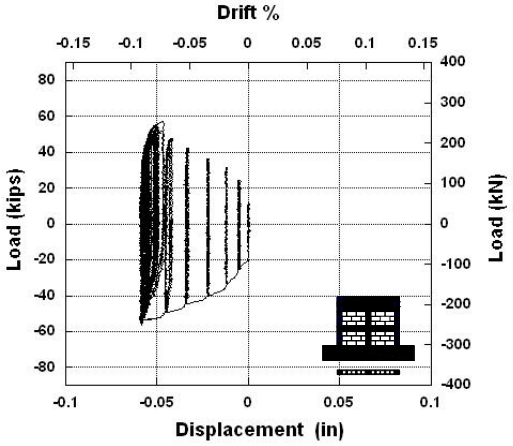

Foundation vs. Load

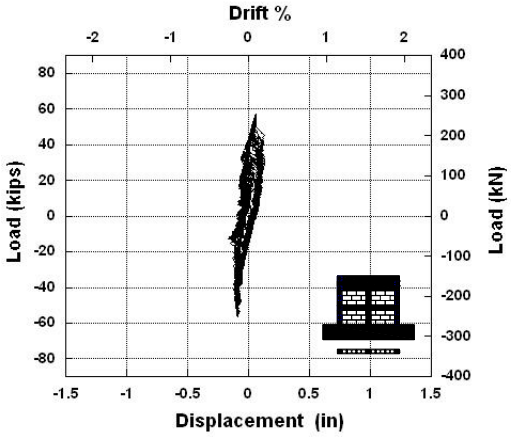

Steel frame vs. load

Figure A.2 Hysteresis loops for Specimen PG127-48I

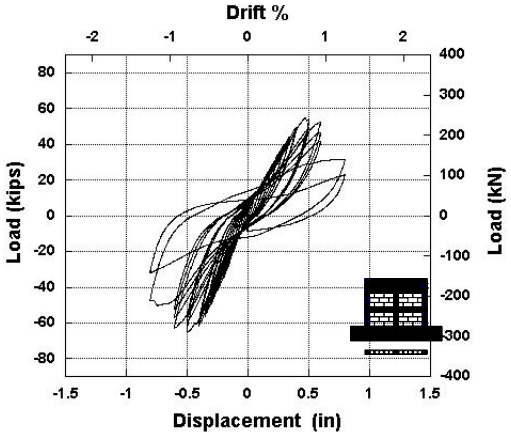

Actuator vs. Load

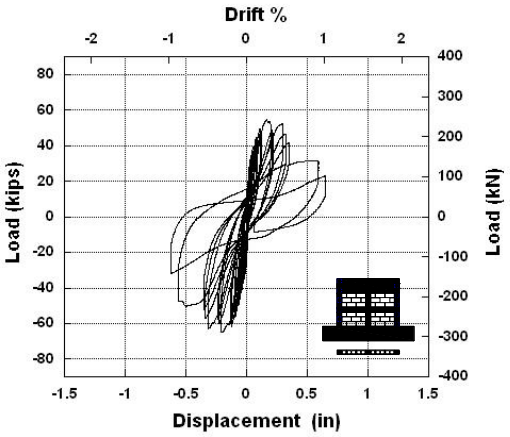

Main jack vs. Load

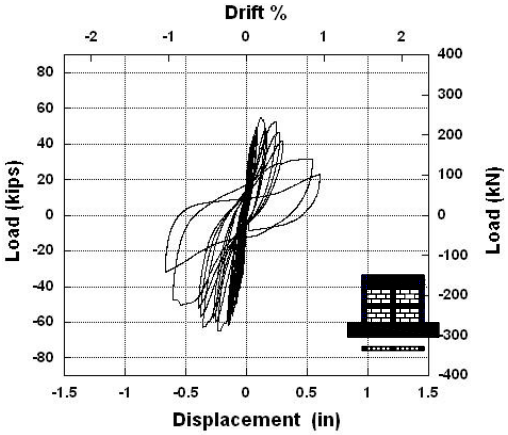

Top of the wall vs. load

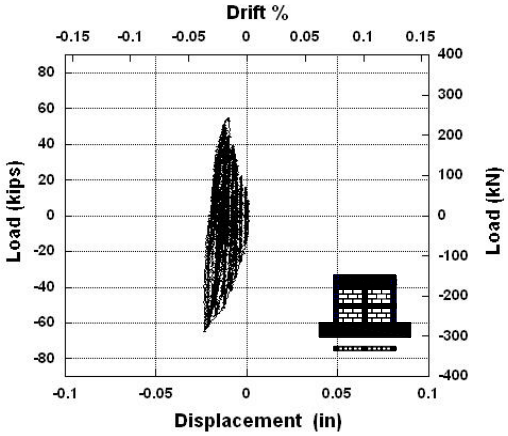

Foundation vs. Load

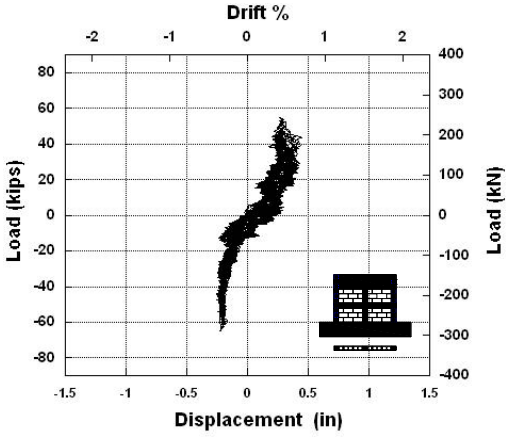

Steel frame vs. load

Figure A.3 Hysteresis loops for Specimen PG180-48

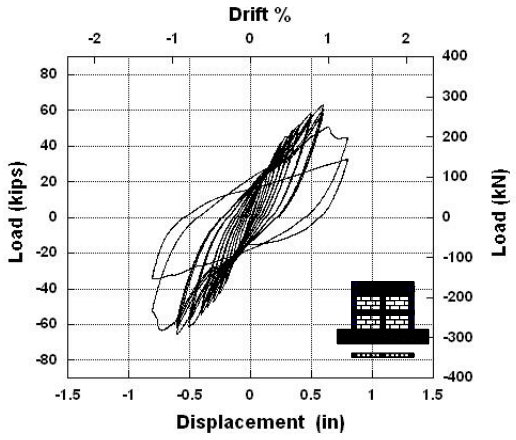

Actuator vs. Load

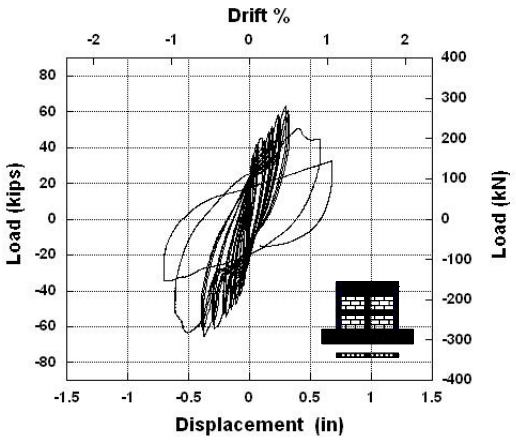

Main jack vs. Load

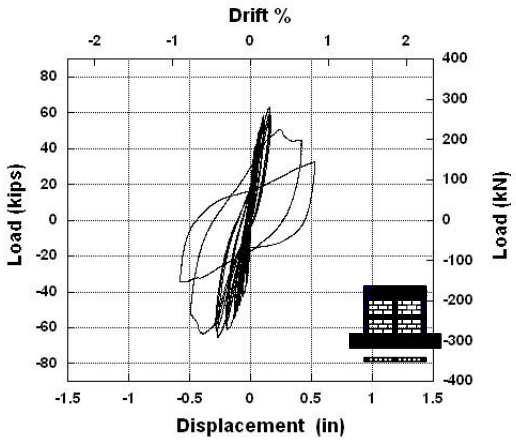

Top of the wall vs. load

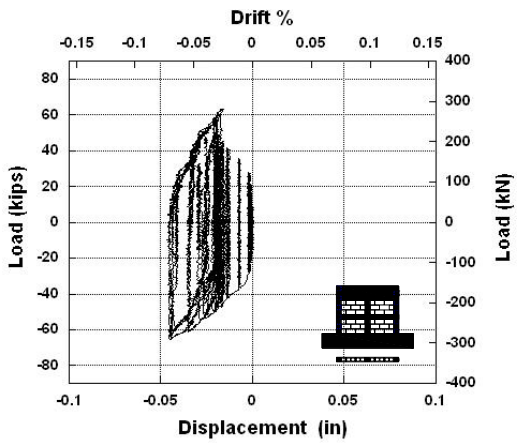

Foundation vs. Load

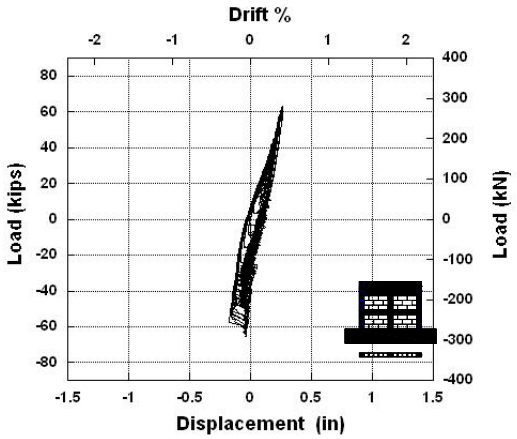

Steel frame vs. load

Figure A.4 Hysteresis loops for Specimen PG254-48

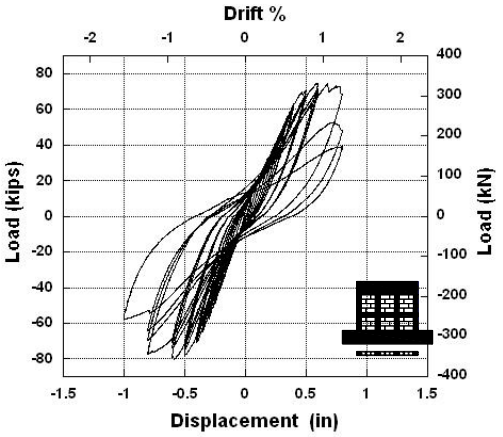

Actuator vs. Load

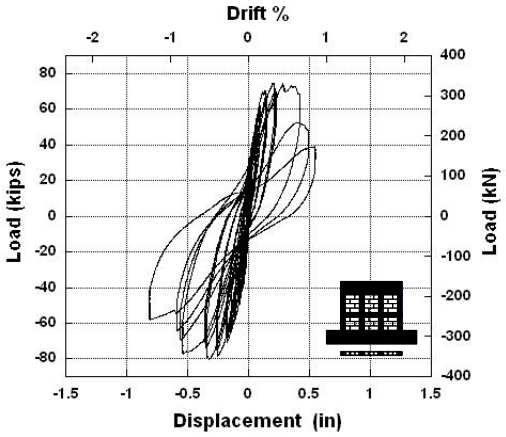

Main jack vs. Load

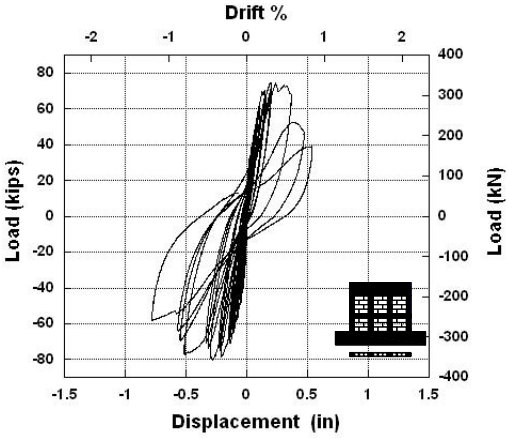

Top of the wall vs. load

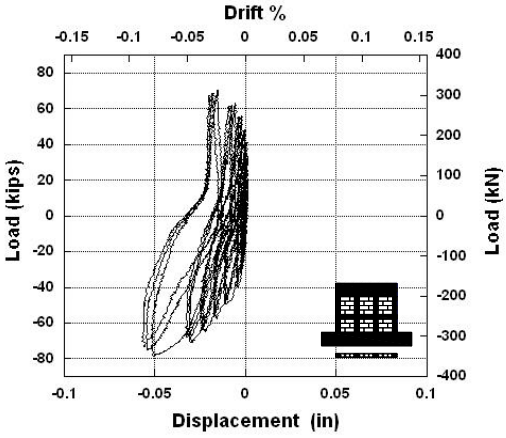

Foundation vs. Load

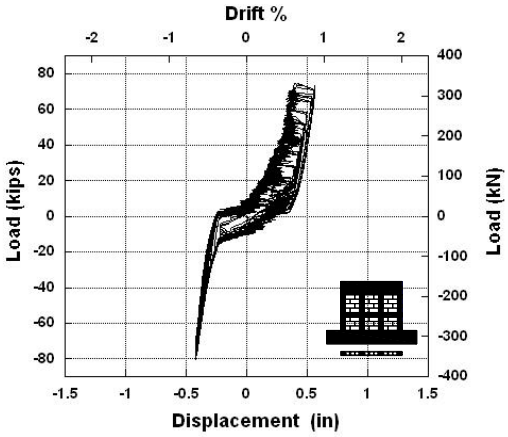

Steel frame vs. load

Figure A.5 Hysteresis loops for Specimen PG127-32

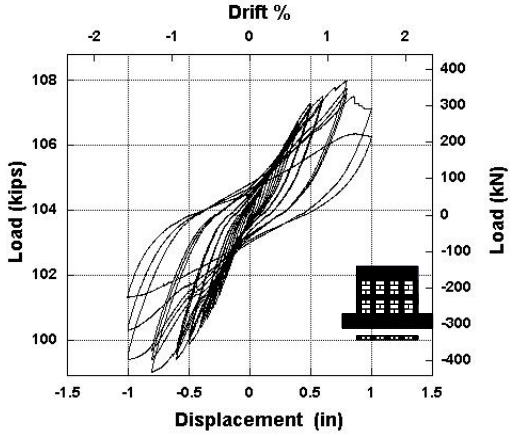

Actuator vs. Load

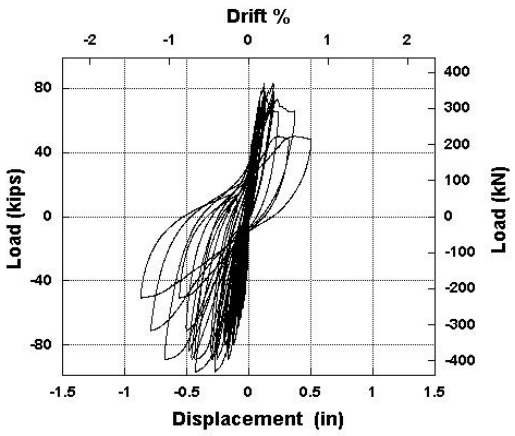

Main jack vs. Load

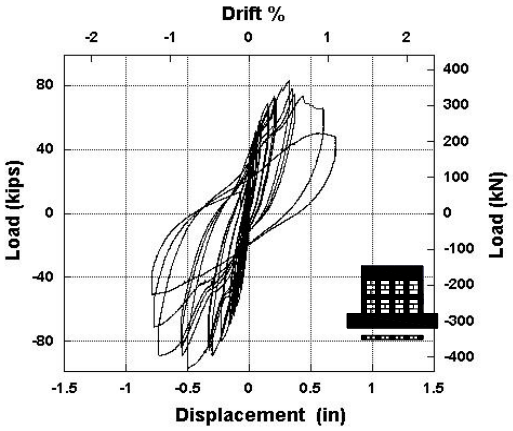

Top of the wall vs. load

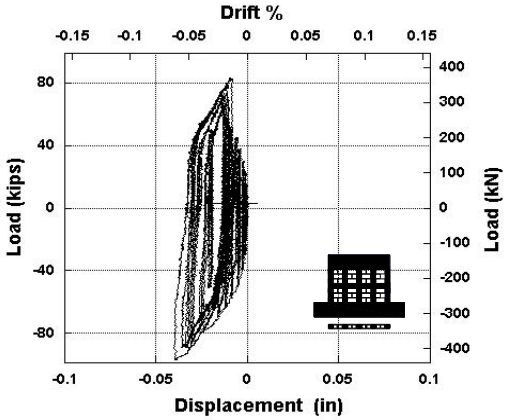

Foundation vs. Load

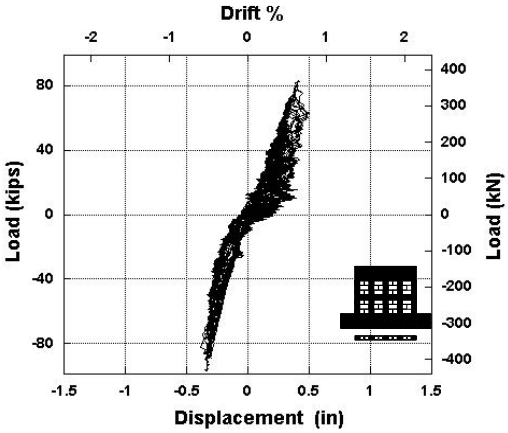

Steel frame vs. load

Figure A.6 Hysteresis loops for Specimen PG127-24

APPENDIX B
HORIZONTAL STRAIN GAGE HYSTERESIS

B.1 Specimen PG127-48

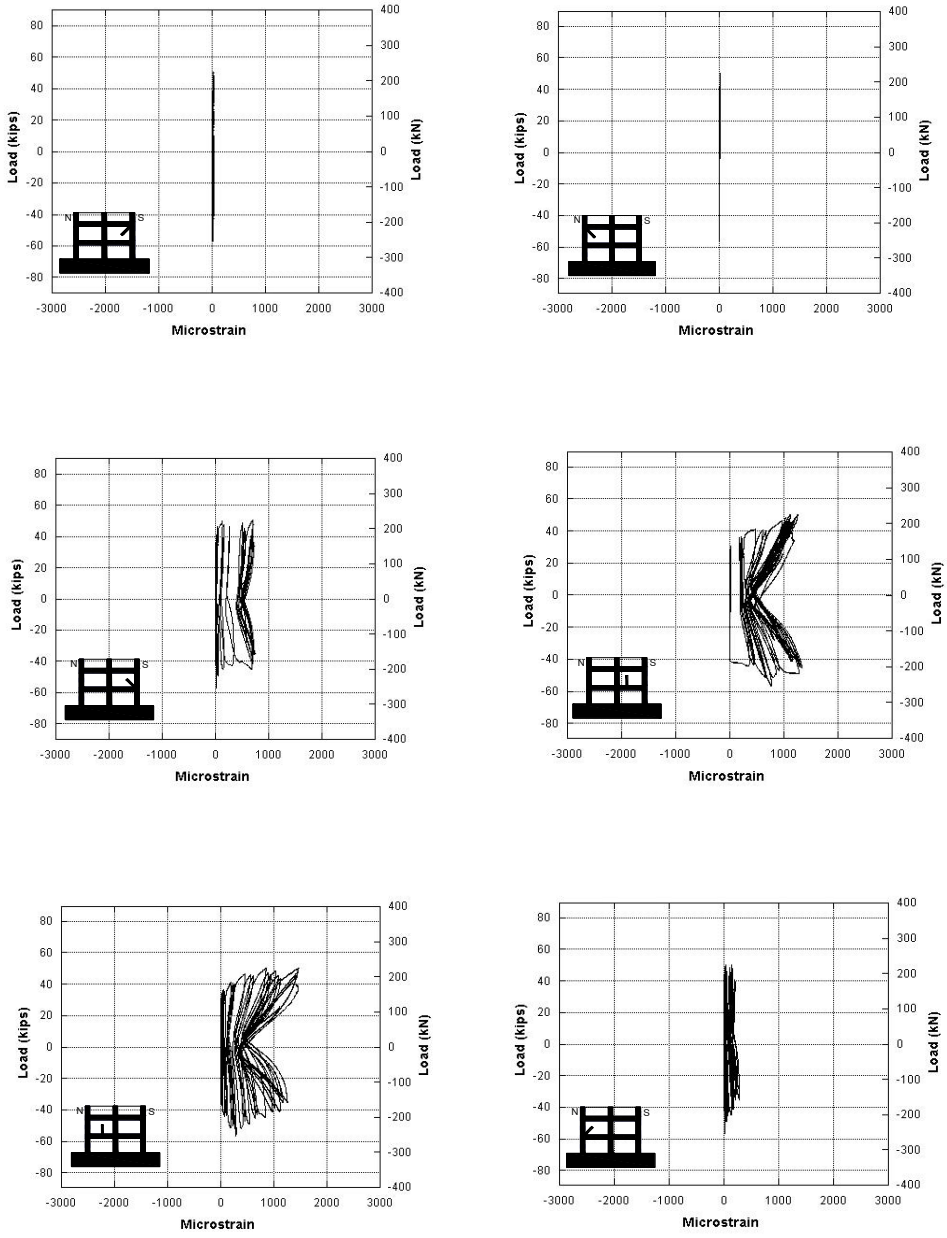

Figure B.1 Horizontal reinforcement hysteresis for specimen PG127-48

B.2 Specimen PG127-48I

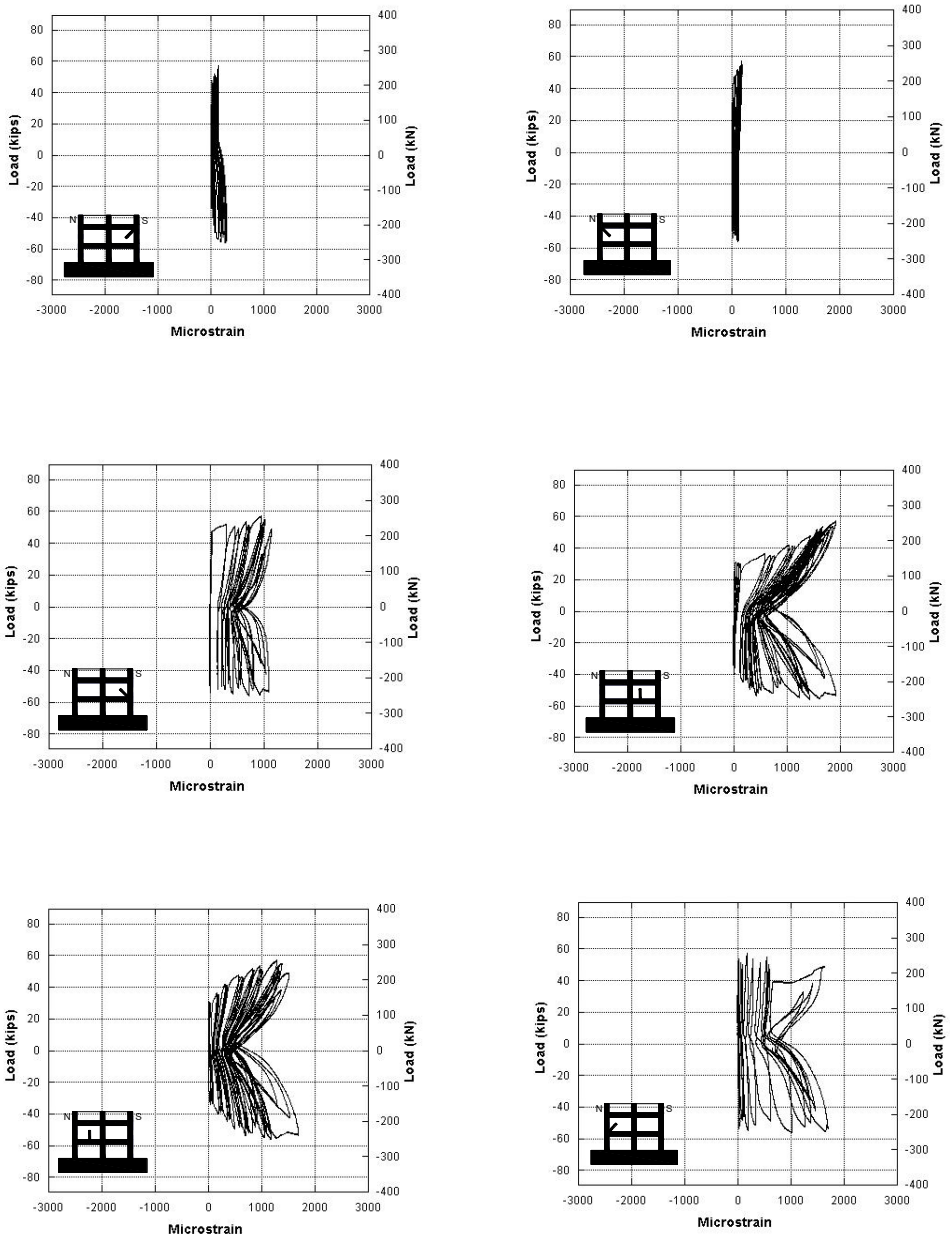

Figure B.2 Horizontal reinforcement hysteresis for specimen PG127-48I

B.3 Specimen PG180-48

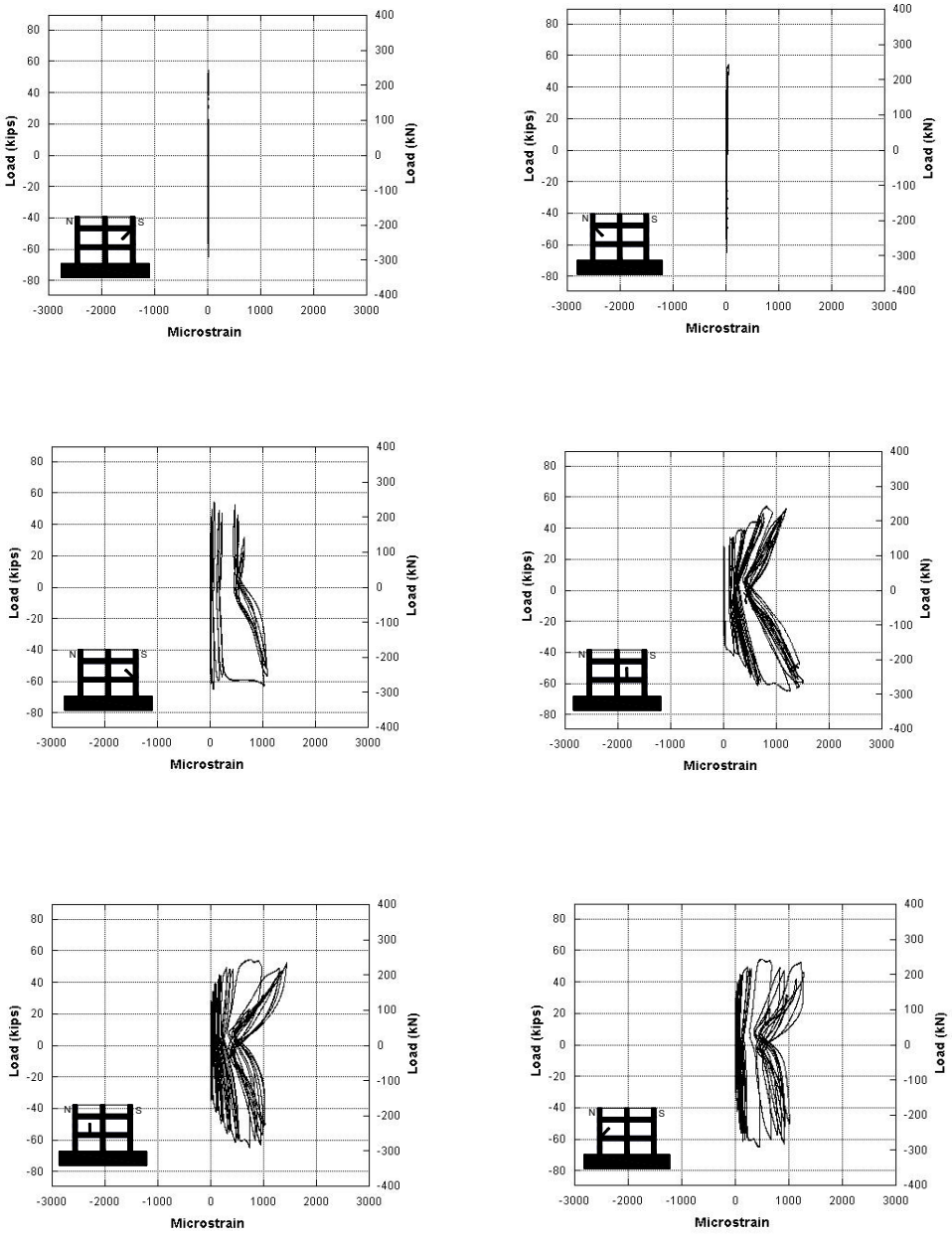

Figure B.3 Horizontal reinforcement hysteresis for specimen PG180-48

B.4 Specimen PG254-48

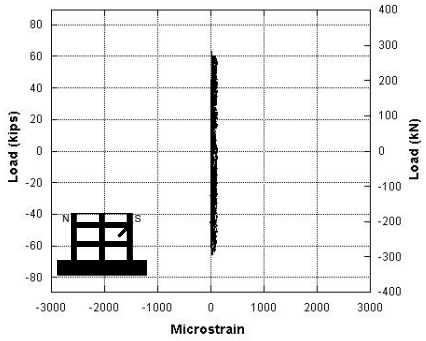

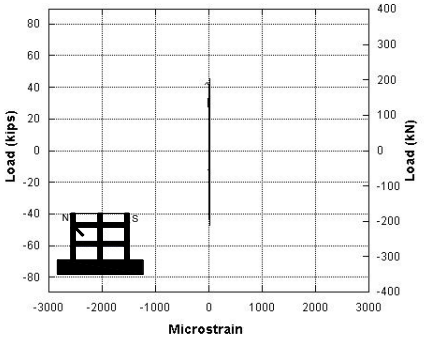

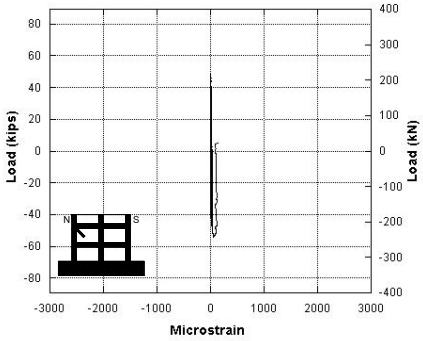

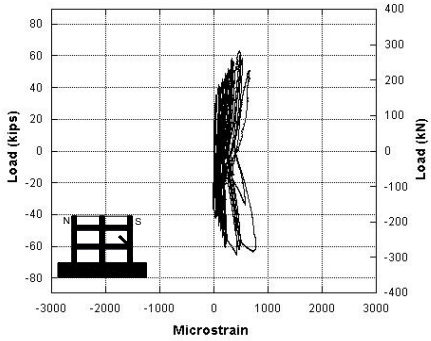

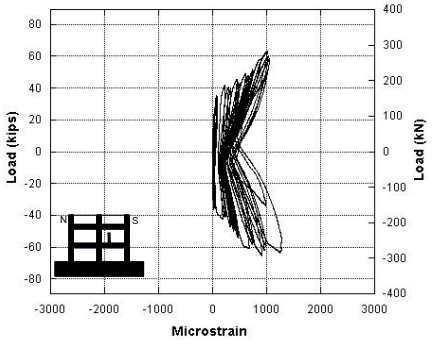

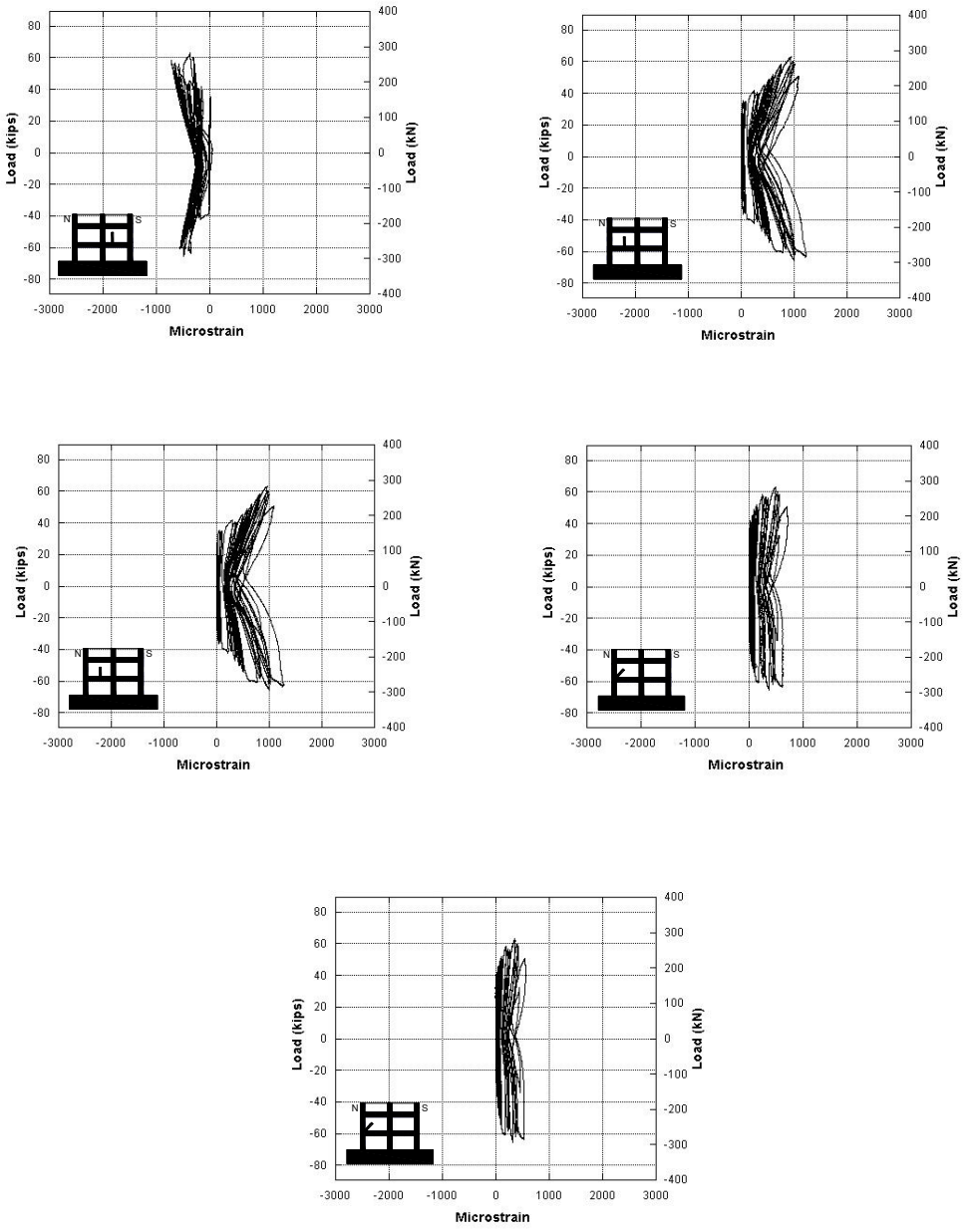

Figure B.4 Horizontal reinforcement hysteresis for specimen PG254-48

B.5 Specimen PG127-32

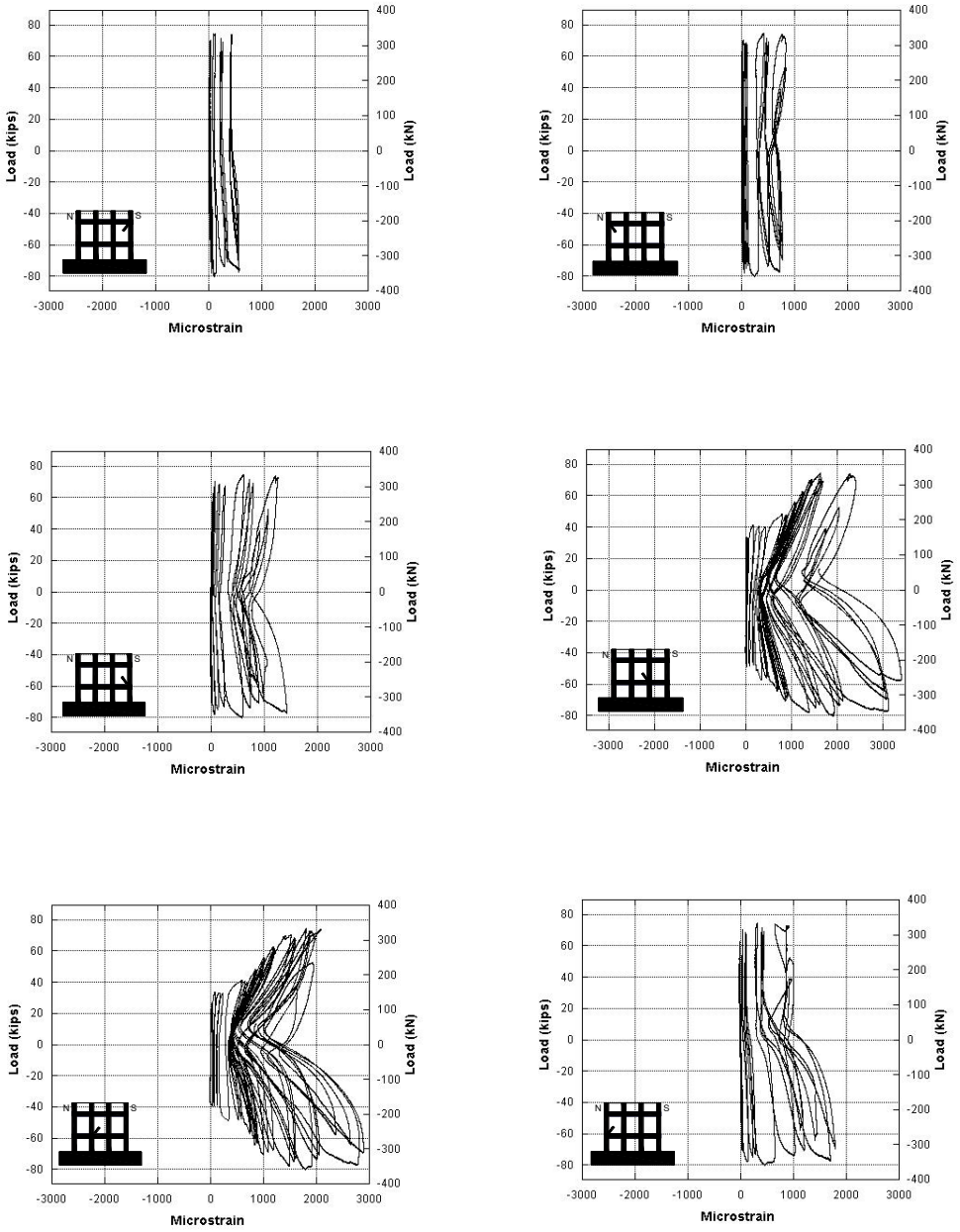

Figure B.5 Horizontal reinforcement hysteresis for specimen PG127-32

B.6 Specimen PG127-24

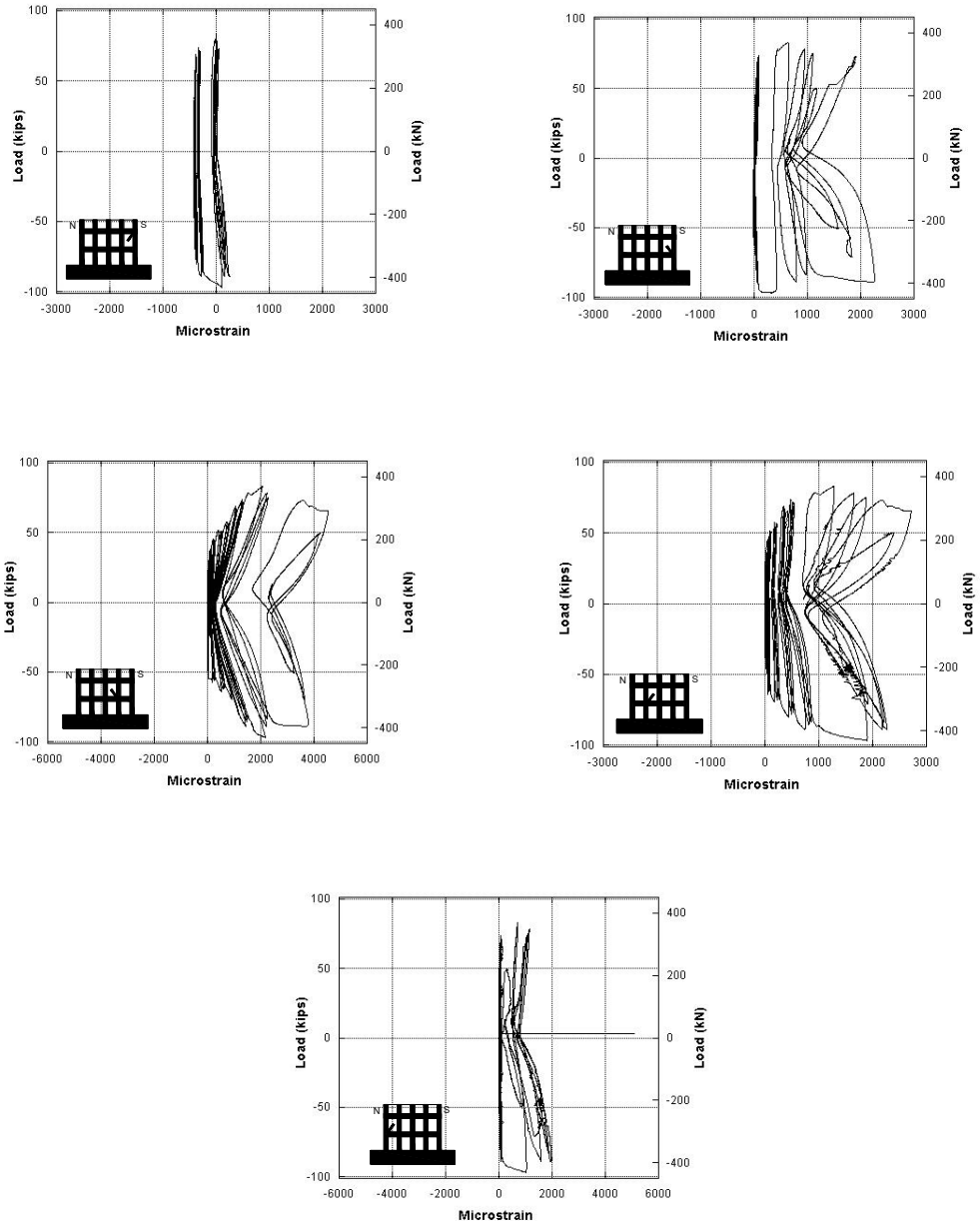

Figure B.6 Horizontal reinforcement hysteresis for specimen PG127-24

APPENDIX C
VERTICAL STRAIN GAGE HYSTERESIS

C.1 Specimen PG127-48

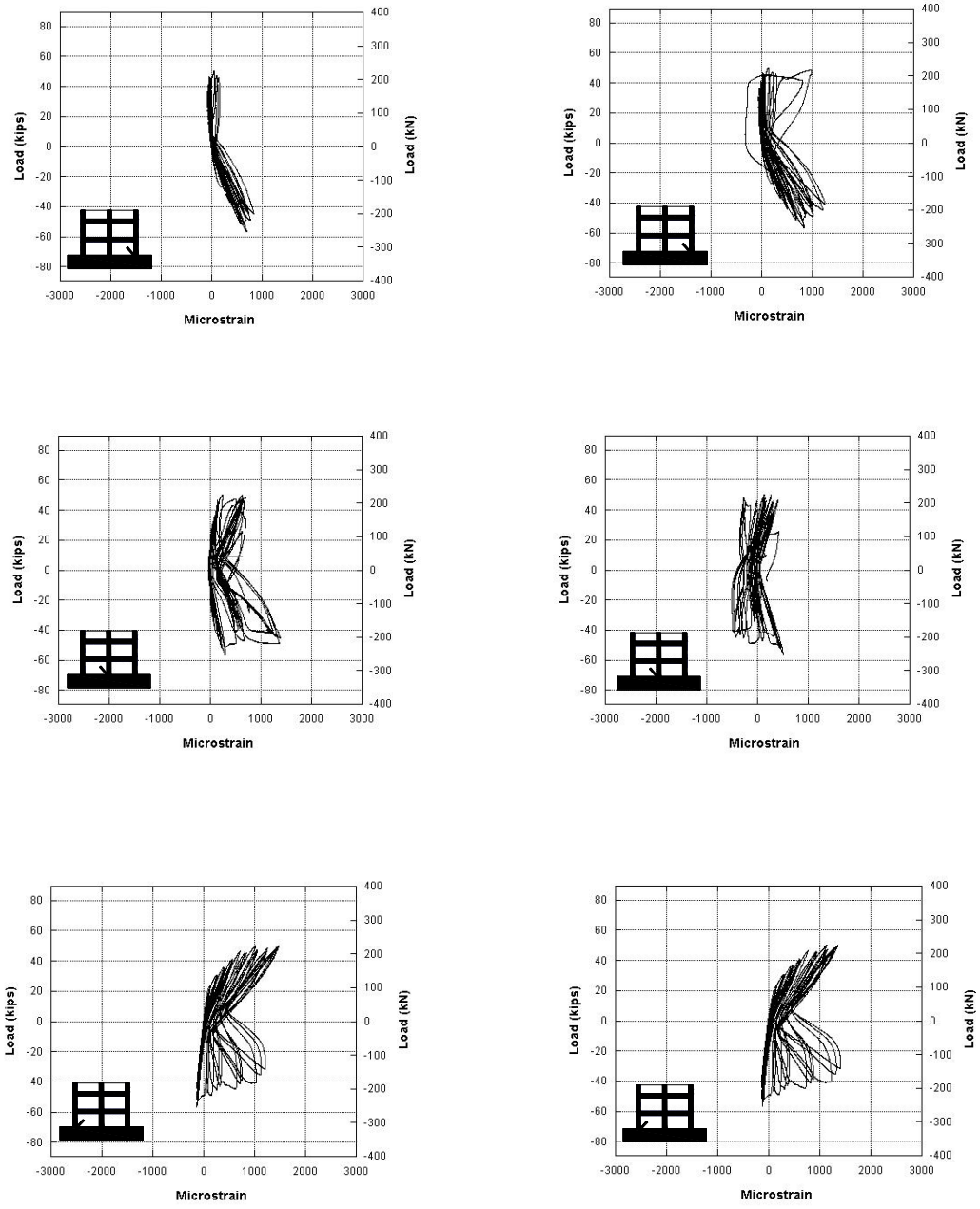

Figure C.1 Vertical reinforcement hysteresis for specimen PG127-48

C.2 Specimen PG127-48I

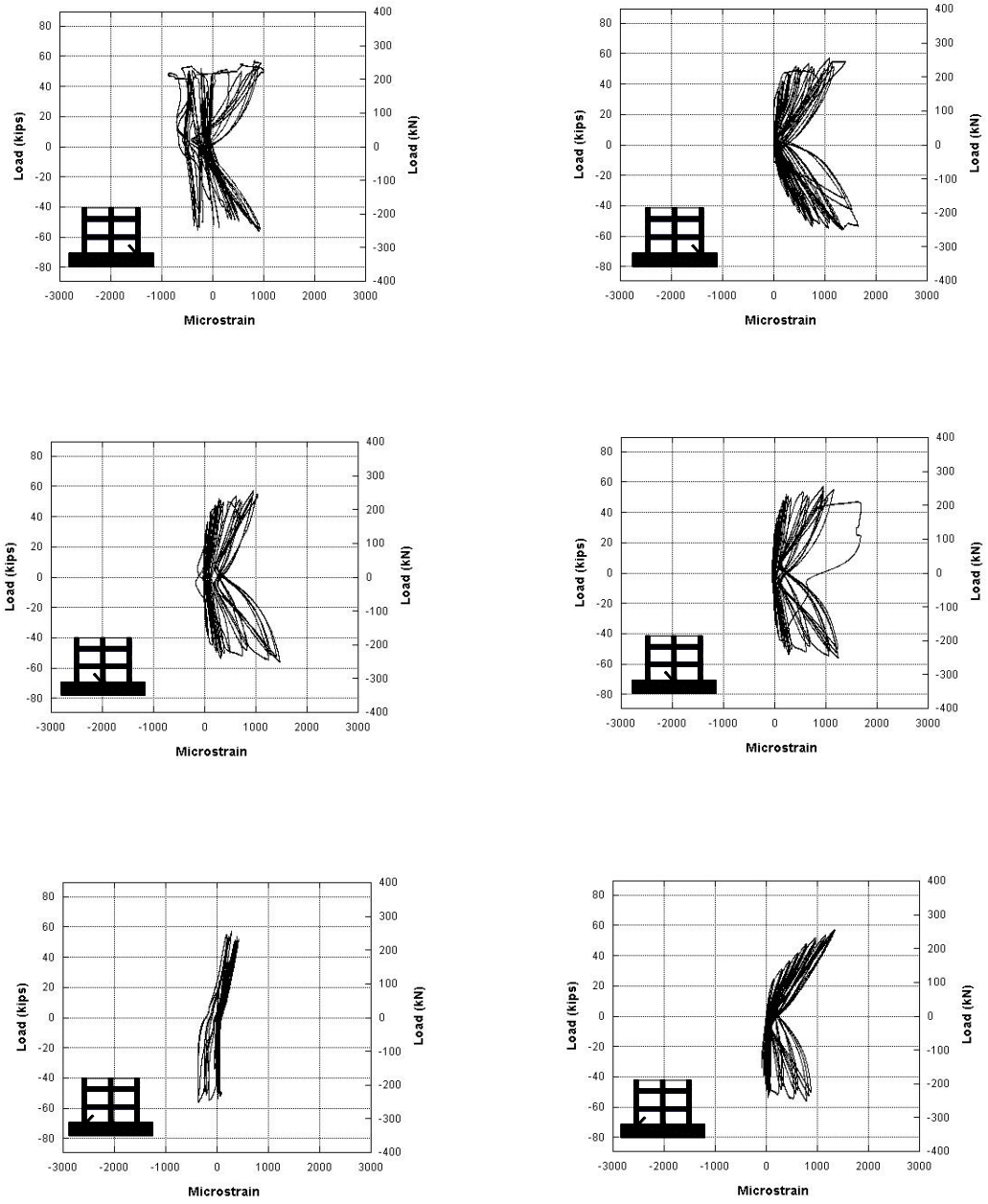

Figure C.2 Vertical reinforcement hysteresis for specimen PG127-48I

C.3 Specimen PG180-48

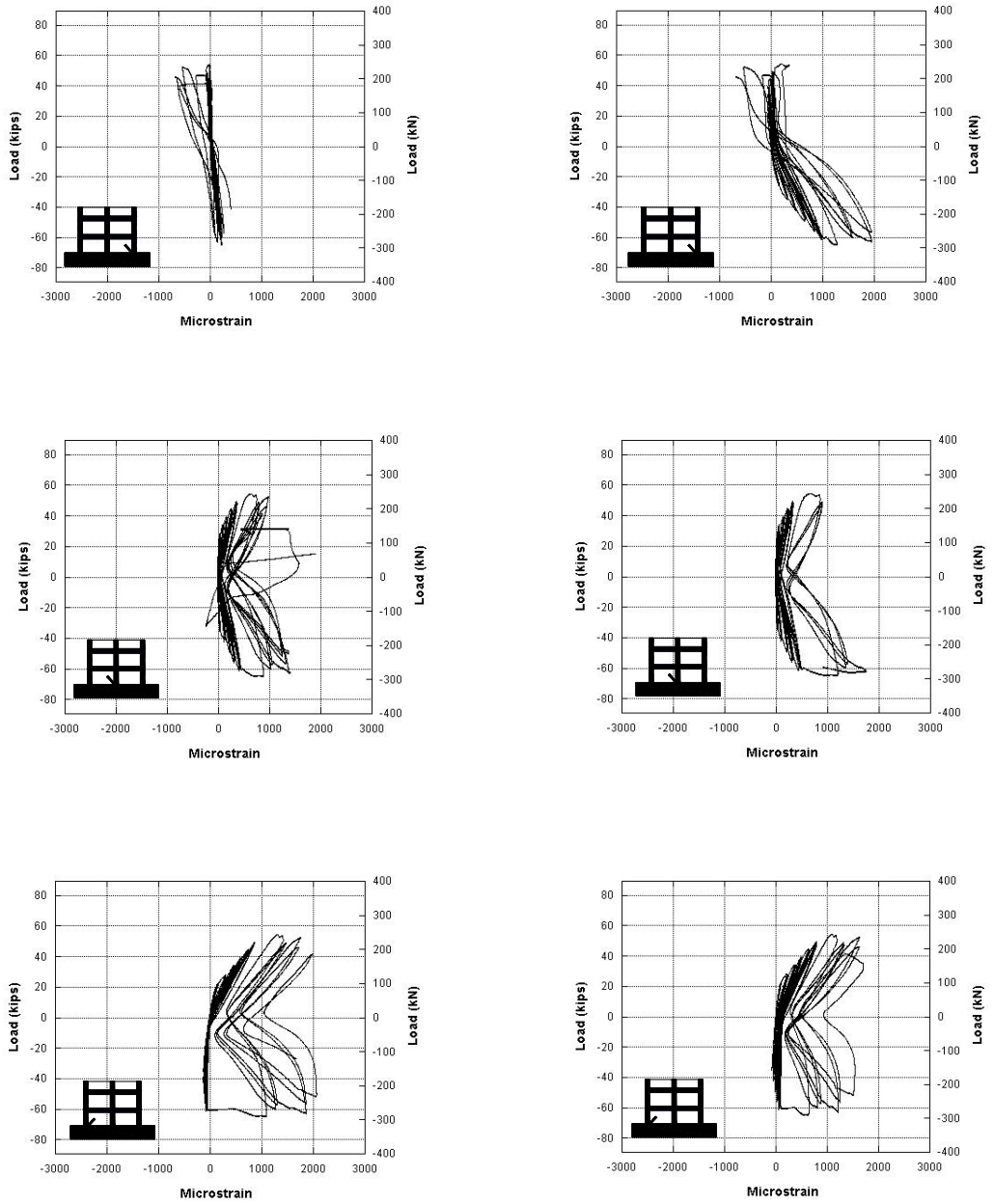

Figure C.3 Vertical reinforcement hysteresis for specimen PG180-48

C.4 Specimen PG254-48

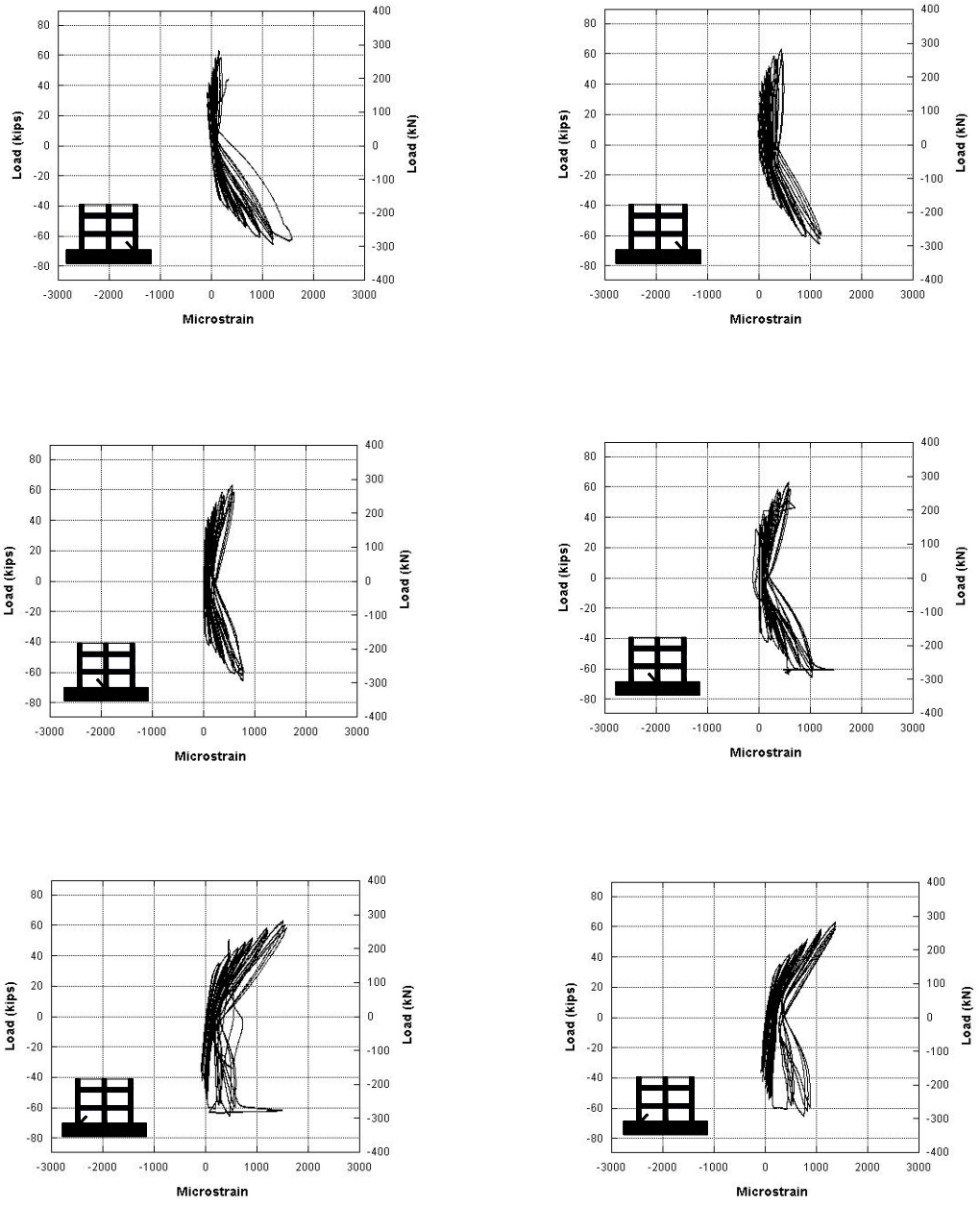

Figure C.4 Vertical reinforcement hysteresis for specimen PG254-48

C.5 Specimen PG127-32

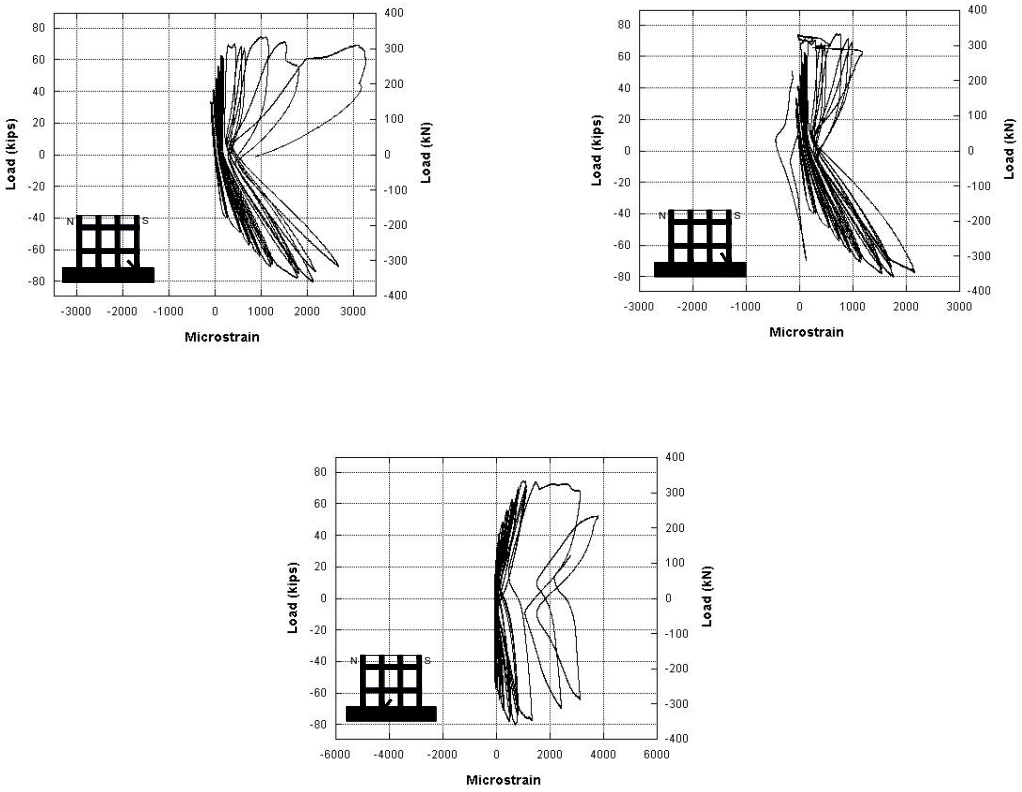

Figure C.5 Vertical reinforcement hysteresis for specimen PG127-32

C.6 Specimen PG127-24

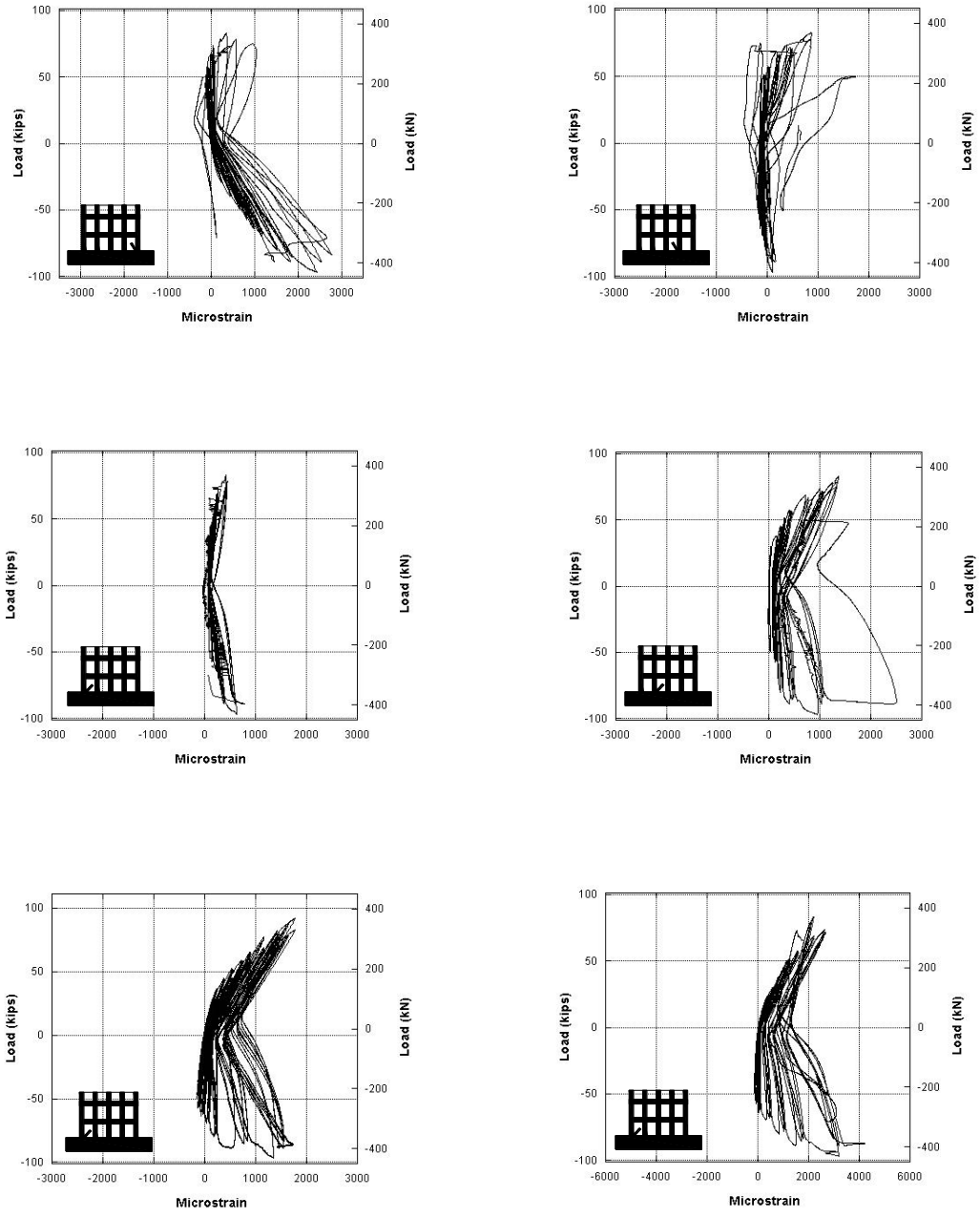

Figure C.6 Vertical reinforcement hysteresis for specimen PG127-24

APPINDEX D
LOCATION OF STRAIN GAGES

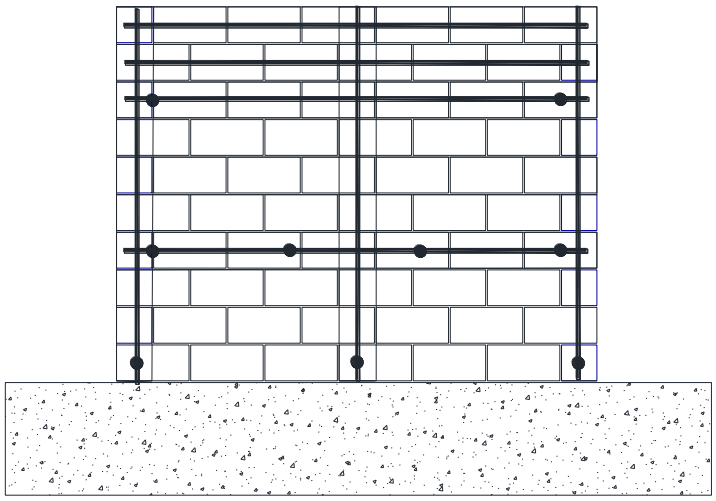

Figure D.1 Location of strain gages for PG127-48, PG127-48I, PG180-48, and PG254-47

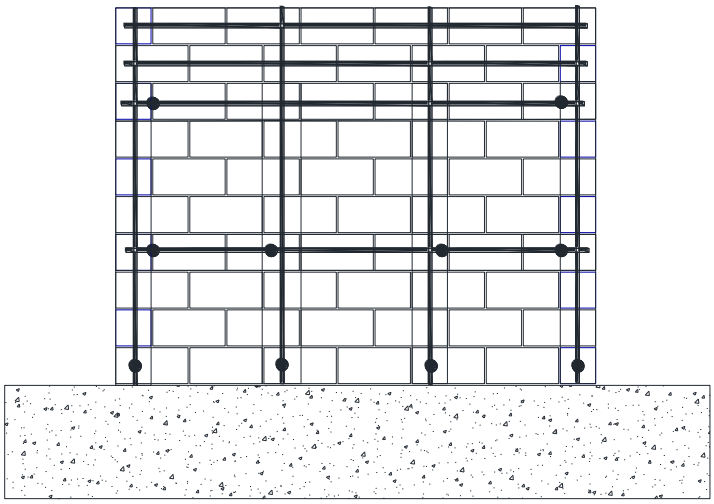

Figure D.2 Location of strain gages for specimen PG127-32

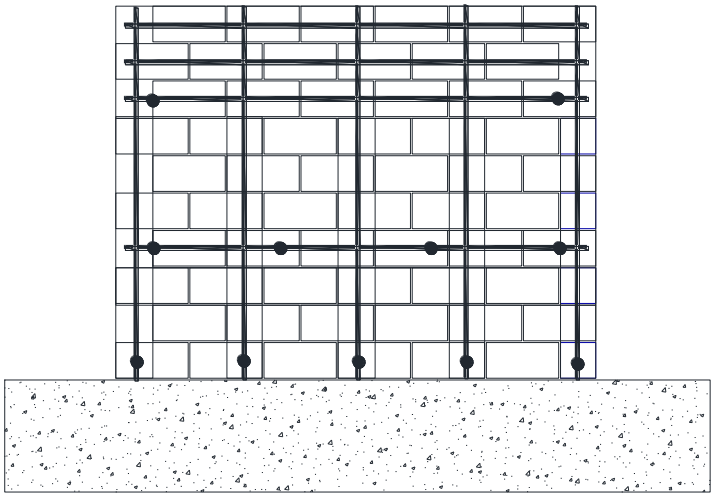

Figure D.3 Location of strain gages for specimen PG127-24

APPINDEX E
LOCATION OF POTENTIOMETERS

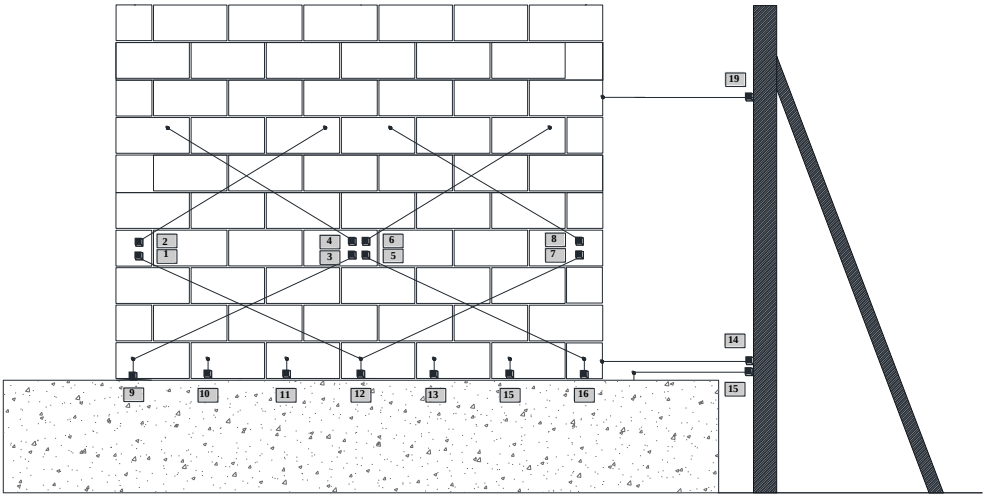

Figure E.1 Location of Potentiometers for PG127-48, PG127-48I, PG180-48, and PG254-47

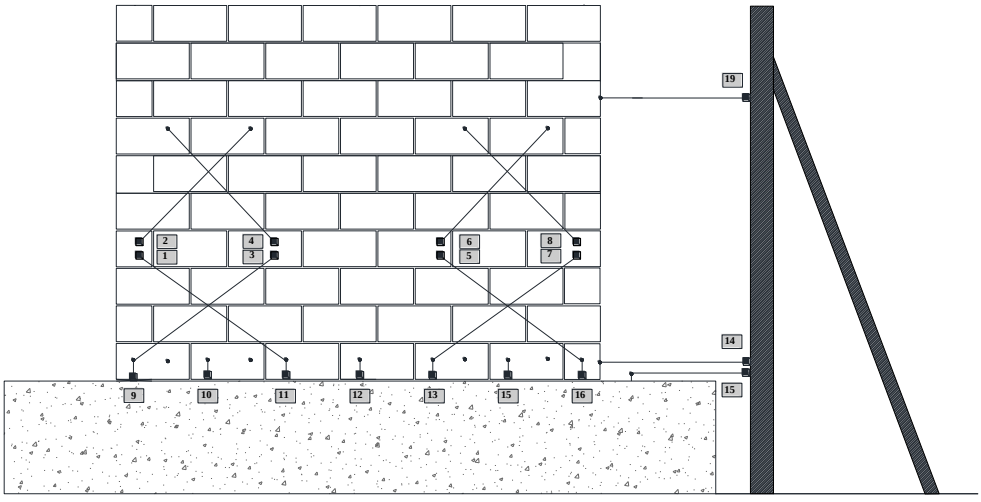

Figure E.2 Location of Potentiometers for specimen PG127-32

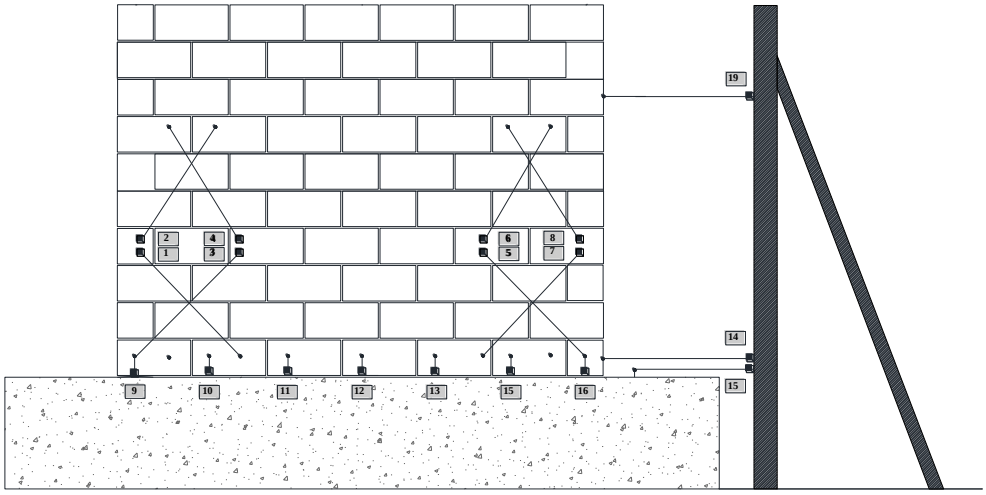

Figure E.2 Location of Potentiometers for specimen PG127-24